UNIVERSITY OF CALIFORNIA
RIVERSIDE

Advanced Surface Plasmon Resonance (SPR) Techniques for Peptide-Based Inhibition Study and Multi-Parametric Cell Analysis

A Dissertation submitted in partial satisfaction
of the requirements for the degree of

Doctor of Philosophy

in

Chemistry

by

Fatimah B.A. Abouhajar

March 2022

Dissertation Committee:
Dr. Quan Cheng, Chairperson
Dr. Min Xue
Dr. Wenwan Zhong

The Dissertation of Fatimah B.A. Abouhajar is approved:

_____

_____

_____

Committee Chairperson

University of California, Riverside

ACKNOWLEDGEMENTS

In the name of Allah, Most Gracious, Most Merciful.

A word of thanksgiving to God, the source of all knowledge, by whose abundant grace this work has come to completion.

There are many people responsible for where I am, and the completion of my dissertation would not have been possible without their support, help and encouragement. First and foremost, I would like to express a deep appreciation for my supervisor, Dr. Cheng for his support, guidance, understanding. His motivation, ideas and feedback have been absolutely invaluable. Dr. Cheng gave me two chances to be a member of this group and welcomed me with open arms. I would like also to extend my sincere thanks to my committee members, Dr. Min Xue and Dr. Wenwan Zhong for taking time out of their ultra-busy schedules to read my dissertation and offer suggestions. My sincere thanks also goes to my previous supervisor at the University of Benghazi, Libya, Dr. Salah Bugreen for his guidance and support during my master's degree. To all my past professors and teachers from my undergraduate and graduate schools, you provided me with the knowledge to accomplish what I have.

It is my pleasure to study at UCR with all the talented researchers and students in a friendly environment. I am very grateful to all my group members at UCR former and present for their valuable help and the wonderful time we spent together. I would like to thank a former graduate student, Dr. Ying Liu for giving me training on SPR, calcinated Au chip preparation and lipid membrane generation. I always remember her valuable help

in getting started in research at UCR. I also owe a great deal of gratitude to Alexander Lambert and Daniel Stuart. They gave me lots of suggestions and practical advice. Discussion with them benefitted my research very much. Thank you, Alex, for taking the time to train me on SPR imaging and preparing a 3D incubator which is not included in this thesis. I'd like to thank Dr. Liza Nor Rais, Dr. Andrew Burris and Bochao Li. Liza was working on her last project and she passed all her experience working with living cells to me. Bochao is the one who trained me on cell cultures. Thank you, Liza, and Bochao, without your help I could not have conducted the project of Studying of Apoptotic Events of HeLa Cells. Thank you, Andy, for helping with AgNP synthesis. My thanks goes to Alexander Malinick, Dr. Kelvin Tran and Dr. Zhengdong Yang for their discussion and useful comments and suggestions on problems I encountered along the way with my research projects. I'd like to thank Dr. Rohit Chaudhuri from Dr. Min Xe's research group, Daniel Stuart and Santino Valiulis for the Corona-virus project. This project was amazing teamwork in which each of us contributed our own specialty and maximized the achievement. I want to thank Qiaoshi Jiang from Dr. Zhong's research group for helping with NTA analysis. I also would like to thank all my group members past and present: Dr. Derek Chen, Dr. Matthew Linman, Dr. Bryce Davis, Dr. Stuart Xe, Cole Ebel and Caleb Pike. It has been a very pleasant and valuable experience for me to work with you. To all visiting scholar's students, I am glad I got a chance to meet you. I would like to express my gratitude to the Libyan Ministry of Higher Education for funding support. I would like to recognize the staff at the International Affairs office and Nina Mandracchia from the Graduate Success Center for their help.

Finally, my heartiest love, respect and thanks goes to my family members. My parents, Basheer and Aisha Abouhajar, whose words of encouragement and push for tenacity ring in my ears. Thank you for all you have done for me. My sisters and brothers who never left my side, you are very special. My three wonderful kids, Muhamed, Hibah and Alabas. You are the driving force of my work and life. Khaled, my husband, for being such a wonderful companion. He is the one who always stands with me and shares my joy and sadness. Khaled, thank you.

ABSTRACT OF THE DISSERTATION

Advanced Surface Plasmon Resonance (SPR) Techniques for Peptide-Based Inhibition Study and Multi-Parametric Cell Analysis

by

Fatimah B.A. Abouhajar

Doctor of Philosophy, Graduate Program in Chemistry
University of California, Riverside, March 2022
Dr. Quan Jason Cheng, Chairperson

The goal of this dissertation focuses on addressing the challenges in advancing biomedical application of SPR techniques, particularly towards drug discovery, cell-drug interactions, and biomarker detection. We first developed and characterized potential peptide inhibitors against the SARS-CoV-2 virus using SPR spectroscopy with a competition assay format. Two peptides were developed with an increasing sequence length based on α-helix of ACE2 PD [22-44] and [30-42] peptides, which were prepared using solid-phase peptide synthesis (SPPS). SPR assays show that these peptides are strong inhibitors to block SARS-CoV-2 spike protein binding to the ACE2 receptor. Results of molecular docking study by PatchDock suggest that both peptides act to block most of the RBD residues that are known to bind to the original ACE2 PD. The work could provide useful information for developing novel anti-SARS-CoV-2 agents without the adverse side effects of small molecules or recombinant proteins. In an effort to augment understanding of cell-based assay with SPR, drug-cell interactions were investigated and monitored in real-time using SPR in combination with optical microscopy. Our results indicate that

different concentrations of propranolol (POA), a beta-blocker, exhibit different modes of interaction with HeLa cells, reflected by both SPR peak angular position (PAP) and peak minimum intensity (PMI). Theoretical SPR curves from models based on confluency were compared to the experimental results, suggesting at a high drug concentration, the experimental SPR response agrees well with microscopic characterization based on confluency. At low concentrations, cell confluency is insufficient to explain the entire SPR response to the apoptotic events, pointing to a complex cytotoxic mechanism. To enhance the biomarker detection sensitivity, we investigated two types of interfaces: an affinity interface based on modified antibody layer and a covalent interface based on thiolated self-assembly monolayer. IgE was chosen as a target model protein biomarker. Results indicate that IgE immobilized by an affinity interface shows a higher binding capacity than those through the covalent interface. In addition, SPR signal amplification using AgNP conjugates was compared on the two interfaces. Furthermore, MD simulation was performed to investigate structural changes and their impact of the amyloid-beta fragments, an Alzheimer's disease biomarker, on the lipid bilayer. Analysis of the simulation results reveals that both Amyloid-beta fragments Aβ (15-27) and Aβ (28-40), along with the POPC lipid bilayer, undergo conformational change in respect to the original structure.

TABLE OF CONTENTS

LIST OF FIGURES

LIST OF TABLES

CHAPTER 1: Introduction

Numerous strategies for biomolecule labeling have been developed that allow for the characterization of biomolecules regarding their structure, or interaction with other molecules.[1, 2] Labeling strategies are used to couple reporter tags, such as radioisotopes, fluorophores, or enzymes, to the target biomolecules (i.e., proteins and nucleotides) to quantitatively assess binding among biomolecules.[3, 4] In addition, the use of molecular labels can cause steric hindrance or change structural configurations, affecting the labeled molecules' affinities for their target biomolecules, which is a major challenge. Label-free detection eliminates the need for specialized tags or dyes, thereby allowing the sensitive measurement of target analytes and enabling the use of native biomolecules suitable for biologically relevant approaches. In the past few decades, a variety of optical biosensor methods have been developed, including surface plasmon resonance (SPR),[5] quartz crystal microbalance (QCM),[6] and ellipsometry.[7] Among the various optical sensing methodologies, the SPR-based system is a representative type of label-free technique for monitoring biomolecular interactions and even living cell analysis in real-time.

Since it was first introduced in the early 1990s, SPR has gained popularity for use in biomolecular studies in real-time to provide specificity, affinity, and kinetic information of these processes. These studies include protein-protein,[8, 9] protein-DNA,[10, 11] enzyme-substrate or inhibitor,[4, 12] receptor-drug,[13, 14] lipid-protein,[15, 16] polysaccharide-protein,[17] cell or virus-protein,[18, 19] among other processes. This optical technique measures the refractive index changes in the vicinity of thin metal layers (i.e., gold, silver, or aluminum

films) in response to biomolecular interactions. Before a sample solution flows across the SPR surface, capturing agents, such as antibodies, enzymes, peptides, and DNAs are immobilized on the surface. Molecular interaction or mass variation near the surface alters the refractive index and thus, can be detected by SPR.

Increases in the effectiveness of the SPR technique led to the development of numerous studies which advanced the potential of the SPR sensor.[20-22] Accordingly, the possible fields of application of SPR technology have expanded to biomedical, environmental, and industrial areas. SPR biosensors can play a prime role in disease diagnosis, drug discovery, foodborne pathogen detection, and so on.[23, 24] Above all, the application of SPR for biomedical purposes is remarkable. So far, various types of SPR measurement systems have been developed for the monitoring of chemical and biological species via the basic theory of SPR detection.[25-27] The work presented in this thesis is focused on the advanced and practical application of SPR-type biosensors, addressing their usefulness and challenges for bioassays. However, we will start with covering the principles of the SPR technique in this introductory chapter.

1.1 Surface Plasmon Resonance (SPR): Principle

1.1.1 SPR Theory

A surface plasmon is an electromagnetic wave propagating at the interface between a metal and a dielectric.[28, 29] Maxwell´s theory of surface plasmons describes the free electrons of metal as an electron liquid of high density (i.e., plasma) and density fluctuations on a surface of this liquid as surface plasmons. In other words, surface

plasmons (SPs) are oscillations of free electrons that propagate along the surface of a metal when it is in contact with a dielectric interface.[30] Therefore, surface plasmons can have a range of energies that depend on the complex dielectric function of the metal (ε_m) and the dielectric function of the adjacent medium (ε_d)[31], as shown by the following equation:

$$k_{sp} = \frac{\omega}{c}\sqrt{\frac{\varepsilon_m \varepsilon_d}{\varepsilon_m + \varepsilon_d}} \qquad (1)$$

where k_{sp} is the wave vector of the SP, ω/c is the wave vector in a vacuum, and the dielectric constant (or permittivity) is the square of the index of refraction.[29]

For practical purposes, Equation 1 can also be expressed in terms of wavelength and refractive index as follows:

$$K_{SP} = \frac{2\pi}{\lambda}\sqrt{\frac{n_m^2 \times n_d^2}{n_m^2 + n_d^2}} \qquad (2)$$

One condition for the generation of SPs is that ε_m and ε_d are of opposite sign, and thus SPs will not be generated for all systems. In addition, ε_m and ε_d are wavelength dependent, and certain regions of the electromagnetic spectrum may be required to generate SPs.[31] One common system used in SPR experiments is a gold film in contact with a water interface. Gold has a negative dielectric function in the IR and visible regions of the electromagnetic spectrum, whereas water has a positive dielectric function.[32] Typical metals that support surface plasmons are gold and silver,[33] but other metals such as aluminum and copper[34] have been used. Gold is usually selected because it is chemically inert to solutions and solutes typically used in biomedical contexts. In addition, gold is

preferred as it is compatible with a number of linking chemistries which will be covered in the next section.

Surface plasmon resonances are not present inherently on these interfaces. Instead, they can be created via excitation by, for example, light. However, because they have a longer wave vector than light waves of the same energy (k_{light} ω/c), they cannot be excited directly by light. The wave vector of a photon must be increased to convert the photon into SPs. This can be accomplished with the use of either a prism or a grating coupler.[29] The setup to excite surface plasmons was first reported by Otto (1968) and Kretschmann and Raether (1968).[35, 36] Since the Otto configuration is rarely employed, we will focus our discussion entirely on the Kretschmann configuration. This configuration is shown in Figure 1.1, which employs p-polarized light that is totally internally reflected (TIR) at the metal surface.

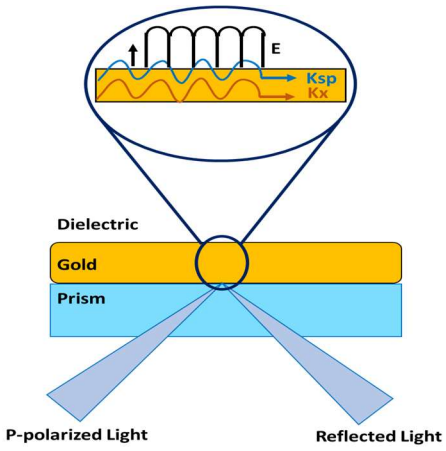

$$K_{SP} = k_x$$

$$\frac{\omega}{c}\sqrt{\frac{\varepsilon_m \varepsilon_d}{\varepsilon_m + \varepsilon_d}} = \frac{\omega}{c}\sin\theta\sqrt{\varepsilon_p}$$

Figure 1. 1 Kretschmann configuration in SPR depicting the conversion of energy from light waves to surface plasmons via a gold/dielectric interface. The equation shows the SPR condition (Ksp=Kx).

When a light beam propagating in a higher refractive index medium reaches the interface with a lower refractive index medium (dielectric interface) at an incident angle

above a critical value, the light is totally reflected at the interface and propagates back into the higher index medium. Although no light is coming out of the prism in TIR, the electrical field of the photons extends into the low index medium.[37] This field is called the evanescent wave because the amplitude of the wave decreases exponentially with increasing distance from the interface surface, decaying over a distance of about one light wavelength.[38] The penetration depth of the evanescent field wave is defined as the distance over which the wave decays to 1/e, or about 37%, of its maximum intensity. The different polarizations of the evanescent field have to be distinguished since they behave differently at the interface. It can be decomposed into a component that is parallel to the plane of incidence (P-polarized light), and perpendicular to the plane of incidence (s-polarized light)

When the P-polarized component of the evanescent field penetrates into the metal layer, the electromagnetic surface plasmon waves are excited and create an enhanced evanescent wave. Therefore, some of the light energy is "lost" into the conductor film, and the surface plasmon angle (θspr) exists when the loss is greatest and the intensity of reflected light reaches a minimum.

The equation for the surface component of a photon's wave vector under TIR conditions K_x is a function of the dielectric constant of the prism (ε_p), and the incidence angle (Θ) of the light on the metal film.[29]

$$k_x = \frac{\omega}{c} sin\ sin\ \theta \sqrt{\varepsilon_p} \qquad (3)$$

At the same time the equation can be expressed in terms of refractive index (n1, higher index medium) and wavelength (λ) as follows:

$$k_x = \frac{2\pi}{\lambda}\, n_1 \; sin\, sin\, \Theta \qquad (4)$$

In order to observe SPR, the matching conditions for the wave vectors of the incident light and SP can be achieved by either tuning the incident angle or the wavelength of the incident light. Using a fixed wavelength light source, surface plasmons will be generated in the metal film at angles where the photon's wave vector (k_{light}) equals the surface plasmon's wave vector (ksp). Since this phenomenon is a conversion of light energy to surface plasmons, the excitation of SPs corresponds to an attenuation of the reflected light intensity. The angle where a complete attenuation of the reflected light occurs is known as the surface plasmon resonance angle and is depicted as a symmetric dip in the reflection spectrum.

$$\theta_{spr} = \left(\frac{1}{n_1} \sqrt{\frac{n_m^2 \times n_d^2}{n_m^2 + n_d^2}} \right) \qquad (5)$$

The position of the resonance angle is affected by the binding of biomolecules to the metal surface. Consequently, SPR is sensitive to changes in the surface characteristics near the interface at a distance of about 300 nm.[39] Thus SPR offers great potential as a surface analytical technique for label-free, nondestructive study of interfacial properties and processes involving both chemical and biological species.

In summary, we can conclude that in an experimental setting where a plane-polarized light is directed through a prism at a certain angle and undergoes total internal reflection on a thin gold surface, the only variable that affects the excitation of surface plasmons is the permittivity of the medium next to the gold surface. The reason for this is

that it is the only variable affecting the wave vector (momentum) of surface plasmons. The evanescent field depth (δz) of surface plasmons depends upon the wavelength of the p-polarized light. Changes only within this evanescent field induce changes in the surface plasmon wave vector. Only when the wave vector of reflected light matches that of the surface plasmons, can plasmons be created. When wave vector matching happens, a sharp dip in the reflected light intensity occurs. On the other hand, the wave vector of the reflected light can be modified by changing the incident angle of the p-polarized light. Thus, by monitoring changes in the angle of minimum light intensity, changes within the medium next to the gold surface can be detected. When the properties (e.g., composition) of the medium change, it changes the permittivity i.e., refractive index (RI) of the medium.

1.1.2 SPR Sensogram and Scanning Modes

There are two modes of SPR: angular-scanning SPR and wavelength-scanning modes SPR spectroscopy, although angular-scanning is more widely practiced. The Kretschmann configuration in the angular scanning mode employs p-polarized light that is totally internally reflected at the metal surface. In this configuration, a laser beam or light-emitting diode (LED) is reflected off the base of a high refractive index prism and the reflected intensity is measured. A thin metal layer, about 51 nm of gold, is located on the prism base which works as the sensor chip, followed by a bulk dielectric (usually water or buffer). The metal layer thickness needs to be precisely controlled in order to obtain the most efficient coupling to the excitation of the surface plasmon for maximum surface sensitivity. Biomolecular interactions taking place at the SPR surface change the surface mass and thus the refractive index within the range of the evanescent field wave. The SPR

angle is therefore altered and is measured as a response signal generating the reflectivity curve (Figure 1.2). The reflectivity curve demonstrates the intensity of reflected light change according to resonance angle shift. The distinct minimum in the reflected light intensity is the peak minimum angle i.e., peak angular position (PAP). The shape and location of the SPR dip (PAP) is monitored to convey information about the sensor surface (e.g., mass and density) and any molecular interaction that caused a change to the refractive index of the medium.

The SPR angle change resulting from biological events can also be monitored in real-time in a continuous manner and forms a sensogram. The whole angle range is measured e.g., every two seconds and the PAP is then expressed in relation to time in the SPR sensogram (Figure 1.3). A sensogram can be drawn also by using a fixed angle scan (wavelength-scanning). Here, the steepest slope at left of the PAP is chosen and the intensity change at this angle is followed continuously. Intensity increases and decreases at this angle translate to peak angular position decreases and increases, respectively. The advantage of fixed angle is its faster response to intensity changes as there is no need to alter the angle of the light. On the other hand, angular scan can monitor the whole SPR curve continuously. Whichever mode used, SPR is capable of measuring changes of the refractive index in the vicinity of the sensor slide in real time.

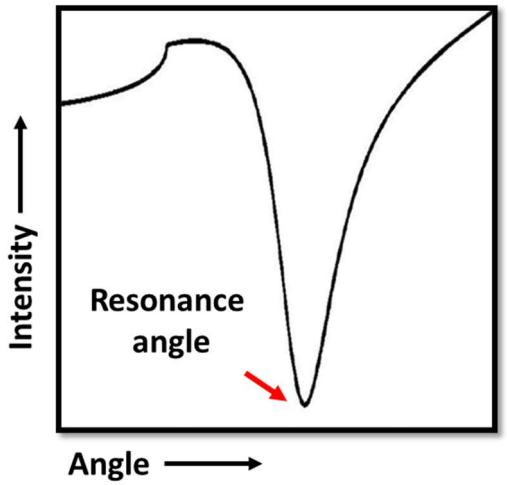

Figure 1. 2 A full SPR curve. Intensity (y-axis) is the intensity of reflected light and Angle (x-axis) is the angle of incident light. At the resonance angle, marked by a red arrow, a sharp drop in the intensity of reflected light is observed (Peak minimum angle).

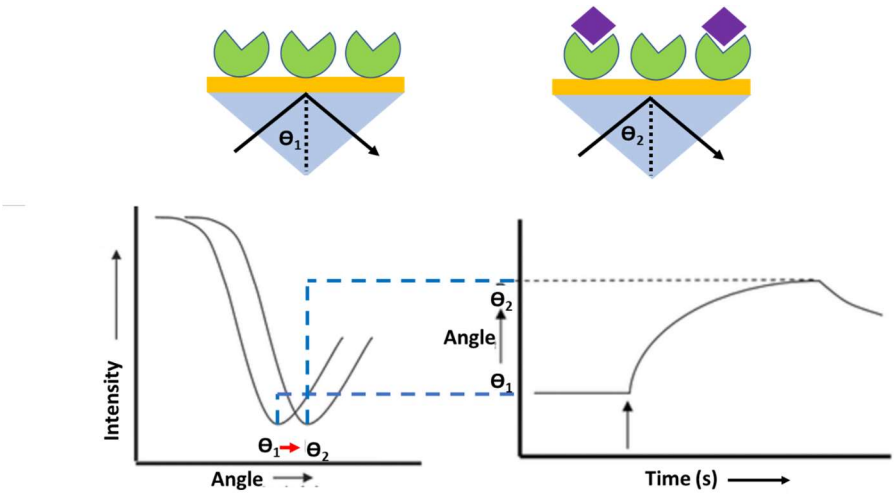

Figure 1. 3 An SPR sensogram: SPR is observed as a sharp shadow in the reflected light from the surface at an angle dependent on the mass of the material at the surface. The SPR angle shifts (from Θ_1 to Θ_2 in the diagram) when biomolecules bind to the surface and change the mass of the surface layer. This change in resonant angle can be monitored in real-time as a plot of resonance signal versus time (Edited from Tudos and Schasfoort 2008).

From figure 1.3, it can be seen how the peak angular position remains constant at first. Then, at the time indicated by the red arrow, the refractive index of the medium within

the evanescent field changes, and the peak minimum angle increases from Θ_1 to Θ_2. Later, the minimum angle starts to shift back towards its original position. This change in peak angular position can be caused by, for example, molecules that adsorb on the gold surface. Because the adsorbing molecules have a different refractive index than the medium, the average refractive index of the medium changes. When the molecules start to detach, the space is occupied again with the medium and the refractive index changes back, closer to the value of plain medium.

The SPR sensorgram generally contains three phases: the association phase, the dissociation phase and the regeneration phase, as shown in figure 1.4. An SPR sensogram provides quantitative information on specificity, activity, affinity and kinetics of biomolecular interactions.

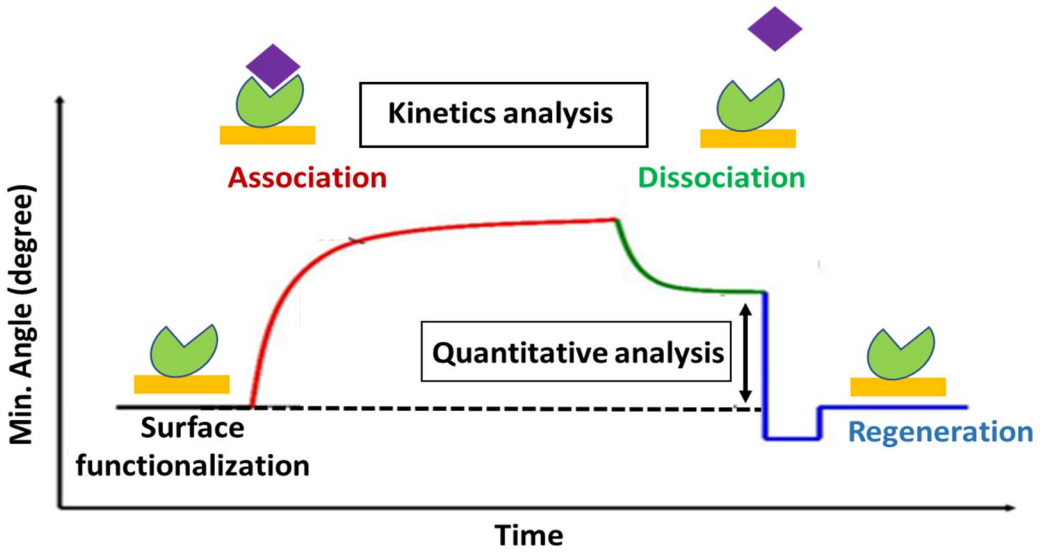

Figure 1. 4 The kinetics of an interaction can be determined from the information in a sensogram.

1.2 Surface modification and immobilization techniques

One of the most important parts of the biosensor is the design of the interface between the biosensor and the chemical or biological system to be studied. Developing a proper interface chemistry to avoid non-specific adsorption and retain the bioactivity of the bio-receptors is important for a successful SPR experiment. Figure 1.5 lists the immobilization strategies to couple biological molecules to a gold surface.

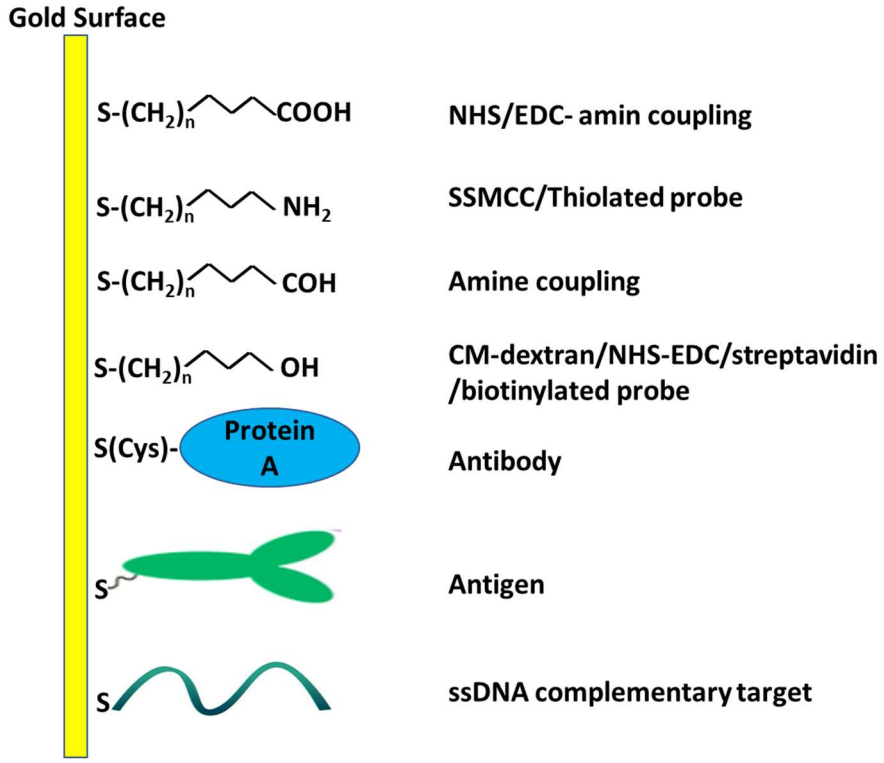

Figure 1. 5 Immobilization methods using chemical linkers with a self-assembled monolayer.

Many coupling strategies utilize a chemical linker layer between the sensor base (the gold layer) and the biological component to achieve these ends. Self-assembled monolayers (SAM) [40] act as ideal linkers in the design of the biosensor. This method increases the freedom of the protein molecules, provides conventional control of the

density of the protein, and helps minimize the non-specific adsorption of the biomolecule to the gold chip[41]. SAMs provide chemical cross-linkers with spacer arms that possess two functional groups; one is a thiol group for linkage to the gold surface, and the other functional group allows for subsequent anchoring of the biological molecule. Several functional groups such as amine (-NH2)[42], Aldehyde (-COH)[43], carboxylic (-COOH)[44], and hydroxylic (-OH)[45] have been used to covalently couple biomolecules to the solid support.

The chemical linker layer can also be used as a substrate for attachment of a polymer coat or hydrogel that renders the surface highly resistant to non-specific adsorption of proteins, nucleotides and drugs. The same polymer also provides a three-dimensional scaffold for receptor immobilization. Formation of hydrogel film composed of carboxymethyl dextran (CM-dextran) covalently linked to the gold surface with a SAM layer is a broadly used method to immobilize the biomolecule in the following reaction.[46]

Membranes also provide a large surface area for biomolecule immobilization. The bilayer lipid membrane is only a few nanometers thick, but the assembly is highly complex and dynamic consisting of two main components: a two-dimensional space made of lipid molecules held together by hydrophobic interactions and self-assembled as a continuous bilayer and proteins embedded within the membrane or transiently associated with it. The bilayer membrane is formed mainly of phospholipid molecules. Phospholipids are a class of lipids consisting of four components: fatty acids, a negatively-charged phosphate group, nitrogen-containing alcohol, and a backbone.[47]

There are many strategies for either covalent or non-covalent (affinity) attachment of bio-receptors to either planar self-assembled surfaces, polymer coats or lipid bilayers. Selection of the correct coupling chemistry requires careful consideration of:

1. the resultant orientation of the bio-receptor,

2. the possible effects of the coupling chemistry on components of the binding interaction (e.g., the receptor bioactivity)

3. the stability of the linkage over the binding assay time and under the conditions used to regenerate the surface, and

4. the availability of sufficient binding sites to the solution phase to interact with the analyte.

For covalent attachment of the bio-receptor to the SAM surface, the reagents must activate the sensor chip surface to produce reactive species. Covalent coupling is then formed by the irreversible binding of reactive functional groups on the outside in a protein onto the activated surface. SAM functionalized with a carboxylic acid group can be activated by 3-(3-dimethylaminopropyl)-carbodiimide (EDC) and N-hydroxysuccinimide (NHS) to form a semi-stable NHS ester, which reacts with an amine in the following reaction to form the amide bond (Figure 1.6a). Amine coupling (e.g., to surface lysine residues or N-terminal residues on a protein receptor) will generally lead to a heterogeneous population of receptors with random orientation on the surface. However, if immobilization is performed at a low pH, the amine terminus is likely to be much more reactive than the gamma-amino group of any lysine residues, in which case amine coupling can give rise to more ordered immobilization.

An aldehyde terminated alkanethiol has been used to couple biomolecules with its amine derivative as well. The interaction between amine and aldehyde groups leads to the formation of a labile Schiff's base that can be stabilized by reduction, creating a stable secondary amine linkage (Figure 1.6b). In addition, thiol (-SH) groups present in cysteine residues[48] or thiol modified biomolecules, ND, or RNA sequences have been directly attached to the gold surface[49] or via connection molecules[50]. An amine terminated alkanethiol (11-mercaptoundecylamine, MUAM) SAM has been reacted with cross linker sulfosuccinimidyl 4-(N-maleimidomethyl) cyclohexane-carboxylate (SSMCC) to forma thiol-reactive maleimide-terminated surface. Thiol modified DNA sequences are then spotted and immobilized for detection of complementary DNA sequences (Figure 1.6c).

Covalent coupling offers a stable, easy, and ligand modification-free method for SPR surface functionalization. Nevertheless, in some cases, there are drawbacks of the use of covalent coupling of biomolecules on a chemically-modified surface. One drawback is the improper orientation of the protein which may result in a reduction in the biosensor sensitivity and reproducibility. In addition, covalent immobilization may involve chemical modification on the active sites of proteins which can potentially affect the analyte-binding activity. To develop a new immobilization procedure to overcome these drawbacks, protein A has been used as an affinity receptor for antibody immobilization. This immobilization relies on the specific interaction with the Fc constant region of the antibody molecules.[51] Using this immobilization method ensures that the binding site of the antibody, located on the Fab variable region, remains easily accessible for binding with the antigen.

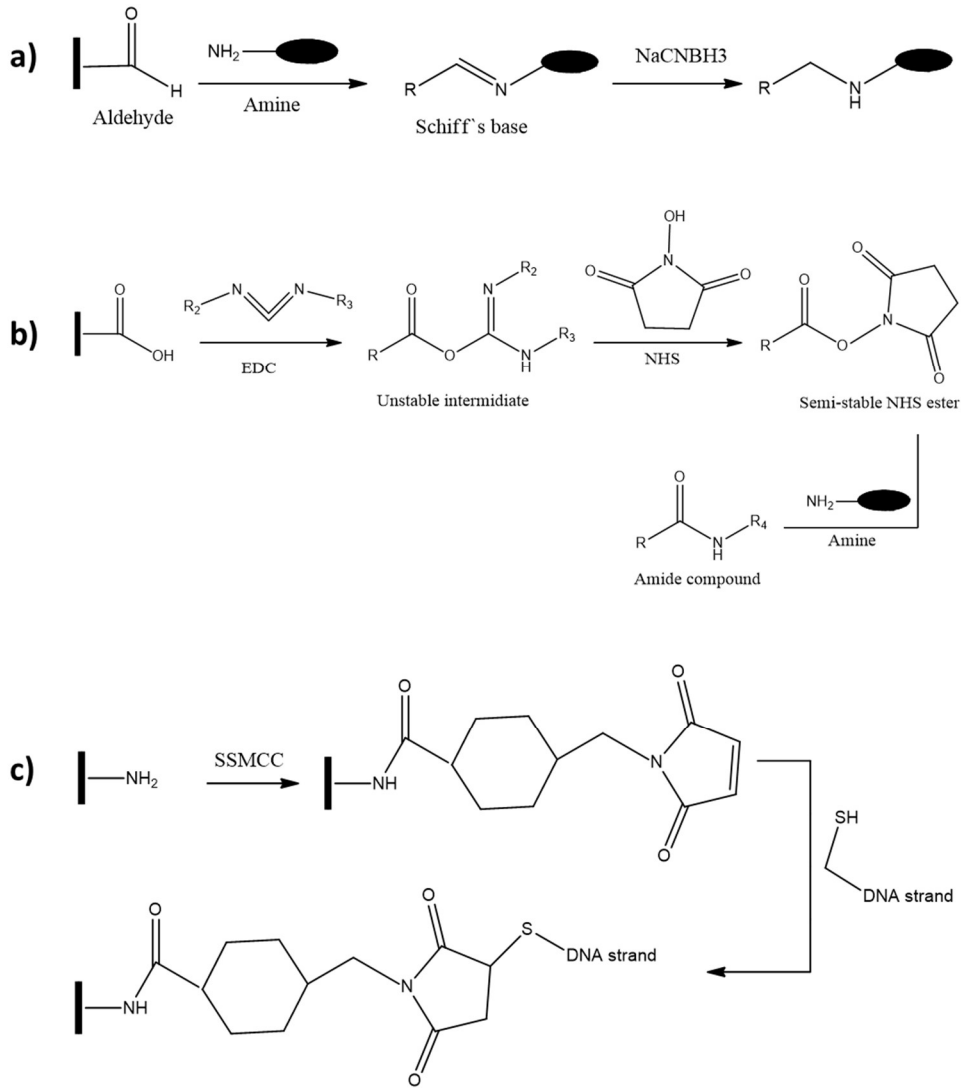

Figure 1. 6 The reaction mechanisms for a) carboxylic acid activated by EDC/NHS to generate amide compound, b) amine chemistry with an aldehyde functionalized surface and c) an amine-functionalized surface reacted with a thiol modified biomolecule with cross-linker SSMCC.

A drawback of protein A-mediated immobilization is the lack of control of the orientation of protein A itself; therefore, different approaches were presented in order to achieve higher orientation control upon immobilization. Lee et al.[52] fabricated an ordered layer-by-layer architecture, with a self-assembled N-succinimidyl-3-(2-pyridyldithio)

propionate (SPDP) layer reacting with the primary amine of protein A. The formation of the protein A layer and the immobilization of IgG molecules were monitored by SPR spectroscopy and AFM topography. Another promising method for immobilizing an oriented antibody to the gold surface is to chemically modify the molecule with a thiol functional group. Wang et al describe using a heteriofunctional linker such as (PEG6-$CONHNH_2$) or (SH-PEG-NH_2) which specifically react with the carbohydrate moiety and carboxyl group, respectively, in the Fc portion of the antibody and result in proper orientation of the antibody.[53]

Another commonly method used to couple the receptor to the surface is using Biotin or streptavidin which are presenting surfaces that can be used to capture biotinylated receptors. The multiple biotin binding sites of streptavidin on each face of the molecule allow biotinylated ligands to be cross-linked by the streptavidin "double adaptor". This method is highly efficient and leads to very stable complexes, but is effectively irreversible.[54, 55]

Many techniques for protein immobilization have been developed in the past years; however, there is no one strategy that can be considered the best one for all protein families and the door is still open for more exploration as it has been the focus of many research groups, including ours in work which will be discussed in Chapter 4.

1.3 Advanced biomedical application of an SPR-Based Biosensor

SPR biosensing appears to be one of the most powerful approaches for monitoring affinity binding of biomolecules and primary screening of druggable molecules. SPR-type

sensors are increasingly used to study a variety of biological entities from small molecular substances such as peptides and glucose to high molecular weight proteins, DNA fragments and even living cells.

1.3.1 Drug discovery

Target identification, screening and optimization of lead candidates are early steps in drug discovery. Techniques that can provide information on compound-target interactions that accelerate the drug discovery process are essential in a competitive industrial environment. The label-free, speed, automation, and high data resolution of SPR-based biosensors make these instruments ideal as drug discovery tools. SPR biosensors provide a reliable method to assess the quality of targets that are destined for further applications. This technology has been used for characterization of target molecules and biopharmaceuticals.[56, 57] Drug discovery biosensor assays currently have been developed that include the screening of compound libraries for binding to target proteins. HIV-1 protease inhibitors have been characterized using SPR analysis.[58, 59] Interactions between thrombin and thrombin inhibitors have also been studied using biosensors to evaluate drug target interactions.[60] Recent advances in data processing have made it possible to routinely detect the binding of low-molecular-mass analytes (< 500 Da).[61]

In general, three experimental setups have been used for drug discovery assay: the direct assay,[62] the competition assay,[63, 64] and the inhibition assay.[65, 66] The setup used for the direct assay involves immobilization of the target and the test compounds are used as analytes. In a competition assay setup, the test compound is mixed with a known ligand, after which the mixture is injected onto the immobilized protein. The competition assay

has two advantages over the direct assay. First, a strong enhancement of the signal is obtained by using a high-molecular-weight reporter molecule.[64] Second, the assay is selective for a certain binding pocket and, therefore, can be used as a follow-up assay after a direct screening.[67] The sensitivity of the competition assay is dependent on the affinity of the reporter ligand. The inhibition assay is common for immunoassays but is also used in receptor-ligand interaction studies. A mixture of the receptor and the test compound is incubated and thereafter flushed over an immobilized high-affinity ligand.

Protein-protein interactions (PPIs) play a fundamental role in all life events and cellular activities, regulating cells' lives and death, as well as mediating various biochemical reactions like signal transduction and metabolism.[68, 69] Thus, PPIs have emerged as a class of promising therapeutic targets for a plethora of medical conditions.[70, 71] At the same time, rational design of PPI inhibitor is considered to be a prospective direction for drug discovery. Our group has investigated a peptide inhibitor against the SARS-CoV-2 coronavirus based on disrupting PPI using a competition assay that will be explained in Chapter 2.

1.3.2 Drug-Cell interaction-based Assay

The SPR technique is not only advantageous due to its real-time and label-free capabilities for dynamic changes at the surface, but also for cellular changes, such as physiology, interactions at the cell surface, and cell detection. The SPR technique enables the monitoring of cellular response, cellular adhesion and cellular products as well as the detection of cancer cells and bacteria cells. Upon receiving stimulation from reactive molecules, mammalian cells respond accordingly. The responses consequently induce SPR

signal changes as interactions between cells and molecules occur.[72-74] In a study in 2007 by Yanase et al.,[73] a large angle of resonance (AR) change in an SPR sensor was observed when RBL-2H3 rat mast cells and PAM212 cells (mouse keratinocyte cell lines) were cultured and activated on a sensor chip by an epidermal growth factor (EGF) or an antigen. In addition, the application of Mycalolide B and Toxin B (cell motility inhibitors) partially inhibited AR changes upon antigen stimulation; no cell movement or morphology changes were observed. These results suggest that AR changes reflect intracellular events other than cell-adhesion area size changes. SPR signal has been used to measure cell growth and size changes as well.[75, 76] Exposure to non-isotonic stimulation can cause the cell volume to change. In particular, hypotonic stimulation results in SPR signal decrease, and the signal reverses to an equilibrium value after additional introduction of isotonic solutions. However, another study shows a decrease in PAP for the cells that actively shrink due to cytoskeleton contraction or inhibition of cellular respiration[77, 78]

A widely used experimental setup when utilizing SPR for living cell sensing uses an approach where cells are cultured on top of a gold surface; the measurement area should have a continuous cell monolayer to ensure that the signals originate from cells and not from empty sensors. Next, solutions containing stimuli flow over the cells, and their response is measured in real-time by SPR. This strategy has been successfully applied to detect and diagnose malignant tumors cells, such as Chinese hamster ovary cells without the use of immunological labels.[79] In addition, living cells uptake of drugs,[80] and extracellular vesicles[81] have been monitored online in this fashion.

The evanescent field penetrates into the cells, and refractive index changes within cells can thus be monitored. Although, the evanescent wave penetration is not deep enough to be impacted by the contact between the drugs and the cell membrane. The SPR signal is caused by morphological changes and rearrangements of the intracellular materials that follow the binding event.[82] However, in the cells, a variety of responses occur that can be responsible for the SPR signal and determining the actual source of the signal is difficult and still not fully understood. The situation is even further complicated by the fact that many different mechanisms can contribute to the SPR signal simultaneously, such as cell spreading/contraction and several concurrent intracellular events.

Additional SPR tools in cell sensing

When using the angular scan, the full angular spectrum is monitored throughout the experiment. Thus, it is possible to gain additional information such as reflected light intensity at the minimum peak of the SPR curve (peak minimum intensity, PMI) and changes at the total internal reflection area (TIR area) (Figure 1.7). Even though these parameters are not commonly utilized, they can further aid in interpreting cellular events. The intensity at peak angular position (PMI) depends on losses of the surface plasmons due to light scattering and absorption, i.e., the more light scatters and absorbs, the fewer surface plasmons are generated and thus the reflected light intensity increases.[80] Scattering is caused by all objects that have a different refractive index than the surrounding liquid. Thus, in cellular assays the increase in PMI is caused by e.g., corrugation of the cell membrane and increasing concentration of cell organelles within the evanescent field.[83, 84] However, these parameters are not yet widely used in cell sensing assay.

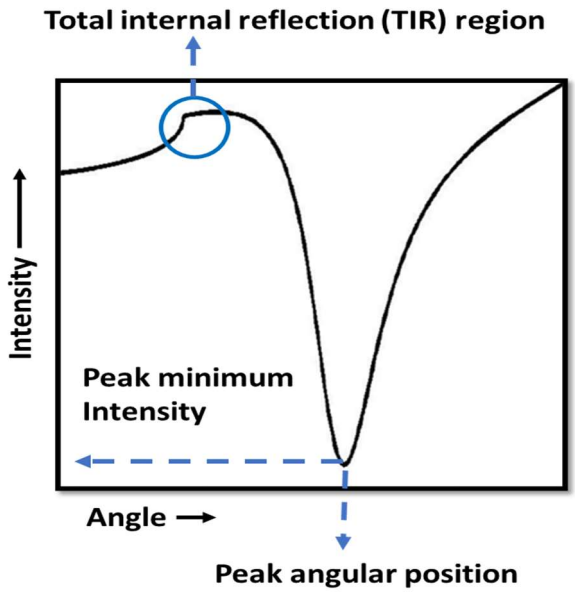

Figure 1. 7 From a full SPR curve, information of the peak minimum intensity (PMI) and changes at the total internal reflection (TIR) area are available (Edited from Viitala et al. 2013).

Our group has previously described how SPR and PAP can be used to monitor HeLa cell morphology change and detachment from substrate surfaces when the cells on the SPR chips undergo an apoptotic phase after being treated with hydrogen peroxide (H2O2), a cell death inducer. The SPR signals were comparable to cell confluency. In addition, this work was verified by a mathematical model that relates the SPR signal to the thickness of cell layers and refractive indexes in the vicinity of the sensing surface. Although cell-based SPR offers huge potential in cancer diagnosis and cell toxicology studies, it remains underrated and is less explored than other SPR biosensors. This gives us motivation to explore more and investigate the full SPR angular spectra in real-time in order to fully utilize its shape or key parameter (i.e., PAP, PMI) for monitoring the apoptosis process during drug-cell interaction as discussed in detail in Chapter 3

1.3.3 Protein Biomarker

Methods for the identification and analysis of biomarkers have gained more attention during recent years and have evolved rapidly. The identification and detection of disease biomarkers are important to foresee outbreaks of certain diseases, thereby avoiding surgery and other invasive and expensive medical treatments for patients. Thus, more research into discovering new biomarkers and new methods for faster and more accurate detection is needed. It is often difficult to detect and measure biomarkers because of their low concentrations and the complexity of their respective matrices. Therefore, it is hard to find and validate accurate screening methods suitable for clinical use. SPR has proven to be useful in biomarker diagnosis due to its sensitivity, portability, small volume sample operation, and capability of multiplexed detection. Researchers have been able to employ SPR in the detection of important biomarkers[85-87]

Nevertheless, SPR biosensors still have some challenges to be addressed in regard to biomarker analysis and detection. First, as we discussed earlier in section 1.2, the interface between the biosensor surface and the biological system to be studied is a vital component of SPR. An interface that provides the right and controlled orientation of the biomolecules results in an increase in biosensor sensitivity and reproducibility. Second, there is an inability to detect ultra-low concentrations of protein biomarkers. To overcome this, the aid of nanoparticles is needed for signal amplification. The continuous development of nanotechnology has enabled the fabrication of advanced nanomaterial-based SPR sensors that have good sensitivity and selectivity. Nanomodification is a useful option to amplify the SPR signal intensity due to the high surface-area-to-volume ratio of

nanomaterials.[88] In addition, it provides versatility for conjugation with many biomolecules including DNA, protein, aptamer, and antibody.[89]

We studied different types of interfaces, specifically affinity and covalent interfaces, for protein biomarker analysis. In addition, the nanoparticle conjugate has been used to compare signal amplification using both interfaces in Chapter 4. This chapter also includes molecular dynamic simulation studies of amyloid-beta fragment (AD biomarker) conformation change near the lipid bilayer.

1.4 Peptide-Based Inhibitors Disrupting Protein-Protein Interactions

As mentioned in section 1.3.1, modulating PPIs is of critical significance in both basic research and clinical translation. It not only facilitates a better understanding of a wide range of biological events but also constitutes the theoretical basis for current therapeutic agents' development. In the era of modern pharmacology, the rational design of a PPI inhibitor is considered to be a prospective direction for drug discovery and possesses enormous potential.

Historically, PPIs have attracted extensive attention in their related research.[90-92] Extensive efforts invested in this topic have retrieved an enormous amount of high-quality PPI system crystal structures, based on which some success has been accomplished in the PPI inhibitor drug design.[93, 94] Nevertheless, due to the of nature biophysical and biochemical limitations, drug discovery targeting PPIs still remains a tough task in both academia and industry. One of the utmost difficulties for PPI inhibitor development is the large, shallow binding surfaces being smooth and lacking well-defined binding pockets.

Such poor surface architecture poses considerable difficulty for ligand binding, as well as confers great challenges toward the design and optimization of drug molecules.[95] Previous crystallography and modeling studies have unveiled that, in contrast to the small molecule binding site which is relatively deep and covers only 300–500 Å2 area, a protein binding interface is generally wide and flat, and its surface area ranges approximately between 1,000–2,000 Å2. [96, 97] Consequently, given the difficult topologies of PPI systems, they are commonly deemed as "undruggable," with limited identification of specific inhibitors directing to them. However, the recent proposal of the "hot spot" concept has greatly promoted the development of PPI inhibitors.[98] It provides an alternative for designing orthosteric ligands to directly target the interaction interface, which mimic the important secondary structure, i.e., the "hot spots" along the PPI interface and disrupts its formation.

The existence of hot spot residues has thus shed light on PPI inhibitor development as it supplies a more specific and well-defined drug target instead of the broad and wide protein interaction surfaces. Through interfering with the hot spot residues within a relatively local region, inhibitor molecules could readily avoid competing with the high-affinity protein binding effector while easily disrupting the overall PPI complexes and exerting therapeutic effects. Researchers have managed to design a great number of PPI inhibitors toward an enormous of historically intractable targets including the immune responses related CD2-CD58,[99] inflammation-related,[100] and apoptosis-related Mcl-1-Bim.[101] Their success depicts the importance of PPI hotspot elucidation and the downstream structure-guided PPI inhibitor discovery. Generally, the rational design of PPI inhibitors depends heavily on reported crystal structures, which can specifically reveal the

principles of protein-protein binding modes. It is significant to develop novel molecular scaffolds with an in-depth understanding of the hot spot residues in each interface.

Although small molecules dominate the drug market so far, peptide inhibitors still represent a class of promising candidates because of their similarity to endogenous ligands, high affinity, and low toxicity due to the limited possibility for accumulation in the body. Furthermore, low molecular weight synthetic peptides have the same advantages as small-molecule inhibitors, including lower manufacturing costs, higher stability, and reduced immunogenicity compared to anti-body therapeutics.[102] Additionally, synthetic peptides are larger compared to small-molecule agents, which may result in stronger interactions when interfering with the interface of PPIs.

In 2010, over 100 peptide drug candidates were reported in clinical trials and in 2019, three new peptide drugs were approved by the US FDA.[103] Early on, peptides were considered poor drug candidates due to the inefficient and expensive synthesis processes, low bioavailability, and limited stability against proteolysis by peptidases in the gastrointestinal tract and serum. Thanks to technological advances, two chemical methodologies: solution-phase synthesis in 1953[104] and solid-phase peptide synthesis in 1963[105] dramatically dropped the cost of peptide manufacturing. The door for development of peptide-based therapeutics was widely opened by introducing peptides with varying sequence lengths, side-chain reactivities and degrees of modification and incorporation of unnatural components.

To overcome the disadvantages of peptides as drug candidates, the field of peptidomimetics was introduced in the early 1990s. A peptidomimetic candidate is usually

based initially on a native peptide, which has been shown to inhibit protein interaction or function and which is then modified artificially to enhance bioavailability, reduce the rate of clearance, and decrease degradation by peptidases.[106, 107] There are numerous reported peptidomimetics.[108] Some examples of peptidomimetics introduce, D-peptides, β-peptides and peptoids.[109] Primarily, changing stereochemistry by inserting D-amino acids has emerged as a promising methodology for designing peptides inhibitors. They are more resistant against proteolytic degradation than their L-enantiomeric counterparts[110] because L-peptides are usually more easily selected by the chiral proteases and quickly cleaved into corresponding amino acid substituents in blood plasma. Such an approach can readily prevent the inhibitor molecules from rapid proteolytic degradation and improve their stability.[111] Notably, these fast-progressing techniques have already obtained reasonable success in an increasing number of critical targets.

1.4.1 Peptides as a drug against viral infections

Human pathogenic viruses pose an enormous threat to human health, society and the economy. This situation is further complicated by the fact that viruses, such as human immunodeficiency virus type 1 (HIV-1), may develop resistance and that viruses keep (re-)emerging (e.g., Ebola and Zika virus).[112, 113] The severe acute respiratory syndrome coronavirus 2 (SARS-CoV-2), which causes the coronavirus disease 2019 (COVID-19), rapidly spread around the world causing many fatalities and crises in the health sector, the economy and society in general.

Even with the successful vaccination effort, issues with vaccines (use in immunocompromised or immune-deficient individuals) should allow room for the

development of therapeutics targeting other pathways. In addition, the development of therapeutics is essential for the treatment of an already infected individuals.

Therapeutic peptides have been validated for the effectively and selectively inhibiting PPIs both in cancer and viruses.[114] For example, Nelfinavir, which was launched into the market in 1997 for the treatment of human immunodeficiency virus (HIV) infectious diseases gives an example of the power and potential of PPI drug discovery.[115]

A straightforward approach to peptide design is to adopt sequences from the interaction sites of proteins. These peptides have the potential to block key protein-protein interactions. Strategies focusing on targeting viral proteins are usually highly specific to the virus of interest. In many cases, peptides are designed to act extracellularly, i.e., to target early steps of viral replication, such as viral envelope glycoprotein activation, receptor attachment, or fusion. This has the advantage that the therapeutic peptide does not need to penetrate the cell membrane and that potential harmful interactions between the viral pathogen and host cells are minimized.

The high potency and selectivity as well as the pharmacological profile and ease of synthesis of peptides enable their translation into clinical applications.[116] Frequently, peptides are highly specific while being tolerable and safe. Importantly, their interactions and degradation pathways are often predictable. Thus, absorption, distribution, metabolism and excretion (ADME) properties can be anticipated and improved.[116, 117] In this respect, administration and targeted tissues play critical roles in ADME and determine therapeutic efficacy. Peptides are rarely orally available and to achieve systemic distribution, they are often delivered intravenously or subcutaneously.[117] Systemically available peptides face

plasma protein binding, proteolytic degradation, metabolization in the liver or free filtration by the kidneys, which may drastically reduce plasma half-life and concentrations at the targeted tissue.[117] Thus, a limitation for the clinical application of peptide inhibitors is their lack of systemic bioavailability.[118]

However, for example, the sites of SARS-CoV-2 infection and replication, i.e., the upper and lower airways, are highly accessible,[119] which renders the need for oral availability or systemic application obsolete. Respiratory diseases are commonly targeted by nasal or oral sprays or inhalation of small molecules allowing for direct delivery to the target organ. Several peptide-based inhalants have already made it into the market. For example, lucinactant is applied as inhalable surfactant replacement to treat respiratory distress syndrome (RDS).[117, 120, 121] Other pulmonary peptide therapeutics such as aviptadil against RDS and pulmonary hypertension, as well as inhalable peptides targeting cystic fibrosis, asthma, and infectious diseases, are currently in clinical trials.[120]

Thus, the oral, nasal, and pulmonary modes of delivery are easy and feasible: absorption and distribution occur directly at the targeted site, the metabolization is reduced, and the elimination occurs mainly via mucus flow which reduces potential side effects. Therefore, locally applied extracellular peptides that do not need to enter the bloodstream to block viral infection might be strong candidates for clinical development.

1.5 Molecular Dynamin Simulation (MDS)

The impact of molecular dynamics (MD) simulations in molecular biology and drug discovery has expanded dramatically in recent years. Molecular dynamics (MD)

simulations predict how every atom in a protein or other molecular system will move over time based on a general model of the physics governing interatomic interactions.[122] These simulations can capture different and important biomolecular process, including conformational change, ligand binding, and protein folding, revealing the positions and motion of every atom at every point of the simulation time. Software to perform this kind of calculation e.g., Charmm,[123] NAMD,[124] Amber,[125] Gromacs,[126] Gromos,[127] and DL_POLY[128] and to visualize and analyze their output are VMD,[129] gOpenMol,[130] nMoldyn,[131] etc. Today MD simulations are routinely used by many users. The importance of MD simulation lies in its ability to probe molecular properties that are difficult or impossible to access through wet-lab experiments. Therefore, in the last project of my thesis (see chapter 4) MD simulation using NAMD and VMD was used to analyze peptide conformation change near lipid bilayers.

The first molecular dynamic simulation of a macromolecule of biological interest was published in 1977.[132] After which, simulations have begun to appear frequently in experimental structural biology papers, where they are used both to interpret experimental results and to guide experimental work. This, in particular is noticed in, although certainly not limited to, neuroscience; simulations have been used to study proteins critical to neuronal signaling,[133-135] to assist in the development of drugs targeting the nervous system,[136, 137] and to reveal mechanisms of protein aggregation associated with neurodegenerative disorders.[138, 139]

The basic idea behind an MD simulation is straightforward. Given the positions of all of the atoms in a biomolecular system (e.g., a protein surrounded by water and perhaps

a lipid bilayer), one can calculate the force exerted on each atom by all of the other atoms. Thus, Newton's laws of motion can be used to predict the spatial position of each atom as a function of time. In particular, as one steps through time, it is possible to calculate the forces on each atom and then use those forces to update the position and velocity of each atom. The resulting trajectory is basically a three-dimensional movie that describes configuration of the system at the atomic level at every point during the simulated time interval.

The forces in an MD simulation are calculated using a mathematical model known as a molecular mechanic's force field. The force field (FF) parameters are typically obtained either from quantum mechanical calculations or by fitting to experimental data such as X-ray crystallography, NMR, infrared, Raman, etc. Molecules are simply defined as a set of atoms that are held together by simple elastic (harmonic) forces and the FF replaces the true potential with a simplified model valid in the region being simulated.[140] There are many force fields available in the literature, having different degrees of complexity and oriented to treat different kinds of systems. However, a typical expression for an FF may look like this[141]:

$$U = \sum_{bonds} \frac{1}{2} k_i^b (r - r_0)^2 + \sum_{angles} \frac{1}{2} k_i^a (\theta - \theta_0)^2 + \sum_{dihedrals} \frac{v_n}{2} [1 + cos(n_i \emptyset_i + \delta_i)]$$

$$+ \sum_{improper} V_{imp} + \sum_{Lj} 4\epsilon_{ij} \left(\frac{\sigma_{ij}^{12}}{r_{ij}^{12}} - \frac{\sigma_{ij}^{6}}{r_{ij}^{6}}\right)] + \sum_{elec} \frac{q_i q_j}{r_{ij}} \qquad (6)$$

where the first four terms refer to intramolecular or local contributions to the total energy (bond stretching, angle bending, and dihedral and improper torsions), and the last two terms serve to describe the repulsive and Van der Waals interactions (Lennard-Jones potential) and the Coulombic interactions

As shown in equation 6 a typical force field incorporates terms that capture for example, electrostatic (Coulombic) interactions between atoms, spring-like terms that model the preferred length of each covalent bond, and terms capturing several other types of interatomic interactions. Such force fields are inherently approximate. Comparison of simulations with a variety of experimental data indicates that force fields have improved substantially over the past decade.[142] It is important to notice that, in a classical MD simulation, no covalent bonds form or break, so no chemical processes can be studied

Many MD simulation studies aim to observe biomolecular processes in action, with particular emphasize on important functional processes such as ligand binding, ligand-induced conformational change, protein folding, or membrane transport. This can allow one to answer questions about the structural basis for events that are difficult to address experimentally. In what order do substructures form during protein folding?[143] How does binding of a ligand to a GPCR's extracellular surface cause changes on the intracellular side, where the G protein binds?[144] More generally, what is the structural basis for allostery in proteins?[145] How do intrinsically disordered proteins assemble to form fibrils?[146, 147]

These simulations are powerful for several reasons. First, they capture the position and motion of every atom at every point in time, which is very difficult with any experimental technique. Second, the simulation conditions are precisely known and can be

carefully controlled: the initial conformation of a protein, which ligands are bound to it, whether it has any mutations or post-translational modifications, which other molecules are present in its environment, its protonation state, the temperature, the voltage across a membrane, and so on. By comparing simulations performed under different conditions, one can identify the effects of a wide variety of molecular perturbations. Of course, experiments play an essential role in validating the simulation methodology[122]: comparisons of simulation and experimental data serve to test the accuracy of the calculated results and to provide criteria for improving the methodology.

1.6 Thesis Outline

My research goal is to demonstrate the great potential of SPR biosensors in advanced applications, mainly toward drug discovery, cell-drug interaction base assays, and biomarker analysis. Specifically, my research aims to address their usefulness and challenges for bioassay. Chapter 2 of this dissertation focuses on developing and investigating a potential peptide inhibitor against SARS-CoV-2 virus based on disrupting PPI. Targeting early steps of a viral infection such as receptor attachment is a promising therapeutic target. To improve SPR sensitivity of studying the binding of small peptides, a competition assay was performed. In addition, molecular docking was performed to understand in-depth the interaction between the receptor and the designed peptide.

Analysis of cellular events using SPR is still new and less explored than other SPR biosensor assays, before we observe a rapid growth for this type of application several challenges and limitations need to be addressed. For one example, the SPR sensing range

is only 300 nm from the sensor surface and the diameter of cells range between 1 to 30 μm, so inherently SPR is limited to only detecting events occurring around a small portion of the cell. Another example is that in the cell a variety of responses occur that can be responsible for the SPR signal and determining the actual source of the signal is difficult and still not well understood. In Chapter 3, I demonstrated how analyzing the full SPR angular spectra in order to fully utilize its shape and key parameters (PAP and PMI) can help gain more information for monitoring cell-drug interactions.

Lack of sufficient sensitivity and proper sensing interfaces could be an issue of SPR sensors while detecting and analyzing protein biomarkers. Chapter 4 focuses on investigating two types of interfaces: an affinity interface based on developing chemically modified antibody self-assembly and a covalent interface base on thiolated self-assembly monolayer. SPR signal amplification using a AgNP conjugate was compared using the two interfaces. My work in this chapter also includes MD simulation. The key concept of Alzheimer`s disease biomarker is based on conformation change and aggregation of amyloid beta proteins; therefore, we perform an MD simulation to investigate confirmation change of amyloid-beta fragments near the lipid bilayer.

REFERENCES

1. Stephanopoulos, N.; Francis, M. B., Choosing an effective protein bioconjugation strategy. *Nat Chem Biol* **2011,** *7* (12), 876-84.

2. Tugarinov, V.; Kanelis, V.; Kay, L. E., Isotope labeling strategies for the study of high-molecular-weight proteins by solution NMR spectroscopy. *Nat Protoc* **2006,** *1* (2), 749-54.

3. Phelan M.L., N. S., Generation of bioreagents for protein chips. *Proteomics.* **2003,** *3*, 2123–2134.

4. Fong C.-C., L. W.-P., Leung Y.-C., Lo S.C.-L., Wong M.-S., Yang M. , Study of substrate–enzyme interaction between immobilized pyridoxamine and recombinant porcine pyridoxal kinase using surface plasmon resonance biosenso. *Biochim. Biophys. Acta.* **2002,** *1596*, 95–107.

5. Nelson B.P., G. T. E., Liles M.R., Goodman R.M., Corn R.M. , Surface plasmon resonance imaging measurements of DNA and RNA hybridization adsorption onto DNA microarrays. . *Anal. Chem.* **2001,** *37*, 1-7.

6. Caruso F., R. E., Furlong D.N., Niikura K., Okahata Y. , Quartz Crystal Microbalance Study of DNA Immobilization and Hybridization for Nucleic Acid Sensor Development. *Anal. Chem.* **1997,** *69*, 2043–2049.

7. Arwin H., P. M., Johansen K. , Total internal reflection ellipsometry: principles and applications. *Appl. Opt.* **2004,** *43*, 3028-3036.

8. Madeira, A.; Vikeved, E.; Nilsson, A.; Sjogren, B.; Andren, P. E.; Svenningsson, P., Identification of protein-protein interactions by surface plasmon resonance followed by mass spectrometry. *Curr Protoc Protein Sci* **2011,** *Chapter 19*, Unit19 21.

9. Besenicar, M.; Macek, P.; Lakey, J. H.; Anderluh, G., Surface plasmon resonance in protein-membrane interactions. *Chem Phys Lipids* **2006,** *141* (1-2), 169-78.

10. Majka J., S. C., Analysis of protein-DNA interactions using surface plasmon resonance. . *Adv. Biochem. Eng. Biotechnol* **2007,** *104*, 13–36.

11. Teh H.F., P. W. Y. X., Su X., Thomsen J.S. , Characterization of protein—DNA interactions using surface plasmon resonance spectroscopy with various assay schemes. . *Biochemistry* **2007,** *46*, 2127–2135.

12. Geitmann, M.; Danielson, U. H., Studies of substrate-induced conformational changes in human cytomegalovirus protease using optical biosensor technology. *Anal Biochem* **2004,** *332* (2), 203-14.

13. Rich R.L., H. L. R., Geoghegan K.F., Brown T.A., LeMotte P.K., Simons S.P., Hensley P., Myszka D.G., Kinetic analysis of estrogen receptorligand interactions. *Proc. Natl. Acad. Sci. USA.* **2002,** *99*, 8562–8567.

14. Salamon Z., C. S., Varga E., Yamamura H.I., Hruby V.J., Tollin G. , Plasmon resonance studies of agonist/antagonist binding to the human delta-opioid receptor: New structural insights into receptor-ligand interactions. . *Biophys. J.* **2000,** *79*, 2463–2474.

15. Erb, E. M.; Chen, X.; Allen, S.; Roberts, C. J.; Tendler, S. J.; Davies, M. C.; Forsen, S., Characterization of the surfaces generated by liposome binding to the modified dextran matrix of a surface plasmon resonance sensor chip. *Anal Biochem* **2000,** *280* (1), 29-35.

16. Baron O.L., P. D., Antipolis S. , Protein-lipid interaction analysis by surface plasmon resonance (SPR) *Bio-Protocol* **2014,** *4*, 1-8.

17. Beccati, D.; Halkes, K. M.; Batema, G. D.; Guillena, G.; Carvalho de Souza, A.; van Koten, G.; Kamerling, J. P., SPR studies of carbohydrate-protein interactions: signal enhancement of low-molecular-mass analytes by organoplatinum(II)-labeling. *Chembiochem* **2005,** *6* (7), 1196-203.

18. Miyoshi, H.; Suehiro, N.; Tomoo, K.; Muto, S.; Takahashi, T.; Tsukamoto, T.; Ohmori, T.; Natsuaki, T., Binding analyses for the interaction between plant virus genome-linked protein (VPg) and plant translational initiation factors. *Biochimie* **2006,** *88* (3-4), 329-40.

19. Zhang, H.; Yang, L.; Zhou, B.; Wang, X.; Liu, G.; Liu, W.; Wang, P., Investigation of biological cell-protein interactions using SPR sensor through laser scanning confocal imaging-surface plasmon resonance system. *Spectrochim Acta A Mol Biomol Spectrosc* **2014,** *121*, 381-6.

20. Grasso, G.; D'Agata, R.; Rizzarelli, E.; Spoto, G.; D'Andrea, L.; Pedone, C.; Picardi, A.; Romanelli, A.; Fragai, M.; Yeo, K. J., Activity of anchored human matrix metalloproteinase-1 catalytic domain on Au (111) surfaces monitored by ESI-MS. *J Mass Spectrom* **2005,** *40* (12), 1565-71.

21. Nedelkov D., N. R. W., Analysis of native proteins from biological fluids by biomolecular interaction analysis mass spectrometry (BIA/MS): Exploring the limit of detection, identification of non-specific binding and detection of multi-protein complexes. . *Biosens. Bioelectron.* **2001,** *16*, 1071–1078.

22. Buijs J., F. G. C., SPR-MS in functional proteomics. *Brief. Funct. Genomic. Proteomic.* **2005,** *4*, 39–47.

23. Cooper, M. A., Label-free screening of bio-molecular interactions. *Anal Bioanal Chem* **2003,** *377* (5), 834-42.

24. Homola, J., Present and future of surface plasmon resonance biosensors. *Anal Bioanal Chem* **2003,** *377* (3), 528-39.

25. Kukanskis K., E. J., Melendez J., Murphy T., Miller G., Garner H. , Detection of DNA Hybridization Using the TISPR-1 Surface Plasmon Resonance Biosensor. *Anal. Biochem.* **1999,** *274*, 7-17.

26. Lowe P.A., C. T. J., Davies R.J., Edwards P.R., Kinning T., Yeung D. , New approaches for the analysis of molecular recognition using the IAsys evanescent wave biosensor. . *J. Mol. Recognit.* **1998,** *11*, 194–199.

27. Mullett, W. M.; Lai, E. P.; Yeung, J. M., Surface plasmon resonance-based immunoassays. *Methods* **2000,** *22* (1), 77-91.

28. SA, M., *Plasmonics Fundamentals and Applications*. Springer, New York 2007.

29. H, R., *Surface Plasmons on Smooth and Rough Surfaces and on Gratings*. Springer, Berlin, 1986.

30. Snyder, A. W. L., J. D., Eds. , *Optical Waveguide Theories*. London, New York, 1983.

31. Smith, E. A. C., R. M. , Surface Plasmon Resonance Imaging as a Tool to Monitor Biomolecular Interactions in an Array Based Format. *Appl. Spectrosc* **2003,** *57*, 320A-332A.

32. Johnson, P.; Christy, R., Optical constants of transition metals: Ti, V, Cr, Mn, Fe, Co, Ni, and Pd. *Physical Review B* **1974,** *9* (12), 5056-5070.

33. Wang, G.; Wang, C.; Yang, R.; Liu, W.; Sun, S., A Sensitive and Stable Surface Plasmon Resonance Sensor Based on Monolayer Protected Silver Film. *Sensors (Basel)* **2017,** *17* (12).

34. Tanabe, I.; Tanaka, Y. Y.; Watari, K.; Hanulia, T.; Goto, T.; Inami, W.; Kawata, Y.; Ozaki, Y., Far- and deep-ultraviolet surface plasmon resonance sensors working in aqueous solutions using aluminum thin films. *Sci Rep* **2017,** *7* (1), 5934.

35. Otto, A., Excitation of nonradiative surface plasma waves in silver by the method of frustrated total reflection. *Zeitschrift für Physik A Hadrons and nuclei* **1968,** *216* (4), 398-410.

36. Kretschmann E and Raether H. Radiative Decay of Non-Radiative Surface plasmon excited by light. *Z Naturforsch A* **1986,** *23*, 2135-2136.

37. Mirabella, F. M., Internal Reflection Spectroscopy. *Applied Spectroscopy Reviews* **2006,** *21* (1-2), 45-178.

38. F, M., Principles of Surface Plasmon Resonance. In *Real-Time Analysis of Biomolecular Interactions*, Nagata K., H. H., Ed. Springer, Tokyo. , 2000.

39. Harding, S. E., Surface Plasmon Resonance. In *Protein-Ligand Interactions: hydrodynamics and calorimetry*, 2001; pp 137-170.

40. Ulman, A., Formation and Structure of Self-Assembled Monolayers. *Chem. Rev.* **1996,** *96*, 1533−1554.

41. Katsumi Uchida, H. O., Mitsuhiro Kaneko, Kazunori Kataoka, and Yukio Nagasaki, A Reactive Poly(ethylene glycol) Layer To Achieve Specific Surface Plasmon Resonance Sensing with a High S/N Ratio: The Substantial Role of a Short Underbrushed PEG Layer in Minimizing Nonspecific Adsorption. *Anal. Chem.* **2005,** *77*, 1075-1080.

42. Lee, H. J. W., A. W.; Li, Y.; Corn, R. M. , Fabricating RNA Microarrays with RNA-DNA Surface Ligation Chemistry. *Anal. Chem.* **2005,** *77*, 7832-7837.

43. D'Souza S.F., G. S. S., Immobilization of invertase on rice husk using polyethylenimine. *J. Biochem. Biophys. Methods* **2002,** *52*, 59–62.

44. Wei Liu, Y. C. a. M. Y., Surface plasmon resonance imaging of limited glycoprotein samples. *Analyst* **2008,** *133*, 1268-1273.

45. Nanduri, V.; Sorokulova, I. B.; Samoylov, A. M.; Simonian, A. L.; Petrenko, V. A.; Vodyanoy, V., Phage as a molecular recognition element in biosensors immobilized by physical adsorption. *Biosens Bioelectron* **2007,** *22* (6), 986-92.

46. S. Lofas and B. J. Johnsoon, A novel hydrogel matrix on gold surfaces in surface plasmon resonance sensors for fast and efficient covalent immobilization of ligands. *Chem. Soc. Chem. Commun.* **1990,** *21*, 1526-1528.

47. Berg, J. M. T., J. L.; Stryer, L. Biochemistry; , *Biochemistry 5th ed - Jeremy M. Berg, John L. Tymoczko, Lubert Stryer.pdf*. New York, , 2002.

48. Younggyu Kim, S. O. H., Natalie R. Gassman, You Korlann,† Elizabeth V. Landorf, Frank R. Collart, and Shimon Weiss, Efficient Site-Specific Labeling of Proteins via Cysteines. *Bioconjugate Chem.* **2008,** *19*, 786–791.

49. Vaisocherova, H.; Zhang, Z.; Yang, W.; Cao, Z.; Cheng, G.; Taylor, A. D.; Piliarik, M.; Homola, J.; Jiang, S., Functionalizable surface platform with reduced nonspecific protein adsorption from full blood plasma--material selection and protein immobilization optimization. *Biosens Bioelectron* **2009,** *24* (7), 1924-30.

50. Jennifer M. Brockman, A. G. F., and Robert M. Corn, A Multistep Chemical Modification Procedure To Create DNA Arrays. *J. Am. Chem. Soc.* **1999,** *121*, 8044-8051.

51. Iijima, M.; Kadoya, H.; Hatahira, S.; Hiramatsu, S.; Jung, G.; Martin, A.; Quinn, J.; Jung, J.; Jeong, S. Y.; Choi, E. K.; Arakawa, T.; Hinako, F.; Kusunoki, M.; Yoshimoto, N.; Niimi, T.; Tanizawa, K.; Kuroda, S., Nanocapsules incorporating IgG Fc-binding domain derived from Staphylococcus aureus protein A for displaying IgGs on immunosensor chips. *Biomaterials* **2011,** *32* (6), 1455-64.

52. Lee, W.; Lee, D.-B.; Oh, B.-K.; Lee, W. H.; Choi, J.-W., Nanoscale fabrication of protein A on self-assembled monolayer and its application to surface plasmon resonance immunosensor. *Enzyme and Microbial Technology* **2004,** *35* (6-7), 678-682.

53. Wang, X.; Mei, Z.; Wang, Y.; Tang, L., Comparison of four methods for the biofunctionalization of gold nanorods by the introduction of sulfhydryl groups to antibodies. *Beilstein J Nanotechnol* **2017,** *8*, 372-380.

54. Peter Nilson, B. P. e. a., Real-Time Monitoring of DNA Manipulation Using Biosensor Technology. *Analytical Biochemistry* **1995,** *224*, 400-408.

55. Kristine Kilsa Jensen, H. Ø., Peter E. Nielsen, and Bengt Norden, Kinetics for Hybridization of Peptide Nucleic Acids (PNA) with DNA and RNA Studied with the BIAcore Technique. *Biochemistry* **1997,** *36*, 5072-5077.

56. Mangold, U., Dax, C. I., Saar, K., Schwab, W., Kirschbaum, B., and Mullner, S., Identification and characterization of potential new therapeutic targets ininflammatory and autoimmune diseases. *Eur. J. Biochem.* **1999,** *266*, 1184–1191.

57. Atwell, S., Ultsch, M., De Vos, A. M., and Wells, J. A., Structural Plasticity in a Remodeled Protein-Protein Interface. *Science* **1997,** *278*, 1125–1128.

58. Hamalainen, M. D., Markgren, P.-O., Schaal, W., et al. (2000), , Characterization of a set HIV protease Inhibitor Using Binding Kinetics Data from a Biosensor-Based Screen. *Biomol. Screen.* **2000,** *5*, 353–360.

59. Markgren, P.-O., Hamalainen, M., and Danielson, U. H. , Fluorometric Method for Measurement of Peroxyl Radical Scavenging Activities of Lipophilic Antioxida. *Anal. Biochem* **1998,** *265*, 340–350.

60. Karlsson, R.; Kullman-Magnusson, M.; Hamalainen, M. D.; Remaeus, A.; Andersson, K.; Borg, P.; Gyzander, E.; Deinum, J., Biosensor analysis of drug-target interactions: direct and competitive binding assays for investigation of interactions between thrombin and thrombin inhibitors. *Anal Biochem* **2000,** *278* (1), 1-13.

61. P., P., Surface Plasmon Resonance: Applications in Understanding Receptor–Ligand Interaction. *Applied Biochem. and Biotech.* **2005,** *126*, 79-91.

62. W., H., A new strategy for improved secondary screening and lead optimization using high-resolution SPR characterization of compound-target interactions. . *J Mol Recognit.* **2005,** *18*.

63. Alterman M., S. H., Safsten P., P1/P1` modified HIV protease inhibitors as tools in two new sensitive surface plasmon resonance biosensor screening assays. *Eur. J. Pharm. Sci.* **2001,** *13*, 203-212.

64. Wear, M. A.; Patterson, A.; Malone, K.; Dunsmore, C.; Turner, N. J.; Walkinshaw, M. D., A surface plasmon resonance-based assay for small molecule inhibitors of human cyclophilin A. *Anal Biochem* **2005,** *345* (2), 214-26.

65. Kroger D., H. F., Vogel H., Ligand binding to nicotinic acetylcholine receptor investigated by surface plasmon resonance *Anal. Chem.* **1999,** *71*, 3157-3165.

66. Kumbhat, S.; Shankaran, D. R.; Kim, S. J.; Gobi, K. V.; Joshi, V.; Miura, N., Surface plasmon resonance biosensor for dopamine using D3 dopamine receptor as a biorecognition molecule. *Biosens Bioelectron* **2007,** *23* (3), 421-7.

67. Nordstrom H, G. T., Hamalainen M, et. al.,, Identification of MMP-12 Inhibitors by Using Biosensor-Based Screening of a Fragment library. *J. Med. Chem.* **2008,** *51*, 3449-3459.

68. Li, X.; Dai, J.; Ni, D.; He, X.; Zhang, H.; Zhang, J.; Fu, Q.; Liu, Y.; Lu, S., Insight into the mechanism of allosteric activation of PI3Kalpha by oncoprotein K-Ras4B. *Int J Biol Macromol* **2020,** *144*, 643-655.

69. Luck, K. et al. A reference map of the human binary protein interactome. *Nature* **2020,** *580* (7803), 402-408.

70. Davenport, A. P.; Scully, C. C. G.; de Graaf, C.; Brown, A. J. H.; Maguire, J. J., Advances in therapeutic peptides targeting G protein-coupled receptors. *Nat Rev Drug Discov* **2020,** *19* (6), 389-413.

71. Cunningham, A. D.; Qvit, N.; Mochly-Rosen, D., Peptides and peptidomimetics as regulators of protein-protein interactions. *Curr Opin Struct Biol* **2017,** *44*, 59-66.

72. Hide, M.; Tsutsui, T.; Sato, H.; Nishimura, T.; Morimoto, K.; Yamamoto, S.; Yoshizato, K., Real-time analysis of ligand-induced cell surface and intracellular reactions of living mast cells using a surface plasmon resonance-based biosensor. *Anal Biochem* **2002,** *302* (1), 28-37.

73. Yanase, Y.; Suzuki, H.; Tsutsui, T.; Hiragun, T.; Kameyoshi, Y.; Hide, M., The SPR signal in living cells reflects changes other than the area of adhesion and the formation of cell constructions. *Biosens Bioelectron* **2007,** *22* (6), 1081-6.

74. Tanaka, M.; Hiragun, T.; Tsutsui, T.; Yanase, Y.; Suzuki, H.; Hide, M., Surface plasmon resonance biosensor detects the downstream events of active PKCbeta in antigen-stimulated mast cells. *Biosens Bioelectron* **2008,** *23* (11), 1652-8.

75. Robelek, R.; Wegener, J., Label-free and time-resolved measurements of cell volume changes by surface plasmon resonance (SPR) spectroscopy. *Biosens Bioelectron* **2010,** *25* (5), 1221-4.

76. Baumgarten, S.; Robelek, R., Surface plasmon resonance (SPR) sensors for the rapid, sensitive detection of the cellular response to osmotic stress. *Sensors and Actuators B: Chemical* **2011,** *156* (2), 798-804.

77. Chabot, V.; Cuerrier, C. M.; Escher, E.; Aimez, V.; Grandbois, M.; Charette, P. G., Biosensing based on surface plasmon resonance and living cells. *Biosens Bioelectron* **2009,** *24* (6), 1667-73.

78. Cuerrier, C. M.; Chabot, V.; Vigneux, S.; Aimez, V.; Escher, E.; Gobeil, F.; Charette, P. G.; Grandbois, M., Surface Plasmon Resonance Monitoring of Cell Monolayer Integrity: Implication of Signaling Pathways Involved in Actin-Driven Morphological Remodeling. *Cell Mol Bioeng* **2008,** *1* (4), 229-239.

79. Hiragun, T.; Yanase, Y.; Kose, K.; Kawaguchi, T.; Uchida, K.; Tanaka, S.; Hide, M., Surface plasmon resonance-biosensor detects the diversity of responses against epidermal growth factor in various carcinoma cell lines. *Biosens Bioelectron* **2012,** *32* (1), 202-7.

80. Viitala, T.; Granqvist, N.; Hallila, S.; Ravina, M.; Yliperttula, M., Elucidating the signal responses of multi-parametric surface plasmon resonance living cell sensing: a comparison between optical modeling and drug-MDCKII cell interaction measurements. *PLoS One* **2013,** *8* (8), e72192.

81. Koponen, A.; Kerkela, E.; Rojalin, T.; Lazaro-Ibanez, E.; Suutari, T.; Saari, H. O.; Siljander, P.; Yliperttula, M.; Laitinen, S.; Viitala, T., Label-free characterization and real-time monitoring of cell uptake of extracellular vesicles. *Biosens Bioelectron* **2020,** *168*, 112510.

82. Suutari, T. S., T.; Karaman, D.S.E.; Saari, H.; Desai, D.; Kerkelä, E.; Laitinen, S.; Hanzlikova, M.; Rosenholm, J.M.; Yliperttula,; al., M. e., Real-Time Label-Free Monitoring of Nanoparticle Cell Uptake. . *Small* **2016,** *12*, 6289–6300.

83. Vala, M.; Robelek, R.; Bockova, M.; Wegener, J.; Homola, J., Real-time label-free monitoring of the cellular response to osmotic stress using conventional and long-range surface plasmons. *Biosens Bioelectron* **2013,** *40* (1), 417-21.

84. Yashunsky, V.; Lirtsman, V.; Zilbershtein, A.; Bein, A.; Schwartz, B.; Aroeti, B.; Golosovsky, M.; Davidov, D., Surface plasmon-based infrared spectroscopy for cell biosensing. *J Biomed Opt* **2012,** *17* (8), 081409-1.

85. Jung S.-H., J. J.-W., Suh I.-B., Yuk J. S., Kim W.-J., Choi E.Y., Kim Y.-M., Ha K.-S. , Analysis of C-reactive protein on amide-linked N-hydroxysuccinimide-dextran arrays with a spectral surface plasmon resonance biosensor for serodiagnosis. . *Anal. Chem.* **2007,** *79*, 5703–5710.

86. Uludag, Y.; Tothill, I. E., Cancer biomarker detection in serum samples using surface plasmon resonance and quartz crystal microbalance sensors with nanoparticle signal amplification. *Anal Chem* **2012,** *84* (14), 5898-904.

87. Tang, D. P.; Yuan, R.; Chai, Y. Q., Novel immunoassay for carcinoembryonic antigen based on protein A-conjugated immunosensor chip by surface plasmon resonance and cyclic voltammetry. *Bioprocess Biosyst Eng* **2006,** *28* (5), 315-21.

88. Antiochia, R.; Bollella, P.; Favero, G.; Mazzei, F., Nanotechnology-Based Surface Plasmon Resonance Affinity Biosensors for In Vitro Diagnostics. *Int J Anal Chem* **2016,** *2016*, 2981931.

89. Merkoci, A., Nanoparticles-based strategies for DNA, protein and cell sensors. *Biosens Bioelectron* **2010,** *26* (4), 1164-77.

90. Devkota, P.; Wuchty, S., Controllability analysis of molecular pathways points to proteins that control the entire interaction network. *Sci Rep* **2020,** *10* (1), 2943.

91. Milroy, L. G.; Grossmann, T. N.; Hennig, S.; Brunsveld, L.; Ottmann, C., Modulators of protein-protein interactions. *Chem Rev* **2014,** *114* (9), 4695-748.

92. Tsai, C. J.; Ma, B.; Nussinov, R., Protein-protein interaction networks: how can a hub protein bind so many different partners? *Trends Biochem Sci* **2009,** *34* (12), 594-600.

93. Schmidt, T.; Bergner, A.; Schwede, T., Modelling three-dimensional protein structures for applications in drug design. *Drug Discov Today* **2014,** *19* (7), 890-7.

94. Sledz, P.; Caflisch, A., Protein structure-based drug design: from docking to molecular dynamics. *Curr Opin Struct Biol* **2018,** *48*, 93-102.

95. Ni, D.; Lu, S.; Zhang, J., Emerging roles of allosteric modulators in the regulation of protein-protein interactions (PPIs): A new paradigm for PPI drug discovery. *Med Res Rev* **2019,** *39* (6), 2314-2342.

96. Lo Conte, L., Chothia, C., and Janin, J. , The Atomic Structure of Protein-ProteinRecognition Sites. *J. Mol. Biol.* **1999,** *285*, 2177–2198.

97. Ran, X.; Gestwicki, J. E., Inhibitors of protein-protein interactions (PPIs): an analysis of scaffold choices and buried surface area. *Curr Opin Chem Biol* **2018,** *44*, 75-86.

98. Bogan, A. A., and Thorn, K. S. , Anatomy of Hot Spots in Protein Interfaces. *J. Mol. Biol.* **1998,** *280*, 1-9.

99. Liu, J., Ying, J., Chow, V. T., Hruby, V. J., and Satyanarayanajois, S. D. , Structure-activity studies of peptides from the "hot-spot" region of human Cd2 protein: development of peptides for immunomodulation. *J. Med. Chem.* **2005,** *48*, 6236–6249.

100. Liu, L.; Ghosh, N.; Slivka, P. F.; Fiorini, Z.; Hutchinson, M. R.; Watkins, L. R.; Yin, H., An MD2 hot-spot-mimicking peptide that suppresses TLR4-mediated inflammatory response in vitro and in vivo. *Chembiochem* **2011,** *12* (12), 1827-31.

101. Denis, C.; Sopkova-de Oliveira Santos, J.; Bureau, R.; Voisin-Chiret, A. S., Hot-Spots of Mcl-1 Protein. *J Med Chem* **2020,** *63* (3), 928-943.

102. Vlieghe, P.; Lisowski, V.; Martinez, J.; Khrestchatisky, M., Synthetic therapeutic peptides: science and market. *Drug Discov Today* **2010,** *15* (1-2), 40-56.

103. Vigneaud Vd, R. C., Swan CJM, Roberts CW, Katsoyannis PG, Gordon S. . , The synthesis of an octapeptide amide with the hormonal activity of oxytocin. *J. Am. Chem. Soc.* **1953,** *75*, 4879–4880

104. RB., M., Solid phase peptide synthesis. I. The Synthesis of a Tetrapeptide. *J. Am. Chem. Soc.* **1963,** *85*, 2149–2154

105. Vagner, J.; Qu, H.; Hruby, V. J., Peptidomimetics, a synthetic tool of drug discovery. *Curr Opin Chem Biol* **2008,** *12* (3), 292-6.

106. Lenci, E.; Trabocchi, A., Peptidomimetic toolbox for drug discovery. *Chem Soc Rev* **2020,** *49* (11), 3262-3277.

107. Avan, I.; Hall, C. D.; Katritzky, A. R., Peptidomimetics via modifications of amino acids and peptide bonds. *Chem Soc Rev* **2014,** *43* (10), 3575-94.

108. Yan R, Z. Y., Li Y, Xia L, Guo Y, Zhou Q. , Structural basis for the recognition of SARS-CoV-2 by full-length human ACE2. *Science* **2020,** *367*, 1444–1448.

109. Lee, A. C.; Harris, J. L.; Khanna, K. K.; Hong, J. H., A Comprehensive Review on Current Advances in Peptide Drug Development and Design. *Int J Mol Sci* **2019,** *20* (10).

110. de la Fuente-Nunez, C.; Reffuveille, F.; Mansour, S. C.; Reckseidler-Zenteno, S. L.; Hernandez, D.; Brackman, G.; Coenye, T.; Hancock, R. E., D-enantiomeric peptides that eradicate wild-type and multidrug-resistant biofilms and protect against lethal Pseudomonas aeruginosa infections. *Chem Biol* **2015,** *22* (2), 196-205.

111. Pallerla, S.; Naik, H.; Singh, S.; Gauthier, T.; Sable, R.; Jois, S. D., Design of cyclic and d-amino acids containing peptidomimetics for inhibition of protein-protein interactions of HER2-HER3. *J Pept Sci* **2018,** *24* (2).

112. Kuritzkes, D. R., Drug resistance in HIV-1. *Curr Opin Virol* **2011,** *1* (6), 582-9.

113. Mourya, D. T.; Yadav, P. D.; Ullas, P. T.; Bhardwaj, S. D.; Sahay, R. R.; Chadha, M. S.; Shete, A. M.; Jadhav, S.; Gupta, N.; Gangakhedkar, R. R.; Khasnobis, P.; Singh, S. K., Emerging/re-emerging viral diseases & new viruses on the Indian horizon. *Indian J Med Res* **2019,** *149* (4), 447-467.

114. Lau, J. L.; Dunn, M. K., Therapeutic peptides: Historical perspectives, current development trends, and future directions. *Bioorg Med Chem* **2018,** *26* (10), 2700-2707.

115. Wlodawer, A., Rational approach to aids drug design through structural biology. *Annu. Rev.* **2002,** *53*, 595–614.

116. Fosgerau, K.; Hoffmann, T., Peptide therapeutics: current status and future directions. *Drug Discov Today* **2015,** *20* (1), 122-8.

117. Kovalainen M, M. J., Riikonen J, Pesonen U, Vlasova M, Salonen J, Lehto VP, Järvinen K, Herzig KH. , Novel delivery systems for improving the clinical use of peptides. . *Pharmacol Rev.* **2015,** *67*, 541-61.

118. Bruno, B. J.; Miller, G. D.; Lim, C. S., Basics and recent advances in peptide and protein drug delivery. *Ther Deliv* **2013,** *4* (11), 1443-67.

119. Wolfel, R.; Corman, V. M.; Guggemos, W.; Seilmaier, M.; Zange, S.; Muller, M. A.; Niemeyer, D.; Jones, T. C.; Vollmar, P.; Rothe, C.; Hoelscher, M.; Bleicker, T.; Brunink, S.; Schneider, J.; Ehmann, R.; Zwirglmaier, K.; Drosten, C.; Wendtner, C., Virological assessment of hospitalized patients with COVID-2019. *Nature* **2020,** *581* (7809), 465-469.

120. Bodier-Montagutelli, E.; Mayor, A.; Vecellio, L.; Respaud, R.; Heuze-Vourc'h, N., Designing inhaled protein therapeutics for topical lung delivery: what are the next steps? *Expert Opin Drug Deliv* **2018,** *15* (8), 729-736.

121. Labiris, N. R.; Dolovich, M. B., Pulmonary drug delivery. Part I: physiological factors affecting therapeutic effectiveness of aerosolized medications. *Br J Clin Pharmacol* **2003,** *56* (6), 588-99.

122. McCammon, M. K. a. J. A., Molecular dynamics simulations of biomolecules. *nature structural biology* **2002,** *9*, 646-652.

123. Brooks, B. R. et. al. CHARMM: the biomolecular simulation program. *J Comput Chem* **2009,** *30* (10), 1545-614.

124. Scalable P. et al. molecular dynamics with NAMD. *J Comput Chem* **2005,** *26*, 1781-802.

125. Case D. et. al. The Amber Biomolecular Simulation Programs. *J. Comput. Chem.* **2005,** *26*, 1668–1688.

126. Van Der Spoel D., L. E., Hess B., Groenhof G, Mark A. E., Berendsen H.J.C., GROMACS: Fast, flexible, and free *J. Comput. Chem.* **2005,** *26*, 1701–1718.

127. Christen M. et. al. The GROMOS software for biomolecular simulation: GROMOS05 *J. Comput. Chem.* **2005,** *26*, 1719–1751.

128. Smith, W.; Yong, C. W.; Rodger, P. M., DL_POLY: Application to molecular simulation. *Molecular Simulation* **2002,** *28* (5), 385-471.

129. Humphrey W., D. A., and Schulten K., VMD Visual Molecular Dynamics. *J. Mol. Graph.* **1996,** *14*, 33-38.

130. Bergman D. L., L. L., and Laaksonen A., Visualization of solvation structures in liquid mixtures. *J. Mol. Graphics Mod.* **1997,** *15*, 301–306.

131. Róg T., M. K., Hinsen K., and Kneller G. R., nMoldyn: A program package for a neutron scattering oriented analysis of molecular dynamics simulations. *J. Comput. Chem.* **2003,** *24*, 657–667.

132. Andrew McCammon J., G. B. R. K. M., Dynamics of folded proteins. *Nature* **1977,** *267*, 585-590.

133. Dawe, G. B.; Musgaard, M.; Aurousseau, M. R. P.; Nayeem, N.; Green, T.; Biggin, P. C.; Bowie, D., Distinct Structural Pathways Coordinate the Activation of AMPA Receptor-Auxiliary Subunit Complexes. *Neuron* **2016,** *89* (6), 1264-1276.

134. Delemotte, L.; Tarek, M.; Klein, M. L.; Amaral, C.; Treptow, W., Intermediate states of the Kv1.2 voltage sensor from atomistic molecular dynamics simulations. *Proc Natl Acad Sci U S A* **2011,** *108* (15), 6109-14.

135. Dror, R. O.; Green, H. F.; Valant, C.; Borhani, D. W.; Valcourt, J. R.; Pan, A. C.; Arlow, D. H.; Canals, M.; Lane, J. R.; Rahmani, R.; Baell, J. B.; Sexton, P. M.; Christopoulos, A.; Shaw, D. E., Structural basis for modulation of a G-protein-coupled receptor by allosteric drugs. *Nature* **2013,** *503* (7475), 295-9.

136. Manglik, A.; Lin, H.; Aryal, D. K.; McCorvy, J. D.; Dengler, D.; Corder, G.; Levit, A.; Kling, R. C.; Bernat, V.; Hubner, H.; Huang, X. P.; Sassano, M. F.; Giguere, P. M.; Lober, S.; Da, D.; Scherrer, G.; Kobilka, B. K.; Gmeiner, P.; Roth, B. L.; Shoichet, B. K., Structure-based discovery of opioid analgesics with reduced side effects. *Nature* **2016,** *537* (7619), 185-190.

137. McCorvy, J. D.; Butler, K. V.; Kelly, B.; Rechsteiner, K.; Karpiak, J.; Betz, R. M.; Kormos, B. L.; Shoichet, B. K.; Dror, R. O.; Jin, J.; Roth, B. L., Structure-inspired design of beta-arrestin-biased ligands for aminergic GPCRs. *Nat Chem Biol* **2018,** *14* (2), 126-134.

138. Khandogin J., a. B. C. L., Linking folding with aggregation in Alzheimer's beta-amyloid peptides. *Pro. Natl. Acad. Sci. USA* **2007,** *104*, 16880-16885.

139. Wu, C.; Shea, J. E., Structural similarities and differences between amyloidogenic and non-amyloidogenic islet amyloid polypeptide (IAPP) sequences and implications for the dual physiological and pathological activities of these peptides. *PLoS Comput Biol* **2013,** *9* (8), e1003211.

140. González, M. A., Force fields and molecular dynamics simulations. *École thématique de la Société Française de la Neutronique* **2011,** *12*, 169-200.

141. Stephen C. Hoops Kenneth W. Anderson and Kenneth M. Merz, J., Force Field Design for Metalloproteins. *J. Am. Chem. Soc.* **1991,** *113*, 8262-8270.

142. Lindorff-Larsen, K.; Maragakis, P.; Piana, S.; Eastwood, M. P.; Dror, R. O.; Shaw, D. E., Systematic validation of protein force fields against experimental data. *PLoS One* **2012,** *7* (2), e32131.

143. Lindorff-Larsen K., P. S., Dror R. O., Shaw D. E., How Fast-Folding Proteins Fold. *Science 2011*, *334*.

144. Dror, R. O.; Arlow, D. H.; Maragakis, P.; Mildorf, T. J.; Pan, A. C.; Xu, H.; Borhani, D. W.; Shaw, D. E., Activation mechanism of the beta2-adrenergic receptor. *Proc Natl Acad Sci U S A* **2011,** *108* (46), 18684-9.

145. Hertig, S.; Latorraca, N. R.; Dror, R. O., Revealing Atomic-Level Mechanisms of Protein Allostery with Molecular Dynamics Simulations. *PLoS Comput Biol* **2016,** *12* (6), e1004746.

146. Dedmon M.M., L.-L. K., Christodoulou J., Vendruscolo M., and Dobson C. M., Mapping Long-Range Interactions in α-Synuclein using Spin-Label NMR and Ensemble Molecular Dynamics Simulations. *J. Am. Chem. Soc.* **2005,** *127*, 476-477.

147. K., N. H. D. a. H. C., Molecular dynamics simulations of spontaneous fibril formation by random-coil peptides. *Pro. Natl. Acad. Sci. USA.* **2004,** *101*, 16180–16185.

CHAPTER 2: Analysis of Inhibition of SARS-Cov-19 Spike Protein Binding to ACE2 Receptor using ACE2-Derived Peptides by Surface Plasmon Resonance Spectroscopy

ABSTRACT

The Novel coronavirus SARS-CoV-2 entry into host cells is mediated by its spike protein (S glycoprotein), and the angiotensin-converting enzyme 2 (ACE2) has been identified as an essential cellular receptor. As such, one strategy to avoid the virus infection is to design peptides based upon extracting the human ACE2 peptidase domain α 1 helix, which would bind to the coronavirus surface protein, preventing viral entry into host cells. Here, we employed a competition assay using SPR to investigate two peptide inhibitors of increasing sequence length based on the α 1 helix of ACE2 PD, respectively [30-42] and [22-44] peptides. Moreover, we identified the critical amino acid residues of the RBD/ACE2 derived peptide using molecular docking, PatchDock. Both peptides were found to block most of the RBD residues that are known to bind to the original ACE2 PD. In addition, they inhibited spike mediated infection with comparable efficiency which may highlight that the addition of extra amino acid residues does not necessarily provide an increase in binding efficiency or inhibition of the peptide toward the spike protein. In fact, the shorter peptide was found to reach maximal inhibition at lower concentrations than the longer peptide

INTRODUCTION

The outbreak of coronavirus disease 2019 (COVID-19) caused by severe acute respiratory syndrome coronavirus 2 (SARS-CoV-2) has infected over 97.4 million individuals worldwide, resulting in more than 2.1 million deaths as reported by World Health Organization (WHO) on January 24th of 2021. Sadly, seven months later on August 11th the WHO reported more that 203 million confirmed cases including around 4 million deaths globally, with no end in sight. COVID19 symptoms are highly variable, although the most commonly reported include fever, cough, fatigue, breathing difficulties, and loss of smell and taste.[1] Once the illness worsens, acute respiratory distress syndrome (ARDS), respiratory failure, sepsis and acute kidney injury are common lethal complication.[2] SARS CoV-2 represents not only a significant challenge to human health globally but has also caused crises on social and economic networks.[3]

At the molecular level, SARS-CoV-2 infection is driven by a crucial interaction between the viral spike protein and the human ACE2 protein, whose normal function is to catalyze the hydrolysis of the vasoconstrictor peptide angiotensin II.[4, 5] hACE2 is mainly expressed on endothelial cells of several organs, particularly the cardiovascular system, renal tubular epithelium, and alveolar epithelial type II cells in the lungs.[6, 7] hACE2 is anchored to the cell membrane through a short, single pass transmembrane domain at the C-terminus. The full-length structure of ACE2 consists of two main domains: the protease domain (PD) at the N-terminus and the collectrin-like domain at the C-terminus.[8, 9]

SARS-CoV-2 consists of a 30 kb single-stranded RNA genome that is encapsulated by a lipid bilayer and three distinct structural proteins that are embedded within the lipid membrane: envelope (E), membrane (M), and spike (S).[10] The spike protein is a large (1208 residue), heavily glycosylated polypeptide that forms homotrimers which are what gives Coronavirus its "corona" structure in electron micrographs. Each monomer consists of two subunits (S1 and S2), where the key receptor-binding domain (RBD) corresponding to residues 319-541 falls within the S1 subunit.[11] In a demonstration of the high resolution capabilities of CryoEM technologies, the full length structure of the spike protein was determined to 2.8 Å within months of the global onset of COVID-19 (PDB 6VXX, 6VYB).[12] One of the most valuable insights to arise from these full-length structures was the occurrence of an "open" and "closed" configuration of the RBD relative to the rest of the protein, where only the "open" configuration is able to efficiently bind hACE2.[12, 13] This receptor binding induces the dissociation of the S1 with ACE2, prompting the S2 to transition from a metastable pre-fusion to a more stable post-fusion state that is essential for membrane fusion.[14-16] Therefore, binding to the ACE2 receptor is a critical initial step for SARS-CoV-2 to enter into target cells.

An important structure has also been determined by X-ray crystallography, most notably the SARS-CoV-2 spike protein RBD in complex with hACE2 (PDB-ID: 6M0J, 6LZG, and 6VW1).[17-19] Several ACE2 and s-protein residues have been identified as part of the ACE2/s-protein interaction by inspection of a crystal structure of the complex. Using the published crystal structure of the ACE2/s-protein RBD complex, amino acids at the ACE2 motifs and the viral s-protein RBD in the interface core were define. In the

recognition of RBD, the protease domain (PD) of ACE2 mainly engages the α1-helix (Ser19-Gln42), as initially depicted in a recent Nature publication by Lan et al.[19]

Revealing the key amino acid residues at the contact interface between the two proteins provides valuable structural information that can be leveraged for the development of disruptors specific for the SARS-CoV-2/ACE2 protein-protein interaction (PPI).[8, 20] Small-molecule inhibitors are often less effective at disrupting extended protein binding interfaces.[21] Peptides, on the other hand, offer a synthetically accessible solution to disrupt PPIs by binding at interface regions containing multiple contact "hot spots".[22]

Most neutralizing antibodies (nAbs) also aim to abrogate this interaction.[23, 24] CoV nAbs, primarily target the trimeric S glycoproteins, and the majority recognizes epitopes within the RBD that binds the ACE2 receptor.[24-26] However, RNA viruses accumulate mutations over time, which yields antibody resistance and requires the use of antibody cocktails to avoid mutational escape.[27] Not surprisingly, there is now evidence of the emergence of SARS-CoV-2 mutants for which antibodies against the original strain have no or diminished activity.[28] On the other hand, proteins or rigid peptides with specific (multivalent) binding domains could facilitate the development of COVID-19 treatment that are potentially independent of further viral S-protein mutation. Overall, peptide and protein therapies show a high specificity, small interference with biological processes, good tolerance to human organisms, and faster FDA approval times.[29]

Computational studies have been reported where the authors attempted to inhibit the SARS-CoV-2 s-protein interaction with small molecules and peptide-mimetic

inhibitors. One study [30] focused on 23 residues from the first N-terminal helix of ACE2. They used MD simulations and free energy calculations and showed that this 23-residue peptide, as well as a mutated variant, bound to the SARS-CoV2 s-protein RBD with high affinity. Another study [31] utilized similar MD-based methods in an in-silico study, and they report a putative minimum binding epitope from the ACE2 N-terminal helices. This smaller peptide motif had retained binding strength for the s-protein RBD. These two computational studies where the authors report ACE2 mimetic peptide inhibitors of s-protein binding could form the basis for the design of potential peptide-based SARS-CoV-2 therapeutics.

Human recombinant soluble ACE2 (hrsACE2) is currently being considered for treatment of COVID-19.[32, 33] However, ACE2 is involved in many key cellular processes, such as blood- pressure regulation and other cardiovascular functions. Therefore, hrsACE2 treatment could lead to dysregulation of those vital processes and subsequently cause deleterious side effects for treated patients. To avoid any interference of the ACE2 homeostasis, we wanted to test whether small ACE2-derived peptides can also interfere with SARS-CoV-2 binding, by blocking binding sites on the S glycoprotein.

To this end, we synthesized and tested short ACE2-derived peptides targeting the viral S glycoprotein as potent binding inhibitor peptides and observed a significant reduction in the binding properties. We accomplished this by utilizing label free approach surface plasmon resonance which provides highly sensitive detection capabilities. The first peptide (Glu22-Ser44) has been selected to mimic the regions of ACE2 that interact with the S1 subunit as determined by the crystal structure.[19] The second one is a truncate of the

first peptide (D30-Q42). Next, we performed a molecular docking using the PatchDock program aimed at gaining an in-depth understanding of the interaction between the SARS-Cov2 RBD and the ACE2-derived peptides.

EXPERIMENTAL

Materials

Recombinant SARS-CoV-2 spike protein, S1 subunit (Val16-Gln690) was purchased from RayBiotech. Human ACE2, His tag (E.coli) was obtained from MP Biomedicals, LLC. 11-mercaptoundecanoic acid (MUA). O-(2-Aminoethyl)-methylpoly-ethylene glycol (PEGamine), N-Hydroxysuccinimide (NHS) and 1-(3-dimethylaminopropyl)-3- ethylcarbodiimide hydrochloride (EDC) were purchased from Sigma-Aldrich (St. Louis, MO). All proteins solutions were prepared in 20 mM phosphate buffered saline (containing 150 mM NaCl, pH 7.4). Rink amide MBHA resin was obtained from Aapptec (Louisville, KY). Fmoc-protected amino acids were obtained from Anaspec (Fremont, CA). Piperidine was purchased from Alfa Aesar (Ward Hill, MA).2-(1H-benzotriazol-1-yl)-1,1,3,3-tetramethyluronium hexafluorophosphate (HBTU, 99.6%) and Diisopropylethylamine (DIEA, 99.5%) were purchased from Chem-Impex (Wood Dale, IL) and ACROS (Germany) respectively. Triisopropylsilane (TIPS) was obtained from TCI (Portland, OR). α-cyano-4-hydroxycinnamic acid (CHCA) was purchased from Sigma Aldrich (St. Louis, MO). Crystal structure of SARS-CoV-2 spike receptor-binding domain bound with ACE2 PD at 2.45 A° resolution with PDB ID: 6m0j was retrieved from RCSB PDB database (https://www.rcsb.org/)

Solid-phase peptide synthesis (SPPS) of linear peptide

CSBio CS336S peptide synthesizer (Menlo Park, CA) was used to synthesize the linear peptide sequences. An automated version of the traditional SPPS coupling process was used. 500 mg of Rink Amide resin with a loading capacity of 0.678 mmol/g was used for the synthesis. Fmoc protected L-amino acids (1 mmol each), DIEA (0.8 M in DMF) and HATU (0.4 M in DMF), 20% piperidine/DMF were prepared, to be utilized by the automated synthesizer. The Fmoc group on the resin was first removed by 20% piperidine/DMF solution. The process of Fmoc and amino acid were alternately followed with beads washed by DMF after each respective step of peptide synthesis.

Cleavage and purification

A solution of TFA, tri-isopropyl silane and water (95:2.5:2.5 by volume) was used as a cleavage cocktail solution to cleave off the peptides from the Rink Amide beads and simultaneously deprotect the peptide from the protecting groups associated with amino acid side chains. The peptides were purified using Reverse Phase-HPLC and analyzed using a MALDI-TOF analysis.

Reverse Phase-HPLC

Thermo Ultimate 3000BX HPLC, equipped with a preparative column (Kinetex 5 μm EVO, 250 Å~ 21.2 mm2) and a multiwavelength UV−vis detector the absorbance at 215, 280, 480, and 560 nm, was used for Reverse-Phase HPLC. 0−100% acetonitrile (with 0.1% TFA) in water (with 0.1% TFA) was maintained as the flow rate at 15 mL/min. The hit peptide was purified using this setup.

Mass spectrometry

A SCIEX 5800 mass spectrometer was used to identify the purified peptides using the MALDITOF technique. The peaks from the mass spectra were compared against the theoretical mass obtained from calculations, to validate the synthesis of the purified peptide

SPR analysis of ACE2-derived peptide inhibition of SARS-CoV-19 spike protein binding

A dual channel SPR spectrometer NanoSPR-321 (NanoSPR, Addison, IL) with a GaAs semiconductor laser light source (λ = 670 nm) was used for all SPR measurements. The device comes with a high-refractive index prism (n = 1.61) and 30 μL flow cell. SPR gold chips were fabricated with a 2 nm thick chromium adhesion layer, followed by deposition of a 46 nm thick gold layer via e-beam evaporation onto cleaned BK-7 glass slides based on previously published procedures.[34] .

Surface interactions were monitored using angular scanning mode which tracks the angle of minimum reflectivity. The gold substrate was incubated in 1 mM MUA ethanol solution for 18 h to form a self-assembled monolayer with carboxyl functional group on the surface. After extensive rinsing with copious ethanol and DI water, the chip was dried under an air stream. The gold substrate was then clamped to a flow cell on a prism. To activate the carboxyl acid group, EDC (0.4 M)/NHS (0.1 M) solution was injected into the flow cell and incubated for 30 min. After 10 min of rinsing, 0.5 μg/ml of spike protein in PBS was injected and incubated for 1 hr to allow formation of covalent amide linkages. Followed by a 10 min rinse to eliminate any residual spike protein in solution. Passivation

of the unused activated carboxyl groups was performed by incubation with 10 mg/ml PEGamine solution for 1 hr. Then the inhibition assay was performed.

Preparation of both receptor and peptide molecules

The human coronavirus spike protein structures and ACE2 structure were downloaded from the RCSB protein data bank. ACE2 structures were modified manually to produce the derived peptide structures. Depending on the peptide needed, the appropriate section of ACE2 was isolated so as to run future docking simulations. In addition, the binding domain on the spike protein was separated from the rest of the structure so as to specify the interactions between the binding domain and ACE2 derived peptides. The structures of the peptides and spike protein binding domain were verified after editing using PyMOL.

Molecular Docking

The MD between human coronavirus spike protein and each peptide understudy were performed using PatchDock web server. PatchDock is developed as geometry-based MD algorithm. It calculates the docking transformation between two molecules to get the best molecular interface complementarity. Which ascertains the peptide posture in relation to the receptor with maximal interface area coverage and minimal steric hindrance.[35] Each ACE2 derived peptide was docked with SARS-CoV-2 RBD by uploading the molecules to the Patchdock server, an automatic server for molecular docking. Clustering RMSD was chosen as 4.0 Å. Results were obtained through automatic server e-mail delivery and the docked complex structures were downloaded. PyMOL was used to analyze the docking

results of RBD/ACE2 derived peptide interaction by identifying the original binding residue between the RBD/ACE2 PD complex.

RESULT AND DISCUSSION

A Small Anti-ACE2 Peptides to Inhibit SARS-CoV-2 Infectivity

The FDA has recently approved three mRNA-based vaccines for COVID-19, but no therapeutics have been proven effective for the treatment of COVID-19.[36] However, a variety of therapeutic approaches are undergoing clinical trials, such as inhibition of RNA-dependent RNA polymerase, viral protease, and virus-cell membrane fusion, in addition to enhancing the immune system, and neutralizing inflammatory response.[37] Several therapeutic agents including remdesivir, favipiravir, and lopinavir-ritonavir have been tested for COVID-19 treatment. Although Remdesivir initially attracted the most attention as a therapeutic potential, a randomized and double-blind multicenter trial found that remdesivir use was not associated with statistically significant clinical benefits.[38] In a case study, favipiravir relieved the symptoms of COVID-19 patients with severe or critical condition patients.[39] A recent clinical trial found no benefit of the lopinavir-ritonavir treatment in severe COVID-19 patients beyond standard care[36]. Antimalarial drugs like chloroquine and hydroxychloroquine have also been tested as potential therapeutics for COVID-19. However, in a randomized clinical trial including more than 4700 patients hospitalized with COVID-19, hydroxychloroquine did not decrease the death incident compared to those who received usual care.[40]

Meanwhile, peptide therapeutics have shown popularity in recent years with 15 new peptide drugs being approved by the FDA in the last five years. Examples of peptide drugs include Scenesse (a 13-mer linear peptide) and Vyleesi (a 7-mer cyclic peptide) which were approved by the FDA in 2019.[41] Generally, peptides are highly selective, effective, and safe making for ideal therapeutics. Moreover, compared to small molecules that often cause side effects via toxic metabolites or nonspecific accumulation in the body, peptides can be metabolized into amino acids in the body and have a rare incidence of side effects.[21, 42]

The N-terminal region of the ACE2 PD is critical for binding to the SARS-CoV-2 spike protein

In order to design a small peptide-based inhibitor that can block the interaction of SARS-CoV-2 spike protein with the ACE2 receptor, we utilized the existing structures and known amino acid interactions necessary for binding of SARS-CoV-2 to ACE2 (Table 2.1). This includes the crystal structure of the ACE2 PD/RBD complex (PDB ID: 6m0j, 6vw1, and 6LZG) in addition to the full length of the ACE2 with SARS-CoV-2 complex (PDB ID: 6M17). Comparisons of the ACE2 interacting residues with SARS-CoV-2 spike protein according to the previous analysis of ACE2/RBD crystal structures[8, 17-19] are shown in Table 2.2. It is clear from the table that the α 1 helix (S19-S44) of ACE2 provides the most contact with the SARs-CoV-2 RBD as well as a small area on the α 2 helix, the short loop between α10/α11, and the linker between β3/β4. Therefore, selection of the peptide-based inhibitor was based on this insight and recent work published by Zhang et al.[43] They suggest that the 23-mer peptide mimics the α-1 helix as a possible drug against SARS-

CoV2 and its affinity to bind the viral RBD has also been demonstrated. The energies involved in the binding of the isolated peptide to the viral RBD is expected to be close to that of the RBD-ACE2 complex, thus raising the possibility of the peptide being competitively replaced by ACE2 in a practical setting.

	ID Structure	Paper Title	Experimental Method	Published Date	Resolution (A°)	Primary publication ref.
1	6M0J	Crystal structure of SARS-CoV-19 spike receptor-binding domain bound with ACE2	X-Ray diffraction	18/03/2020	2.45	19
2	6M17	The 2019-nCov RBD/ACE2-B0AT1 complex	Electron microscopy	11/03/2020	2.90	8
3	6VW1	Structure of SARS-CoV-2 chimeric receptor-binding domain complexed with its receptor human ACE2	X-Ray diffraction	04/03/2020	2.68	18
4	6LZG	Structure of novel coronavirus spike receptor-binding domain complexed with its receptor ACE2	X-Ray diffraction	18/03/2020	2.50	17

Table 2. 1 Crystal structure of ACE2/SARS-CoV-2 complex and the primary publication

Consequently, the [22-44] peptide (Glu22-Ser44, wheat ribbon in fig 2.1B) has been synthesized to mimic the α-1 helix and tested for its ability to interfere with SARS-CoV-2-spike protein/ACE2 binding. In addition, a smaller peptide that was obtained by removing the first 8 and last 2 histidine residues of the original [22-44] peptide leaving only a 13-residue peptide which was also synthesized and tested as an inhibitor of ACE2/S1 complex. This small peptide (Asp30-Gln42, pink ribbon in fig 2.1B) contains most of the key contact with the RBD and represents the central and C-terminal of the isolated α-1 helix of ACE2. We aim to investigate the effect of the peptide length on the blocking efficiency of the Spike protein.

α 1 helix of AEC2 interacting Residues with RBD																									
PDB	S19	T20	I21	E22	E23	Q24	A25	K26	T27	F28	L29	D30	K31	F32	N33	H34	E35	A36	E27	D38	L39	F40	Y41	Q42	S43	S44
6M0J						✓						✓					✓		✓	✓			✓	✓		
6M17						✓			✓			✓	✓			✓	✓		✓	✓			✓	✓		
6VW1	✓					✓			✓	✓			✓			✓	✓		✓	✓			✓	✓		✓
6LZG	✓					✓			✓	✓		✓	✓			✓	✓		✓	✓			✓	✓		✓

α 2,10,11 helix and loop (β3/β4) of AEC2 interacting Residues with RBD													
PDB	L79	A80	Q81	M82	Y83	Q325	E329	N330	K353	G354		D355	R357
6M0J									✓				
6M17				✓					✓	✓		✓	✓
6VW1	✓			✓	✓	✓	✓	✓	✓	✓		✓	✓
6LZG	✓			✓	✓	✓	✓	✓	✓	✓		✓	✓

Table 2. 2 Comparison of ACE2 interacting residues with SARS-CoV-2 spike protein. Upper table represents ACE2 amino acids provided by α 1 helix. Lower table represents ACE2 amino acids provided by α 2, the short loop between α10/α11, and the link between β3/β4

Evaluation of Blocking Efficiency Using Competition Surface Plasmon Resonance (SPR)

SPR is a classic technique to study the interaction of two different proteins. However, direct analysis of the interaction between small molecules, such as small peptides, and a protein by SPR is always difficult as a result of low signal change from small molecules.[44] We, therefore, utilized a competition assay to evaluate the binding of the peptide to the SARS-CoV-2- spike protein using SPR spectroscopy. Figure 2.1A provides a schematic of the competition assay. 50 μg/ml of SARS-CoV-2-spike protein was immobilized on a self-assembled monolayer with a carboxyl functional group on the gold chip surface. PBS (pH 7.4) was used as the running buffer. An SPR competitive assay was used to assess the ability of the ACE2-derived peptides to block the interaction between human ACE2 and SARS-CoV-2 spike protein. Peptides with different

concentrations were mixed with 30 µg/ml of human ACE2 protein and injected into the chip coated with SARSCoV-2-spike protein. Free human ACE2 solution (30 µg/ml) was injected as a control. To confirm the specificity of ACE2/spike protein interaction, we conducted an additional independent control experiment using -COOH terminated alkanethiol surface without the spike protein.

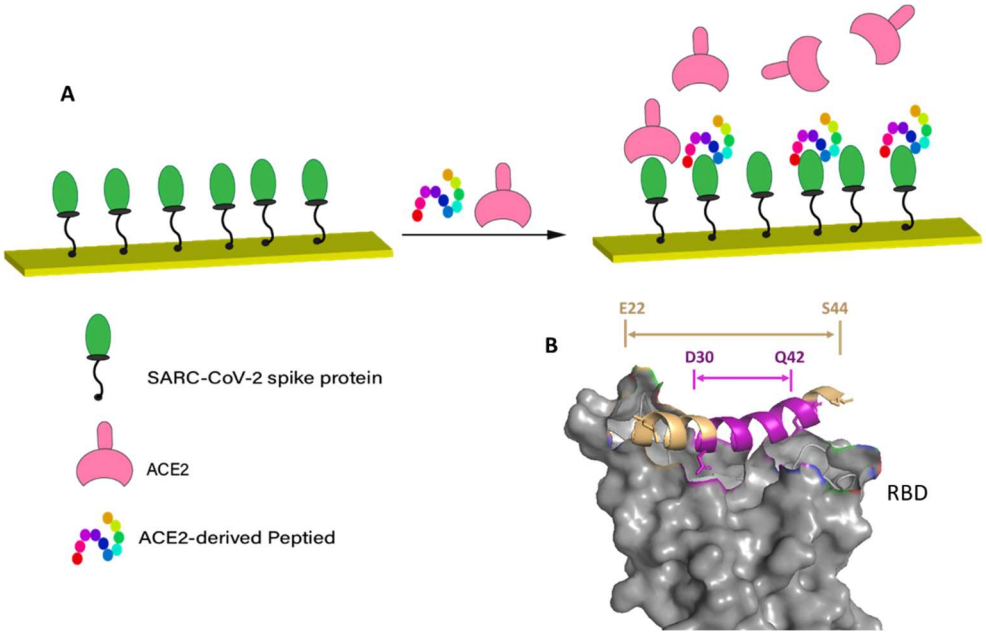

Figure 2. 1 (A) Represent the schematic of the competition assay. (B) Relative location of [30-42] peptide (pink) and [22-44] peptide (wheat and pink) corresponding to PDB ID: 6m0j

Fig (2.2A) shows the SPR binding response of ACE2/spike protein with no inhibition, ACE2/spike protein in presence of 0.1 µg/ml of each peptide, and the independent control which represents ACE2 binding to S1 surface free. The SPR binding shift observed during the independent control experiment is significantly lower, thereby confirming the specificity of the ACE2/spike protein complex under our experimental condition. Figure 2.2 B and D demonstrate that increasing the concentration of both

peptides decreases the binding signal of the ACE2 protein to SARS-CoV-2-spike protein coated on the chip, indicating a concentration dependent inhibition of the peptides to the spike protein.

To visually compare the binding signal between the S1 subunit and ACE2 in the absence of the peptide (0 μg/ml) with the signal after adding the peptides at different concentrations (0.1,1,10,100 μg/ml), we plot the SPR angle response versus the peptide's concentration (fig 2.2 C). We found that the ACE2/spike protein binding results in an angle shift of 0.147±0.009 degree. The [22-44] peptide shows maximum SPR angle inhibition of the ACE2/S1 complex formation with a measured reduction in SPR signal of 0.047±0.009 degree. Interestingly the small peptide, [30-42], shows similar maximum inhibition potential at (0.049°±0.027). This result suggests that both peptides are able to disrupt the ACE2/spike protein interaction. In addition, this could indicate that the central and C-terminal region of the isolated α-1 helix of ACE2 is the essential motif important for disrupting the ACE2/S1 interaction since both peptides show similar max inhibition effects.

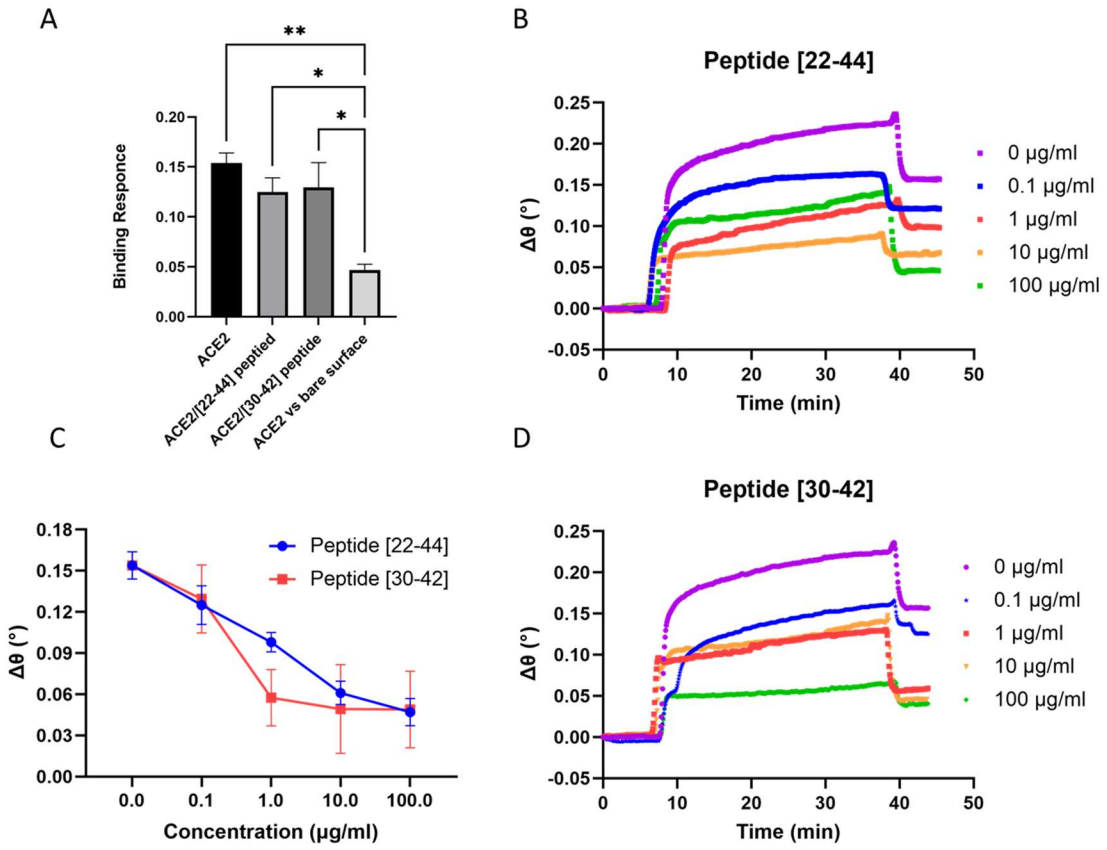

Figure 2. 2 Evaluation of blocking efficiency of the ACE2-derived peptide to spike protein using competition SPR. A) Specific binding measured between the Spike protein on the surface with ACE2. B) SPR sensogram with [22-44] peptide. C) Graph showing the reduction of SPR binding signal. D) SPR sensogram with [30-42] peptide.

Based on the crystal structure of SARS-CoV-2 spike protein and ACE2 receptor (PDB ID: 6m0j) solved by Lan et al. [19] the polar residues [24,30,35,37,38,41,42] of ACE2 helix-1 are the key interfacial interactions and are able to form a network of hydrogen bonds with the SARS-CoV-2 spike protein. Accordingly, we can exhibit 6 critical amino acids that are part of both peptides under our study (at the central and C-terminal region). While [22-44] peptide has only one extra critical residue at the N-terminal region of the peptide. Moreover, it has been highlighted in the modeling study of RBD/ACE2 that the

residues 37, 38, 41, and 42 are the key interfacial interactions between ACE2 and the RBD/spike protein.[45] Taken together, these structural insights and MD study lend support to our result of [22-44] and [30-42] as peptide disruptors of the ACE2/S1 interaction and that the central and C-terminal of the isolated α-1 helix of ACE2 contain more critical residue compared to N-terminal of the isolated α 1 helix of ACE2 PD.

When examining figures 2.2 B, C, D in more detail, it was found that the [30-42] peptide reached higher blocking efficiency and achieved saturation of the spike protein at lower concentration compared to the [22-44] peptide. In the case of the [30-42] peptide, a 0.057°±0.02 reduction of SPR signal was observed at 1 μg/ml. At the same concentration, the [22-44] peptide shows only 0.098°±0.007 reduction of the SPR signal. In addition, at 10 μg/ml the [30-42] peptide shows maximum neutralization to the spike protein. On the other hand, the [22-44] peptide indicates similar maximum neutralization, however at a higher concentration (100 μg/ml). This is possibly attributed to the presence of two consecutive serine residues in the [22-44] peptide, which could affect its flexibility. As it has been shown that presence of two consecutive serine residues affect the [37-45] peptide binding affinity to spike protein.[46]

Next, we determine the half-maximal inhibitory concentration (IC50) of each peptide. Figures 2.3A and 2.3B show that the [22-44] and [30-42] peptides blocked the SARS-CoV-2 spike protein/ACE2 interaction with an IC50 value of 2.00 and 0.65 μg/ml respectively. This implies that the two peptides exhibit strong affinity to the spike protein although the [22-44] peptide has extra amino acid residues. Related to the novel coronavirus, it was suggested by Yang et al.[47] that the additional amino acids do not

influence the overall affinity of the peptide for SARS-CoV-2 S1 subunit. Their experimental study used two peptides [22-44] and [22-57] which showed similar inhibition potential of the ACE2/spike complex. This was also supported by their MD simulation which showed the [22-57] peptide established fewer hydrogen bonds when compared to that of the shorter one, [22-44] peptide. Moreover, it was reported that the residues 21-43 of the same human ACE2 α 1-helix (similar to [22-44] peptide understudy) can strongly bind to SARS-CoV-2 RBD with micromolar affinity (KD= 1.3μM)[13] that is comparable to the full length ACE2 binding to RBD[20].

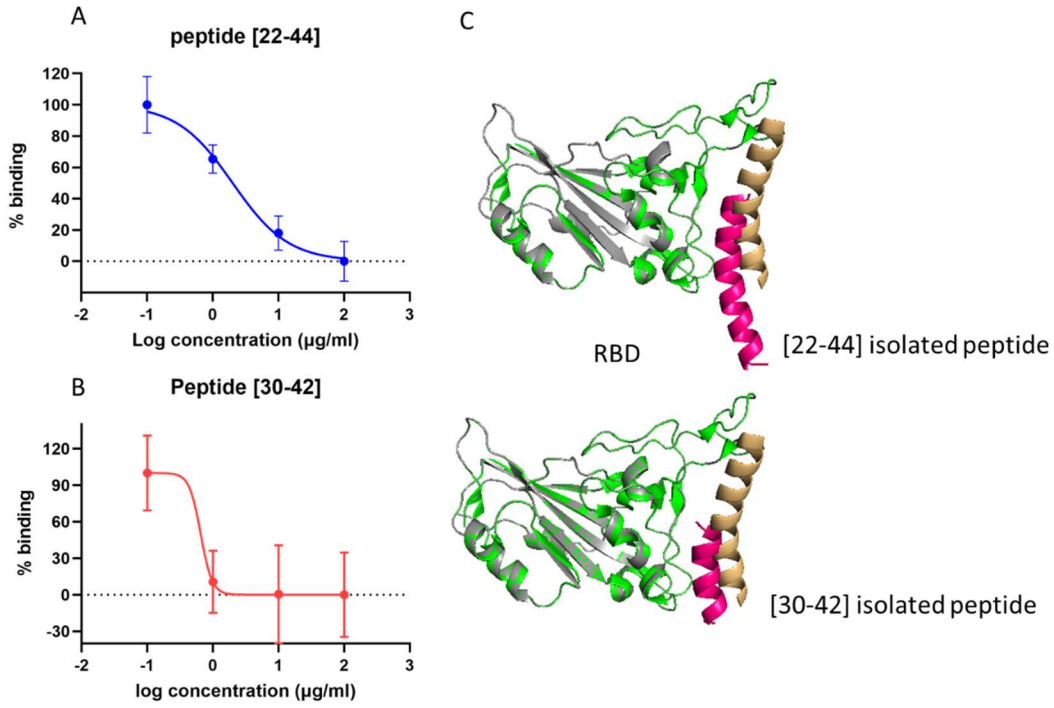

Figure 2. 3 A, B) Doses dependent blocking of the spike protein using [22-44] peptide and [30-42] respectively. C) structural alignment of both the docked result of the peptide/RBD complex and the α 1 helix/RBD complex which were constructed from the ACE2/RBD complex (PDB ID 6m0j).

Molecular Docking of ACE2 derived peptide/RBD interaction

In order to evaluate and compare the two peptides as inhibitors of ACE2/S1 complex, we combined molecular docking with the experimental study. Molecular docking was performed through the PatchDock server to study the binding efficiency and to identify the important amino acid residues that contribute to the binding of the RBD/ACE2 derived peptide complex.

We evaluated the binding structure of the 23 and 13-amino acid chain, [22-44] and [30-42] peptide respectively, alone and without the remainder of the ACE2 PD domain to the SARS-CoV-2 spike protein. To perform a non-biased analysis, we performed a blind docking run whereby we did not specify the binding site during the docking simulations. The obtained results were analyzed by comparing the docked conformations of each peptide within the SARS-CoV-2 spike protein. A contact was defined to exist between a peptide residue and the RBD if any atom of the RBD fell within 3 A° of any atom belonging to the peptide residue.

At the same time, we retrieved the crystal structure of the SARS-CoV-2 spike protein with the ACE2 PD domain (PDB ID: 6M0j) and explored it as the basis of the current study. The interface residues between the SARS-CoV-2 spike protein and the ACE2 PD domain were visualized and interpreted using Pymol software. After a detailed analysis of interface residues, the α 1 helix, which is cradled in a concave groove formed by β5 and β6 sheets of the RBD, provides the majority of the interaction between ACE2/RBD interface (fig.4). Specifically, 8 residues (N487, K417, Q493, Y505, Y449,

T500, N501, G446) in RBD provide contact via hydrogen bond with ACE2 (fig. 2.4A and 2.4B).

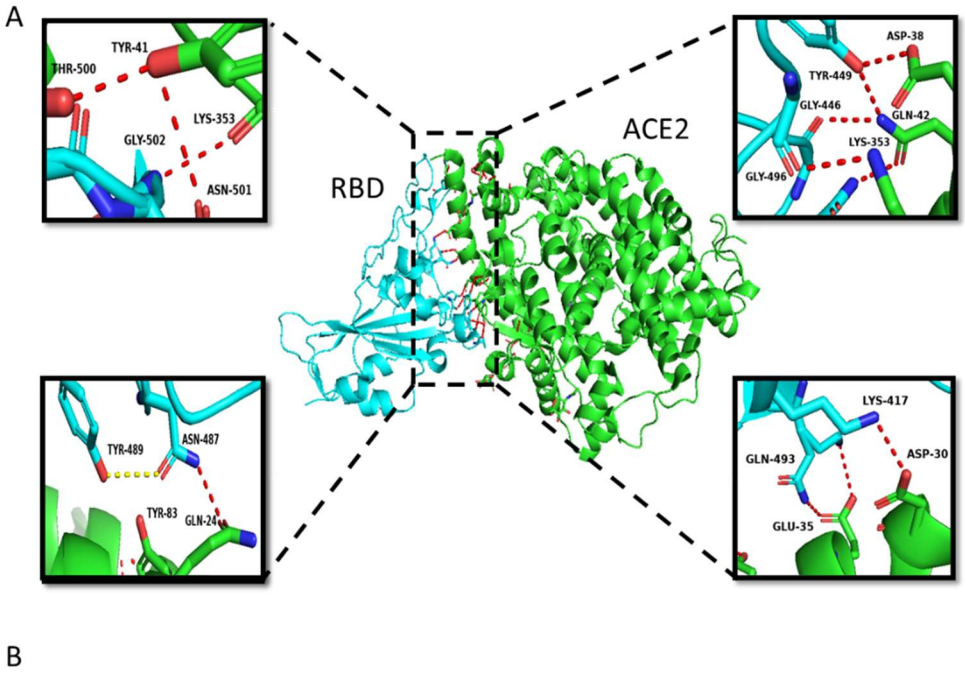

Interaction residues within 3A° region	
SARS-CoV-2 Spike RBD	Human ACE2
K417, G446, Y449, N487, Y489, Q493, T500, N501, and N502	Q24, D30, E35, E37, D38, Y41, Q42, Y83, K353, and R393

Figure 2. 4 Illustration of the interacting interface of the SARS-CoV-2 receptor-binding domain (RBD) (cyan) and hACE2 (green) from PDB-ID: 6M0J. The key interacting residues shown close up as insets. The table shows the interacting residues within a 3A° region that was analyzed using the PyMOL tool

Figure. 2.3C shows the structural alignment of both the docked result of the peptide/RBD complex and the α 1 helix/RBD complex which were constructed from the ACE2/RBD complex (PDB ID 6m0j). It is clear from the docking result that the [30-42]

peptide binds to the concave groove of the RBD that the original ACE2 PD domain also binds. The [22-44] peptide laid on the RBD groove as well; however, only the central and the C-terminus of the peptide show binding. This result aligns very well with the experimental results that the two peptides independently have the potential to inhibit the interaction of the SARS-CoV-2 spike protein and ACE2 complex.

By analyzing the docking results, the critical interacting amino acids of RBD/ACE2 were identified. Examination of the figure 2.5A and 2.5B present that the RBD residues (449, 496, 493,494 500, 502, 505) were blocked by the [30-42] peptide. Similarly, the 35, 37, 38, 41, residues of the [22-44] peptide have the ability to occupy the RBD residues 449, 498, 496, 494,493, 502 by making 6 Hydrogen bonds within 3°A. It is clear that most of the RBD interacting amino acidic residues, as defined by PatchDock analysis, were found to be those within prominent binding sites as predicted by analyzing the Crystal structure of the ACE2/RBD complex (fig. 2.4A and 2.4B). The docking position of the two peptides in the RBD pocket ensured a high possibility to block the interaction with the ACE2 receptor which is in alignment with current experimental study (fig. 2.2).

In addition, inspection of the binding between each peptide and the RBD shows that fewer hydrogen bonds formed between the RBD/ peptide [22-44] complex compared with the RBD/peptide [30-42] complex which make 8 hydrogen bonds. This result is in line with our experimental results in which the [30-42] peptide shows higher inhibition of the ACE2/spike protein interaction for 0.1 to 1 μg/ml concentrations (fig. 2.2C) compared

to the [22-44] peptide. It may be recalled that this result is in synergy with another study which suggests that addition of extra amino acids do not necessarily increase the hydrogen bond or the binding efficiency of the peptide toward the spike protein.[47]

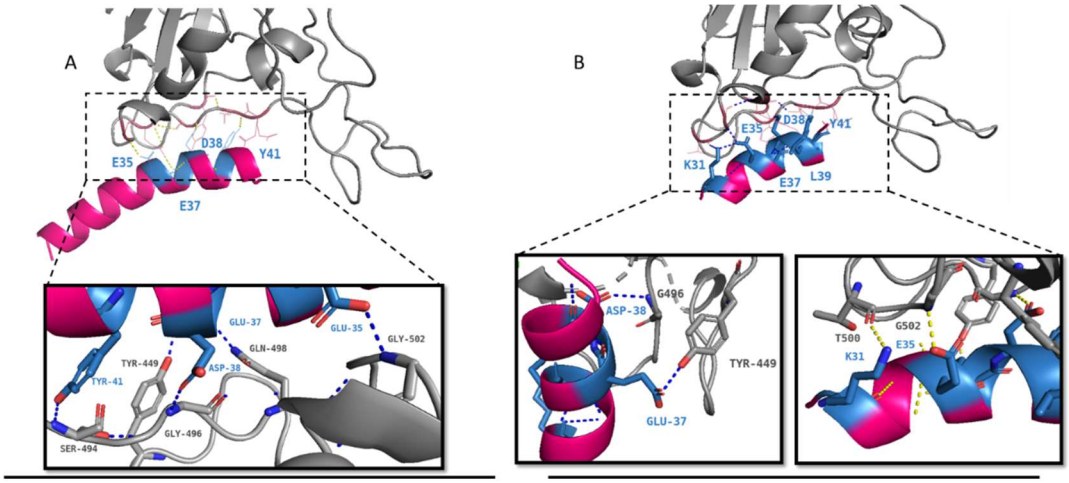

Interaction residues within 3A° region	
SARS-CoV-2 Spike RBD	[22-44] Peptide
Y449, Q493, S494, G496, Q498, and N502	E37, D38, Y41, Y41, and Q42

Interaction residues within 3A° region	
SARS-CoV-2 Spike RBD	[30-42] Peptide
Y449, Y453, Q493, S494, T500, N502, and Y505	K31, E35, E37, D38, L39, Y41, and Q42

Figure 2. 5 Interaction of the A) [22-44] peptide B) [30-42] peptide (pink) with the SARS-CoV-2 receptor-binding domain (RBD) (gray). Molecular docking complex obtained with PachDock.The key interacting residues shown close up as insets. The table shows the interacting residues within a 3A° region that was analyzed using the PyMOL tool.

CONCLUSION

In this manuscript, two peptides were investigated as inhibitors of the ACE/SARS-CoV-2 spike protein using a competition assay. The two inhibitors of different sequence length based on the α 1 helix of ACE2 PD show similar blocking efficiency with the shorter peptide reaching maximal blocking efficiency at a lower concentration. This demonstrates the feasibility of targeting ACE2/spike protein interaction interface with peptide-based inhibitors to inhibit virus infection. We observed a progressive reduction of the SPR

binding signal as a function of the concentration confirming specific inhibition. The [30-42] peptide which is a truncate of the longer peptide, highlights the importance of the amino acid residues at the central and C-terminus of the isolated α 1 helix of ACE2 for interaction with the spike protein. Moreover, we identified the critical residues of the RBD/ACE2 derived peptide interface using molecular docking, PachDock. Analyzing the docking results revealed that the peptide inhibitors block most of the RBD residues that bind with ACE2 as predicted by analyzing the crystal structure of the ACE2/RBD complex. The results of our molecular docking and experimental inhibition assay are in alignment indicating that small inhibitory peptide can be utilized to inhibit the ACE/SARS-CoV-2 spike protein complex. This may be developed as an anti-SARS-CoV-2 treatment of the viral infection without the adverse side effects that exist for many other small molecule or recombinant protein therapeutic avenues.

REFERENCES

1. Giorli, A.; Ferretti, F.; Biagini, C.; Salerni, L.; Bindi, I.; Dasgupta, S.; Pozza, A.; Gualtieri, G.; Gusinu, R.; Coluccia, A.; Mandala, M., A Literature Systematic Review with Meta-Analysis of Symptoms Prevalence in Covid-19: the Relevance of Olfactory Symptoms in Infection Not Requiring Hospitalization. *Curr Treat Options Neurol* **2020,** *22* (10), 36.

2. Chen, T.; Wu, D.; Chen, H.; Yan, W.; Yang, D.; Chen, G.; Ma, K.; Xu, D.; Yu, H.; Wang, H.; Wang, T.; Guo, W.; Chen, J.; Ding, C.; Zhang, X.; Huang, J.; Han, M.; Li, S.; Luo, X.; Zhao, J.; Ning, Q., Clinical characteristics of 113 deceased patients with coronavirus disease 2019: retrospective study. *BMJ* **2020,** *368*, m1091.

3. Nicola, M.; Alsafi, Z.; Sohrabi, C.; Kerwan, A.; Al-Jabir, A.; Iosifidis, C.; Agha, M.; Agha, R., The socio-economic implications of the coronavirus pandemic (COVID-19): A review. *Int J Surg* **2020,** *78*, 185-193.

4. Li, W. H.; Moore, M. J.; Vasilieva, N.; Sui, J. H.; Wong, S. K.; Berne, M. A.; Somasundaran, M.; Sullivan, J. L.; Luzuriaga, K.; Greenough, T. C.; Choe, H.; Farzan, M., Angiotensin-converting enzyme 2 is a functional receptor for the SARS coronavirus. *Nature* **2003,** *426* (6965), 450-454.

5. Li, W.; Zhang, C.; Sui, J.; Kuhn, J. H.; Moore, M. J.; Luo, S.; Wong, S. K.; Huang, I. C.; Xu, K.; Vasilieva, N.; Murakami, A.; He, Y.; Marasco, W. A.; Guan, Y.; Choe, H.; Farzan, M., Receptor and viral determinants of SARS-coronavirus adaptation to human ACE2. *EMBO J* **2005,** *24* (8), 1634-43.

6. Zipeto, D.; Palmeira, J. D. F.; Arganaraz, G. A.; Arganaraz, E. R., ACE2/ADAM17/TMPRSS2 Interplay May Be the Main Risk Factor for COVID-19. *Front Immunol* **2020,** *11*, 576745.

7. Zhao, Y.; Zhao, Z.; Wang, Y.; Zhou, Y.; Ma, Y.; Zuo, W., Single-Cell RNA Expression Profiling of ACE2, the Receptor of SARS-CoV-2. *Am J Respir Crit Care Med* **2020,** *202* (5), 756-759.

8. Renhong Yan, Y. Z., Yaning Li, Lu Xia, Yingying Guo, Qiang Zhou, Structural basis for the recognition of SARS-CoV-2 by full-length human ACE2. *Science* **2020,** *367*, 1444-1448.

9. Towler, P.; Staker, B.; Prasad, S. G.; Menon, S.; Tang, J.; Parsons, T.; Ryan, D.; Fisher, M.; Williams, D.; Dales, N. A.; Patane, M. A.; Pantoliano, M. W., ACE2 X-ray structures reveal a large hinge-bending motion important for inhibitor binding and catalysis. *J Biol Chem* **2004,** *279* (17), 17996-8007.

10. Chen, N.; Zhou, M.; Dong, X.; Qu, J.; Gong, F.; Han, Y.; Qiu, Y.; Wang, J.; Liu, Y.; Wei, Y.; Xia, J. a.; Yu, T.; Zhang, X.; Zhang, L., Epidemiological and clinical characteristics of 99 cases of 2019 novel coronavirus pneumonia in Wuhan, China: a descriptive study. *The Lancet* **2020,** *395* (10223), 507-513.

11. Ke, Z.; Oton, J.; Qu, K.; Cortese, M.; Zila, V.; McKeane, L.; Nakane, T.; Zivanov, J.; Neufeldt, C. J.; Cerikan, B.; Lu, J. M.; Peukes, J.; Xiong, X.; Krausslich, H. G.; Scheres, S. H. W.; Bartenschlager, R.; Briggs, J. A. G., Structures and distributions of SARS-CoV-2 spike proteins on intact virions. *Nature* **2020,** *588* (7838), 498-502.

12. Walls, A. C.; Park, Y. J.; Tortorici, M. A.; Wall, A.; McGuire, A. T.; Veesler, D., Structure, Function, and Antigenicity of the SARS-CoV-2 Spike Glycoprotein. *Cell* **2020,** *181* (2), 281-292 e6.

13. Xiong, X.; Qu, K.; Ciazynska, K. A.; Hosmillo, M.; Carter, A. P.; Ebrahimi, S.; Ke, Z.; Scheres, S. H. W.; Bergamaschi, L.; Grice, G. L.; Zhang, Y.; Collaboration, C.-N. C.-B.; Nathan, J. A.; Baker, S.; James, L. C.; Baxendale, H. E.; Goodfellow, I.; Doffinger, R.; Briggs, J. A. G., A thermostable, closed SARS-CoV-2 spike protein trimer. *Nat Struct Mol Biol* **2020,** *27* (10), 934-941.

14. Gui, M.; Song, W.; Zhou, H.; Xu, J.; Chen, S.; Xiang, Y.; Wang, X., Cryo-electron microscopy structures of the SARS-CoV spike glycoprotein reveal a prerequisite conformational state for receptor binding. *Cell Res* **2017,** *27* (1), 119-129.

15. Song, W.; Gui, M.; Wang, X.; Xiang, Y., Cryo-EM structure of the SARS coronavirus spike glycoprotein in complex with its host cell receptor ACE2. *PLoS Pathog* **2018,** *14* (8), e1007236.

16. Kirchdoerfer, R. N.; Wang, N.; Pallesen, J.; Wrapp, D.; Turner, H. L.; Cottrell, C. A.; Corbett, K. S.; Graham, B. S.; McLellan, J. S.; Ward, A. B., Stabilized coronavirus spikes are resistant to conformational changes induced by receptor recognition or proteolysis. *Sci Rep* **2018,** *8* (1), 15701.

17. Wang, Q.; Zhang, Y.; Wu, L.; Niu, S.; Song, C.; Zhang, Z.; Lu, G.; Qiao, C.; Hu, Y.; Yuen, K. Y.; Wang, Q.; Zhou, H.; Yan, J.; Qi, J., Structural and Functional Basis of SARS-CoV-2 Entry by Using Human ACE2. *Cell* **2020,** *181* (4), 894-904 e9.

18. Shang, J.; Ye, G.; Shi, K.; Wan, Y.; Luo, C.; Aihara, H.; Geng, Q.; Auerbach, A.; Li, F., Structural basis of receptor recognition by SARS-CoV-2. *Nature* **2020,** *581* (7807), 221-224.

19. Lan, J.; Ge, J.; Yu, J.; Shan, S.; Zhou, H.; Fan, S.; Zhang, Q.; Shi, X.; Wang, Q.; Zhang, L.; Wang, X., Structure of the SARS-CoV-2 spike receptor-binding domain bound to the ACE2 receptor. *Nature* **2020,** *581* (7807), 215-220.

20. Daniel Wrapp, N. W., Kizzmekia S. Corbett, Jory A. Goldsmith, Ching-Lin Hsieh, Olubukola Abiona, Barney S. Graham, Jason S. McLellan, Cryo-EM structure of the 2019-nCoV spike in the prefusion conformation. *Science* **2020,** *367*, 1260-1263.

21. Smith, M. C.; Gestwicki, J. E., Features of protein-protein interactions that translate into potent inhibitors: topology, surface area and affinity. *Expert Rev Mol Med* **2012,** *14*, e16.

22. Josephson, K.; Ricardo, A.; Szostak, J. W., mRNA display: from basic principles to macrocycle drug discovery. *Drug Discov Today* **2014,** *19* (4), 388-99.

23. Tai, W.; He, L.; Zhang, X.; Pu, J.; Voronin, D.; Jiang, S.; Zhou, Y.; Du, L., Characterization of the receptor-binding domain (RBD) of 2019 novel coronavirus: implication for development of RBD protein as a viral attachment inhibitor and vaccine. *Cell Mol Immunol* **2020,** *17* (6), 613-620.

24. Zhe Lv, Y.-Q. D., Qing Ye, Lei Cao, Chun-Yun Sun, Changfa Fan, Weijin Huang, Shihui Sun, Yao Sun, Ling Zhu, Qi Chen, Nan Wang, Jianhui Nie, Zhen Cui, Dandan Zhu, Neil Shaw, Xiao-Feng Li, Qianqian Li, Liangzhi Xie, Youchun Wang, Zihe Rao, Cheng-Feng Qin, Xiangxi Wang, Structural basis for neutralization of SARS-CoV-2 and SARS-CoV by a potent therapeutic antibody. *Science* **2020,** *369*, 1505-1509.

25. Sui, J.; Deming, M.; Rockx, B.; Liddington, R. C.; Zhu, Q. K.; Baric, R. S.; Marasco, W. A., Effects of human anti-spike protein receptor binding domain

antibodies on severe acute respiratory syndrome coronavirus neutralization escape and fitness. *J Virol* **2014,** *88* (23), 13769-80.

26. Wang, C.; Li, W.; Drabek, D.; Okba, N. M. A.; van Haperen, R.; Osterhaus, A.; van Kuppeveld, F. J. M.; Haagmans, B. L.; Grosveld, F.; Bosch, B. J., A human monoclonal antibody blocking SARS-CoV-2 infection. *Nat Commun* **2020,** *11* (1), 2251.

27. Alina Baum, B. O. F., Elzbieta Wloga, Richard Copin, Kristen E. Pascal, Vincenzo Russo, Stephanie Giordano, Kathryn Lanza, Nicole Negron, Min Ni, Yi Wei, Gurinder S. Atwal, Andrew J. Murphy, Neil Stahl, George D. Yancopoulos, Christos A. Kyratsous, Antibody cocktail to SARS-CoV-2 spike protein prevents rapid mutational escape seen with individual antibodies. *Science* **2020,** *369*, 1014–1018

28. Wibmer, C. K.; Ayres, F.; Hermanus, T.; Madzivhandila, M.; Kgagudi, P.; Oosthuysen, B.; Lambson, B. E.; de Oliveira, T.; Vermeulen, M.; van der Berg, K.; Rossouw, T.; Boswell, M.; Ueckermann, V.; Meiring, S.; von Gottberg, A.; Cohen, C.; Morris, L.; Bhiman, J. N.; Moore, P. L., SARS-CoV-2 501Y.V2 escapes neutralization by South African COVID-19 donor plasma. *Nat Med* **2021,** *27* (4), 622-625.

29. Benjamin Leader, Q. J. B. a. D. E. G., Protein therapeutics: a summary and pharmacological classification. *Naturere reviews | drug discovery* **2008,** *7*, 21-39.

30. Saurabh, S.; Purohit, S. S., A Modified ACE2 peptide mimic to block SARS-CoV2 entry. *bioRxiv* **2020**.

31. Renzi, F.; Ghersi, D., ACE2 fragment as a decoy for novel SARS-Cov-2 virus. *bioRxiv* **2020**, 1-6.

32. Zhang, H.; Penninger, J. M.; Li, Y.; Zhong, N.; Slutsky, A. S., Angiotensin-converting enzyme 2 (ACE2) as a SARS-CoV-2 receptor: molecular mechanisms and potential therapeutic target. *Intensive Care Med* **2020,** *46* (4), 586-590.

33. Monteil, V.; Kwon, H.; Prado, P.; Hagelkruys, A.; Wimmer, R. A.; Stahl, M.; Leopoldi, A.; Garreta, E.; Hurtado Del Pozo, C.; Prosper, F.; Romero, J. P.; Wirnsberger, G.; Zhang, H.; Slutsky, A. S.; Conder, R.; Montserrat, N.; Mirazimi, A.; Penninger, J. M., Inhibition of SARS-CoV-2 Infections in Engineered Human

Tissues Using Clinical-Grade Soluble Human ACE2. *Cell* **2020,** *181* (4), 905-913 e7.

34. Hinman, S. S.; Ruiz, C. J.; Drakakaki, G.; Wilkop, T. E.; Cheng, Q., On-Demand Formation of Supported Lipid Membrane Arrays by Trehalose-Assisted Vesicle Delivery for SPR Imaging. *ACS Appl Mater Interfaces* **2015,** *7* (31), 17122-30.

35. Schneidman-Duhovny, D.; Inbar, Y.; Nussinov, R.; Wolfson, H. J., PatchDock and SymmDock: servers for rigid and symmetric docking. *Nucleic Acids Res* **2005,** *33* (Web Server issue), W363-7.

36. Cao, B. et al. Trial of Lopinavir-Ritonavir in Adults Hospitalized with Severe Covid-19. *N Engl J Med* **2020,** *382* (19), 1787-1799.

37. Tu, Y. F.; Chien, C. S.; Yarmishyn, A. A.; Lin, Y. Y.; Luo, Y. H.; Lin, Y. T.; Lai, W. Y.; Yang, D. M.; Chou, S. J.; Yang, Y. P.; Wang, M. L.; Chiou, S. H., A Review of SARS-CoV-2 and the Ongoing Clinical Trials. *Int J Mol Sci* **2020,** *21* (7).

38. Wang, Y. et al., Remdesivir in adults with severe COVID-19: a randomised, double-blind, placebo-controlled, multicentre trial. *The Lancet* **2020,** *395* (10236), 1569-1578.

39. Takahashi, H.; Iwasaki, Y.; Watanabe, T.; Ichinose, N.; Okada, Y.; Oiwa, A.; Kobayashi, T.; Moriya, M.; Oda, T., Case studies of SARS-CoV-2 treated with favipiravir among patients in critical or severe condition. *Int J Infect Dis* **2020,** *100*, 283-285.

40. Group, R. C. et al. Effect of Hydroxychloroquine in Hospitalized Patients with Covid-19. *N Engl J Med* **2020,** *383* (21), 2030-2040.

41. de la Torre, B. G.; Albericio, F., The Pharmaceutical Industry in 2019. An Analysis of FDA Drug Approvals from the Perspective of Molecules. *Molecules* **2020,** *25* (3).

42. Ahrens VM, B.-S. K., Beck-Sickinger AG (12):. doi: 10.4155/fmc.12.76. PMID: 22917246., Peptides and peptide conjugates: therapeutics on the upward path. *Future Med Chem* **2012,** *4* (12).

43. Zhang, G.; Pomplun, S.; Loftis, A. R.; Tan, X.; Loas, A.; Pentelute, B. L., Investigation of ACE2 N-terminal fragments binding to SARS-CoV-2 Spike RBD *bioRxiv* **2020**.

44. Schuck, P.; Zhao, H., The role of mass transport limitation and surface heterogeneity in the biophysical characterization of macromolecular binding processes by SPR biosensing. *Methods Mol Biol* **2010,** *627*, 15-54.

45. Wang, Y.; Liu, M.; Gao, J., Enhanced receptor binding of SARS-CoV-2 through networks of hydrogen-bonding and hydrophobic interactions. *Proc Natl Acad Sci U S A* **2020,** *117* (25), 13967-13974.

46. Larue, R. C.; Xing, E.; Kenney, A. D.; Zhang, Y.; Tuazon, J. A.; Li, J.; Yount, J. S.; Li, P. K.; Sharma, A., Rationally Designed ACE2-Derived Peptides Inhibit SARS-CoV-2. *Bioconjug Chem* **2021,** *32* (1), 215-223.

47. Yang, J.; Petitjean, S. J. L.; Koehler, M.; Zhang, Q.; Dumitru, A. C.; Chen, W.; Derclaye, S.; Vincent, S. P.; Soumillion, P.; Alsteens, D., Molecular interaction and inhibition of SARS-CoV-2 binding to the ACE2 receptor. *Nat Commun* **2020,** *11* (1), 4541.

CHAPTER 3: Studying of Apoptotic Events of HeLa Cells Induced by Propranolol (POA) Using Multi-Parametric SPR

ABSTRACT

In vitro, cell-based assays are widely used during the drug discovery and development process to test the biological activity of new drugs. Most of the commonly used cell-based assays, however, cannot measure in real-time or without labeling. In this study, a multi-parameter surface plasmon resonance approach combined with living cell sensing has been utilized to monitor drug-cell interactions in real-time, under constant flow, and without labels. The multi-parameter surface plasmon resonance approach provided fully specific signal patterns for various cell behaviors when stimulating cells with drugs that induce cell apoptosis. Utilizing SPR angular spectra and its shape or key parameters (i.e., SPR peak angular position, SPR peak minimum intensity) allows better understanding and provides plausible explanations for the type of cellular changes, e.g., morphological or mass redistribution in cells, that were induced in the HeLa cell monolayers during drug stimulation. The present study indicates that different concentrations of propranolol have different modes of interaction with HeLa cells, which is reflected by both the main SPR peak angular position and the main SPR peak minimum intensity. In addition, to predict the behavior of SPR spectra to the % of cell coverage on sensor slide, theoretical curves from averaging models were compared to the experimental data. Both SPR and microscopic imaging were used to monitor the apoptotic process of HeLa cells when treated with different concentrations of POA. Our experimental results

demonstrate that the change in the cell adhesion area to a sensor chip is insufficient to explain the entire SPR response to the activation of living cells. Furthermore, the multi-parameter surface plasmon resonance approach can simultaneously detect an extensive range of apoptotic events on the same cell population, which is important for improving our mechanistic understanding during drug discovery and development processes.

INTRODUCTION

Understanding apoptosis in disease conditions is essential as it gives insights into the pathogenesis of disease and may also leave clues as to how the disease can be treated. In cancer, there is a loss of balance between cell division and cell death leading to cells that should die never receiving the signals to do so. The problem can arise in any one step along the way of apoptosis. One example is the downregulation of p53, a tumor suppressor gene, which reduces apoptosis and enhances tumor growth and development.[1] Inactivation of p53, regardless of the mechanism, has been linked to many human cancers.[2, 3] However, being a double-edged sword, apoptosis can be the cause of the problem as well as the solution, as many have now ventured into the quest of new drugs targeting various aspects of apoptosis.[4, 5] Therefore, the ability to examine living cells in physiologically relevant environments, to monitor drug-induced cell apoptosis, is of the greatest importance for improving our mechanistic understanding during the drug discovery and development processes.

In vitro, cell-based assays are static and laborious and cannot measure real-time interactions on the cellular level. They often rely on labeled materials for imaging or

detection purposes. They require a secondary detection technique where the final quantification is based on UV- or fluorescence spectroscopy or mass spectrometry. Thus, developing new in vitro cell-based assay methodologies and approaches that enable direct detection through real-time, non-invasive, label-free, and continuous high sensitivity monitoring of cell responses to exogenous stimuli would be desirable.

Surface plasmon resonance (SPR) has attracted a great deal of interest. This is probably because it is widely spread and has established itself as a powerful technique for biosensing applications. However, the evanescent wave measuring techniques generally penetrate approximately 1/2 of the incident light wavelength into the surrounding medium. Thus, for a visible light source, a 300 nm penetration depth with exponential decay of sensitivity as a function of distance from the sensor surface is commonly achieved.[6] As described by Giebel K et al. and Burridge K et al., when cells are brought to interact with the surface of the biosensor, the cell membrane is not homogeneously in contact with the substrate. However, the interaction is mediated through focal contacts (1 μm in width and 2-10 μm in length) where the cell membrane is within 10-15 nm from the surface. Other areas form close contacts where the membrane and the surface are separated by 30-50 nm and extracellular matrix contacts that are at the distance of 100 nm or more.[7, 8] Therefore, SPR continuously detects the effective mean of the refractive index within the evanescent field that includes extracellular fluid. In other words, SPR of relatively short penetration depths are still able to sense the bottom portion of cells

Several studies have demonstrated that SPR is a powerful tool for real-time monitoring of living cell interactions and for studying different cellular processes without

the use of labeling agents. [9-16] Yashunsky and his group combined conventional optical microscopy with SPR instrumentation to obtain simultaneous SPR information and optical images of the cell on the sensor slide. They monitored MDCK cells (Madin Darby canine kidney) for cell sedimentation and deposition to the sensor surface, cell spreading, formation of intercellular contacts, and formation of a continuous cell monolayer. The SPR measurement was initiated by using a sensor without cells. Later, they injected the cells and monitored the SPR response continuously. The refractive index increased rapidly as cells sedimented on the sensor. Later, the RI increase was slower but reached even higher values as cells spread and started forming cell-cell junctions. Eventually, RI reached its maximum when cells occupied the whole sensor surface area and no bare gold surface was visible. In addition to an increased angular position as RI increases, the SPR curve dip became wider and shallower.[17] Yanase et al. correlated the number of cells on a gold sensor to peak angular position (PAP) using rat mast cells RBL-2H3. They observed different concentrations of cells on the sensor surface simultaneously with light microscopy and SPR. Linear correlation was found with an increasing amount of cells causing an increase in peak angular position.[15]

Other groups studied the SPR response to cell apoptosis. Kosaihira et al. used several different pancreatic cancer cell types (MIA PaCa-2, PANC-1, and Suit-2) with different cancer drugs and drug combinations. They combined fluorescence microscopy and SPR in one device and validated the SPR response by monitoring the mitochondrial membrane potential, an indication of cancer drug effect on cells. The SPR response was seen as a decrease in PAP as cells died.[18] Maltais et al. also studied SPR responses for cell

apoptosis using several endothelial cell types (EA. Hy 926, AD-293, and HeLa). Cell death was initiated with different components that induced apoptosis by caspase activation through extrinsic and intrinsic pathways.[19] This led to cell morphology changes such as rounding, nuclear condensation and fragmentation, membrane blebbing, and cell detachment. They confirmed their result using phase-contrast microscopy and a conventional apoptosis assay with annexin V. Results were congruent with Kosaihira[18]: a decrease in RI as cells died. Maltais et al. concluded that it was possible to obtain accurate information of latency, rate, and extent of cell apoptosis by monitoring angular position.

The cell membrane is a semi-permeable barrier allowing fluid exchange between intracellular and extracellular phases. A non-isotonic medium thus causes size alterations in cells. MDCK and NRK-52E (normal rat kidney) cell responses in SPR were studied for their size variations in these conditions.[20-22] An increase in angular position was observed within a hypertonic medium and a decrease within a hypotonic environment. In hypertonic environment, cells shrink, and in a hypotonic, they expand. Responses correlated directly to the cellular volume change increase/decrease. They suggest that the SPR signal relates to the cellular volume change, as the loss of cellular water from the cytosol causes an increased cytoplasmic concentration of intracellular osmolytes and, thus, an increased refractive index close to the sensor surface. However, water flowing from the extracellular space into the cell, dilutes the cytosol, which causes the refractive index within the evanescent field, and thus the SPR signal, to decrease.[20-22] In contrast Cuerrier et al. and Chabot et al. show a decreasing PAP for cells that actively shrink due to cytoskeleton contraction or inhibition of cellular respiration.[9, 16] They suggested that when a cell

cytoskeleton activates, it causes morphological changes by contracting the cell. When this happens, the area occupied by the cells on the gold surface decreases. Thus, SPR "sees" more of the lower RI water content.

In addition to simple cell membrane occupancy on sensor surface or intracellular fluid amount, changes in cell membrane composition such as Actin cytoskeleton rearrangement is one of these cellular responses that are widely acclaimed to be responsible for the SPR signal. MDCK and A7r5 (rat vascular smooth muscle) cell treatment with cytochalasin D and Latrunculin A, respectively.[23, 24] These compounds lead to actin cytoskeleton disassembly by inhibiting actin polymerization, the effect of cytochalasin D, or by inducing depolymerization, the effect of Latrunculin A. Cell monolayer remains intact and cells do not detach. This cytoskeleton degradation resulted in permanent decrease in SPR signal in both cases.

Beside cytoskeleton rearrangement, other intracellular events could contribute to SPR signal as well. Yanase et al. and Horii et al. stimulated mouse keratinocytes (PAM212), basophils and RBL-2H3 mast cells with epidermal growth factor (EGF) or different antigens. They observed cell spreading with confocal microscopy and differential interference contrast microscopy to relate cell spreading and PAP changes. They showed that simple cell spreading, ruffling or cell membrane density changes did not explain the PAP increase completely and the PAP increase was still observable even after they eliminated cell spreading by destroying the actin cytoskeleton. They associated PAP alterations directly to antigen or EGF binding. [11, 12, 15]

Odorant molecules interact with olfactory receptors through G-protein activation. This activation initiates a signaling cascade, where secondary messengers such as cAMP (cyclic adenosine monophosphate) and IP3 (inositol trisphosphate) are produced by action of adenylate cyclase and phospholipase C (PLC), respectively. These signaling pathways also result in an increase of intracellular calcium and the SPR signal.[25] Detecting cell calcium concentration is, in fact, used as a method to measure intracellular activity, and it was thought to be the direct cause also for the increased SPR signal.[25] However, the presence of calcium was later shown not to be responsible for the SPR response.[16]

From these results, it is evident that a variety of responses occur in cells that can be responsible for the SPR signal, and determining the actual source of the signal is difficult and still not fully understood. The situation is even further complicated by the fact that many different mechanisms can contribute to the SPR signal simultaneously, such as cell spreading / contraction and several concurrent intracellular events.

Viitala et al. simulated full surface plasmon resonance angular spectra of cell monolayers and compared the simulation with actual surface plasmon resonance measurements performed with MDCKII cell monolayers in order to better understand the origin of the surface plasmon resonance signal responses during drug stimulation of cells.[26] The monolayer was theoretically divided into three sections in order to clarify the effect of changing different optical properties in it such as change in real (n) and imaginary (k) parts of the refractive index. The first section within the reach of the evanescent field (EF) represents the lower region of the cell monolayer. The second section consists of the rest of the cell (Cell), outside the evanescent. The field and bulk medium layers represent the

third section (Figure 3.1). It was found that increasing the real part (n) of RI at the lower part of the cell (EF), increases PAP; whereas the same change outside the evanescent field (Cell) increases TIR angle (θ). On the other hand, increasing RI (k) by the sample layer within the evanescent field, increases PMI and decreases TIR intensity; whereas when this happens outside the evanescent field, it has no effect on PMI. Viitala et al. used these parameters to differentiate between passive (trans- and paracellular) drug absorption processes during drug-cell interactions.

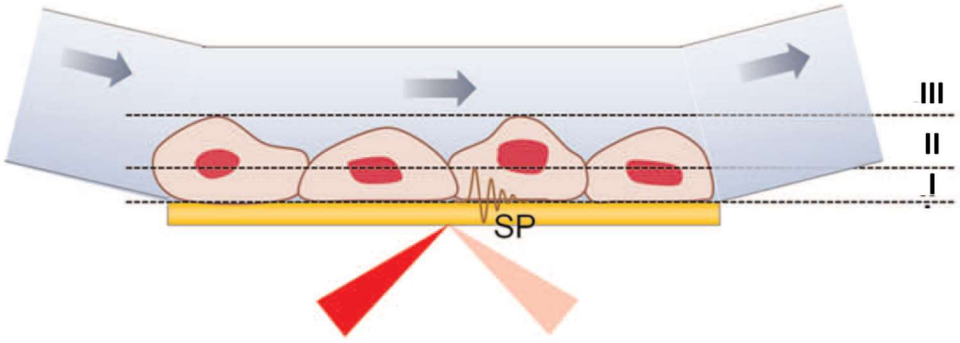

Figure 3. 1 Schematic representation of a cell monolayer divided theoretically into three regions: (I) within the evanescent field (EF) consist of the lower part of the cell monolayer, (II) outside the evanescent field consist of the rest of the cell (Cell), and (III) bulk medium layer (Edited from Viitala et al. 2013).

The full SPR angular spectra have successfully been used in modeling optical properties and thicknesses of both thin organic and inorganic layers.[6, 27, 28] However, a highly unexploited approach of SPR is to measure the full SPR angular spectra in real-time in order to fully utilize its shape or key parameters (i.e., SPR peak angular position, SPR peak minimum intensity and the changes in the total internal reflection region) for monitoring apoptotic process during drug-cell interaction. This might not be critical when

considering traditional biomolecular interactions, but it should play a significant role in living cell sensing. Therefore, analyzing multiple parameters from the full SPR angular spectra would be of interest in order to try to obtain a better quantitative or even qualitative understanding of how SPR could be utilized for living cell sensing.

Over the past few decades, ovarian cancer has become one of the deadliest cancer-related deaths among women worldwide, with nearly 140,000 deaths of women occurring every year.[29, 30] Surgery and chemotherapeutic drugs are the standard treatment for ovarian cancer. Nowadays, despite significant advances in clinical diagnosis and systemic therapy, the overall 5-year overall survival rate is still less than 30%.[31] Therefore, the mechanisms underlying the tumor progression and identification of novel chemotherapy are critical challenges to enhance the therapeutic effect and prolong survival.

The beta-adrenergic receptors (β-ARs) are a class of G-protein coupled receptors (GPCRs) that are targets of the catecholamines epinephrine and norepinephrine. Stimulation of these receptors induces sympathetic nervous system responses, most notably the fight-or-flight reaction. β-ARs were first detected in breast cancer nearly fourty years ago,[32, 33] and it has recently been reported that β-ARs are over-expressed in liver and breast cancer relative to non-diseased epithelium.[34, 35] Pre-clinical studies using breast cancer cell lines have correlated β-AR antagonist (beta blocker) treatment to decreased cell proliferation and migration.[35-37]

Epidemiologic studies have summarized that using β-blockers in clinical settings can reduce the rates of progression for some solid tumors.[38] Results claim that β-blockers

may be secure and inexpensive therapeutic agents for tumors.[39-41] But the molecular mechanism pathways relevant in these responses remain poorly concluded.

There is evidence suggesting that Propranolol may trigger multiple signaling pathways that could contribute to the induction of apoptosis by several proposed mechanisms. Studies suggested apoptosis induced by Propranolol is mediated by promoting caspase-dependent signaling.[42] Other studies show PRO treatment dramatic increase in ROS which initiate ETC in mitochondria and activated apoptotic effector including BAX, Bcl, cytochrome c ultimately triggered apoptotic cell death.[43]

Here we aim to monitor cellular alterations and remodeling occurring in the course of apoptotic reaction of HeLa cell stimulated with POA and taking the advantage of multiparametric SPR.

EXPERIMENTAL SECTION

Materials and Solutions

The human cervical cancer HeLa cell line was purchased from American Type Culture Collection (ATCC) and cryopreserved in a liquid nitrogen storage until use. Dulbecco's Modified Eagle Medium (DMEM), Fetal bovine serum (FBS), penicillin, Streptomycin, 0.05% Trypsin-EDTA and Trypan blue were purchased from Gibco. Propranolol hydrochloride was purchased from Sigma-Aldrich. Buffered salt solution HEPES with pH 7.4 was chosen, as this buffer is recommended to keep the cells viable for a longer time at room temperature without CO_2 supply. The buffer was prepared by dissolving the solid compound (Sigma-Aldrich) in Milli-Q water using 10 mM HEPES,

150 mM NaCl, 5 mM KCl, 1.2 mM $MgCl_2$, 2 mM $CaCl_2$ and 10 mM D-glucose.[44] The buffer was filtered, degassed and autoclaved before use.

Apparatus

For the cell culture, a Class II A/B3 biological safety cabinet, Fisher Scientific ISOTEMP 205 water bath, Pelton & Crane Validator 8 autoclave, CF-80-1 electronic centrifuge, Fisher Scientific CO_2 incubator and Kenmore lab refrigerator were used. Microscopic imaging was done with an Optical microscope with an AmScope digital camera. The refractive index of various liquid solutions was measured with an American Optical ABBE refractometer. SPR data was measured with NanoSPR-321 (NanoSPR, Addison, IL) with a GaAs semiconductor laser light source (λ=670 nm). The device comes with a high-refractive index prism (n=1.61), 30 µl flow cell and an Orion Sage syringe pump. Nanopure water (> 18 MΩ.com), purified through a Barnstead E-Pure filtration system (Thermo Scientific, Rockford, IL), was used for all reagent preparations and rinsing.

Drug preparation

Propranolol hydrochloride (0.030 g) was dissolved in 20 ml of HEPES buffer to form a stock solution with a concentration of 5 mM. The stock solution was filtered through a 0.22-µm microporous membrane and stored at 4˚C for future use. The stock solution was diluted to different concentrations (100, 250, 500 µM and 2, 3 mM) to determine the response of the SPR signal according to HeLa cells stimulation.

HeLa cells Reactivation, seeding

A vial of cryopreserved cells from liquid nitrogen storage was thawed in a 37°C water bath, just until ice was no longer visible. The entire content was transferred into a 15- mL conical centrifuge tube with 3 mL of growth medium (DMEM supplemented with 10% FBS and 1% penicillin). Then, 1 mL of the medium was added into the cell vial, rinsed and added into the centrifuge tube. This step was repeated several times to make sure content from the cell vial was transferred into the centrifuge tube. Once transferred, the cells were centrifuged at 4000 rpm (1799 xg, RCF) for 10 min. After that, the supernatant was carefully aspirated out, minding to not disrupt the cell pellet. Thereafter, the cell pellets were resuspended with 5 ml of growth media in a culture flask and the suspension was checked under a microscope to ensure the cells were uniformly distributed. Finally, the cells were kept in a 37°C, 5% CO_2 humidified incubator.

Culturing of HeLa cells

HeLa cells were cultured in DMEM supplemented with 10% FBS and 1% penicillin and streptomycin. Cells were incubated at 37°C and 5% CO_2 in a humidified incubator. The culture medium was removed at cell subculture then cells were detached from the culture flask by a standard trypsinization protocol. For this purpose, 2 ml of 0.05% trypsin-EDTA was added into the culture flask and placed in the incubator to allow the trypsin to work. The flask was observed under the microscope every minute until the cell was slightly detached from the flask wall and appeared rounded and separated from each other. Thereafter, the Trypsin-EDTA solution was aspirated out and the cells were tapped off the

wall of the flask prior to adding 5 ml of fresh medium to resuspend the cell. Then, the cells were gently pipetted several times to ensure that the cells are transferred and dispersed into the fresh medium. After that, 2 ml of the cell suspension was transferred into a new culture flask and then resuspended in 3 ml of fresh medium. The cells were kept in the incubator and subcultures of confluent cells were performed every 1-2 days where 12 was the maximum Passing number used.

Culturing of HeLa cells on SPR sensor chips

SPR Gold sensor chips were fabricated with a 2-nm thick chromium adhesion layer, followed by deposition of a 50-nm thick gold layer via e-beam evaporation onto cleaned BK-7 glass slides based on previously published procedure[45]. After extensive rinsing with the Nanopure water, pure ethanol and air dried, the gold chip was sterilized by UV radiation for 20 min.

Cleaned gold chip (2.5 X 1.5 cm) was placed in a 6-well culture plate. For cell suspension preparation, HeLa cells were removed from culture flasks by trypsinization and, suspended in 5 mL of the culture medium. 2 mL of this cell suspension and 4 mL of the culture medium were mixed, then 3 ml of this cell suspension were pipetted on top of the SPR chip in each well. The wells` contents were inspected under a microscope for uniform distribution of cells and then kept in the incubator for 1-2 days until their surfaces were covered with ~70-80% layer of cells, prior to use for SPR and microscopic experiments.

Cell Viability Test

Cell viability was examined for selected slides using the trypan blue exclusion test. Cells were trypsinized and resuspended in 0.4 w/v % trypan blue. Cell viability was calculated under 25× magnification using a hematocytometer and expressed as (N viable cells) / (N total cells) × 100%. The trypan blue stained cells were considered nonviable. This allowed for a rapid rough assessment of viability prior to the SPR measurements that were always conducted using slides where >97% of the cells seemed viable.

SPR measurements

The measurements of SPR signal response to HeLa cell stimulation with Propranolol (POA) were performed on a dual channel SPR spectrometer (NanoSPR-321) equipped with a Plasmon Serial software that provides the reflectivity curve and sensorgrams of the real-time minimum angle. HEPES is the running buffer in which the cells were immersed when they were not exposed to a POA solution. Buffer flow rate across the sensor surface was precisely controlled using a Syringe Pump which is also can be set on pause mode for incubation purposes. All SPR measurements were done at room temperature. Prior to measurements, the microfluidic systems consisted of the chambers and inlet/outlet tubing, the injection ports and the device accessories were sterilized by flowing 70% (v/v) ethanol for 30 min and then rinsed with HEBES.

Once the cell had reached confluency on the SPR chip, they were rinsed by immersing the ship into a running buffer. After this, the gold chip was quickly adhered to the prism using a refractive index matching fluid (n= 1.610 Cargille Laboratories New

Jersey). The flow cell consists of two 30 µL flow channels attached afterwards, and the buffer flow was run until a stable baseline was obtained. Subsequently, Propranolol at a different concentration (100, 250, 500 uM and 2,3 mM) was added to the cells and full SPR angular spectrum were monitored for a total period of 2 hr. After the measurement was completed, the outlet was disposed of in a biological container and the instrument parts were cleaned with 70% ethanol. Figure 2 shows experimental set up.

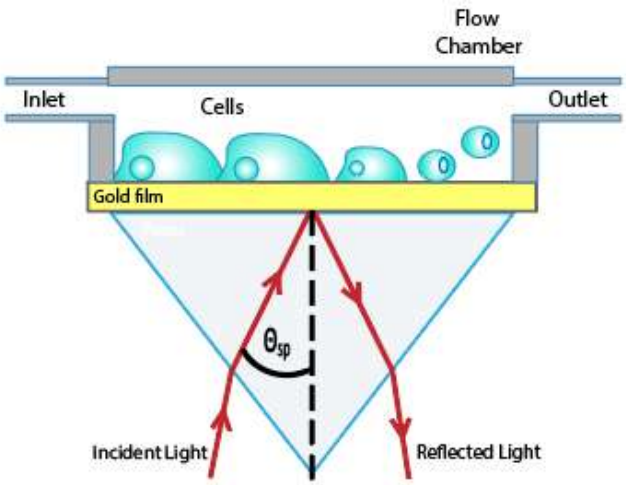

Figure 3. 2 Experimental set up of SPR monitoring apoptotic events of HeLa cells in real time without labeling.

Microscopy measurement

Microscope imaging was performed with the conditions and procedures replicating the SPR experiments. The chips were removed from the incubator, rinsed with the HEPES buffer and placed on the microscope platform using Petridis. 1 mL of POA with different concentrations were added into the gold chip. Images of each gold chip were taken every

15 min, with a total observation period of 2 hr, using a digital microscope camera before and after exposure to POA at 25x magnification. To ensure accuracy, the images were taken at the same spot on the chips.

Cell confluency measurement

The cell coverage on the chip was measured by Fiji/ImageJ software (www.fiji.sc). A calibration was performed using a stage micrometer prior to measurements. To quantify the fraction of covered areas, the cells boundaries were traced manually using the freehand selection tool. Then, the cell interior was filled by means of a fill-hole procedure. In this way, the cell covered area was distinguished from the cell-free area. After that, the threshold function was used. Then, the particle analysis tool was used to calculate the percentage of covered area, which also represents the cell confluency.

RESULTS AND DISCUSSION

SPR angular scan of a HeLa cells monolayer

The SPR sensor slides were verified before each interaction measurement with Propranolol by first measuring the full SPR angular spectrum of the HeLa cell monolayer. Figure (3.3) shows a full SPR curve for a sensor slide without cells and with a HeLa cell monolayer. When a cell monolayer is present, the PAP shifts from 63.4° to 65.3° and PMI increases from 0.06 to 0.07. Also, the TIR region shifted to lower intensity, from around 0.97 to 0.93. These changes are in accordance with experiments done by Yashunsky et al. and Viitala et al. [17, 26] Yashunsky et al. monitored cell monolayer formation concurrently with optical microscopy and SPR. Viitala et al. simulated a full SPR curve of a thick sample

layer on the sensor surface, corresponding to the SPR curve produced by a cell monolayer. In both experiments, the cell monolayer caused the PAP to shift to a higher angle and PMI to increase. In addition, Viitala et al. showed similar TIR intensity changes as observed here.

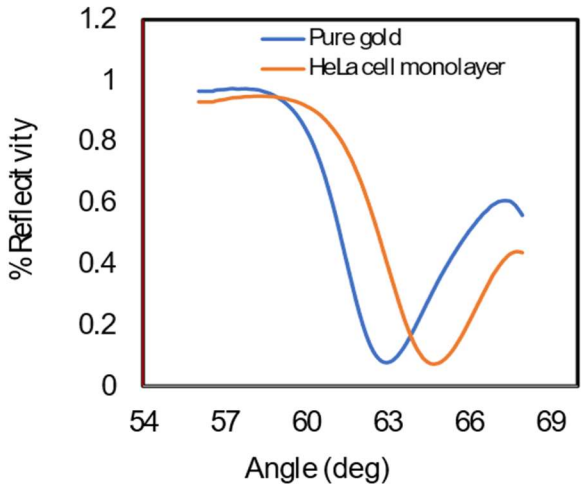

Figure 3. 3 Measured full SPR angular spectra of a pure gold coated SPR sensor slide (blue line) and HeLa cell monolayer immobilized on the SPR sensor slide (red line).

SPR monitoring of cell apoptotic events after stimulation with different concentration of propranolol (POA)

To study apoptotic events triggered by POA using SPR, one channel was dedicated as the experiment channel where the POA was injected, while the other channel was the negative control channel without POA (Fig. 3.4A). The negative control is needed to confirm that the observed changes were caused by direct stimulation by POA and not by other factors such as temperature or the buffer flow shear. Different concentrations of

propranolol were added to the cell and the full SPR angular spectrum was monitored for a total period of 2 hr.

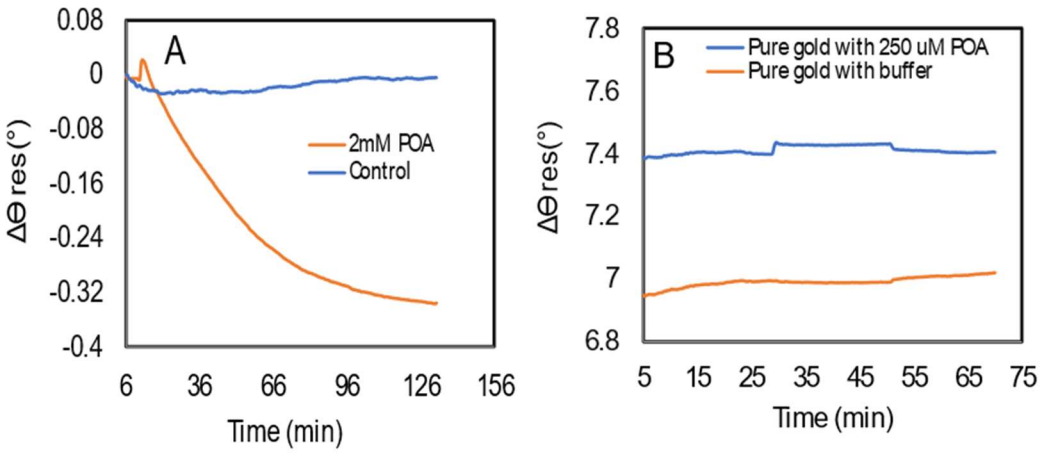

Figure 3. 4 SPR sensogram showing no significant change in control channel (A) and when POA interact with pure gold chip (B)

Main SPR peak angular position showed no significant change when Propranolol was allowed to interact with pure gold (Fig. 3.4B). This validates that the change in main SPR peak angular position reflects real drug-cell interactions and not drug-gold interactions.

Fig. 3.5 summarized the POA-induced responses of HeLa cells, which clearly exhibited that different concentrations of POA have different effects on HeLa cells. At a lower (100, 250 µM) and an intermediate concentration (500 µM), POA results in two distinct reproducible phases: a decay phase with decreased signal and a positive phase with increased signal (Fig. 3.5A). However, a 500 µM concentration showed the greatest amplitude (Fig. 3.5C). In contrast, at higher concentrations (2,3 mM) POA led to only a rapidly decayed signal (Fig. 3.5B).

Interestingly, when HeLa cells were stimulated with propranolol, it was found that not only the main SPR peak angular position changed during stimulation, but also the main SPR peak minimum intensity changed significantly (Fig. 3.6). Peak minimum intensity showed decreased signal and then after 10 min continuous increased signal when cells were stimulated with 500 μM of POA (Fig. 3.6A). In the case of 2 mM POA stimulation, the PMI signal kept decreasing with time (Fig. 3.6C). These results indicate that different concentrations of propranolol have different effects on HeLa cells, which is reflected not only in the main SPR peak angular position but also in the main SPR peak minimum intensity. Thus, instead of analyzing only the main SPR peak angular position changes during drug-cell interaction, it would be more useful to analyze both the main SPR peak angular position and the main SPR peak minimum intensity in order to better understand and distinguish the cellular mass redistribution and morphology change associated with apoptotic events during cell stimulation with different drug concentration.

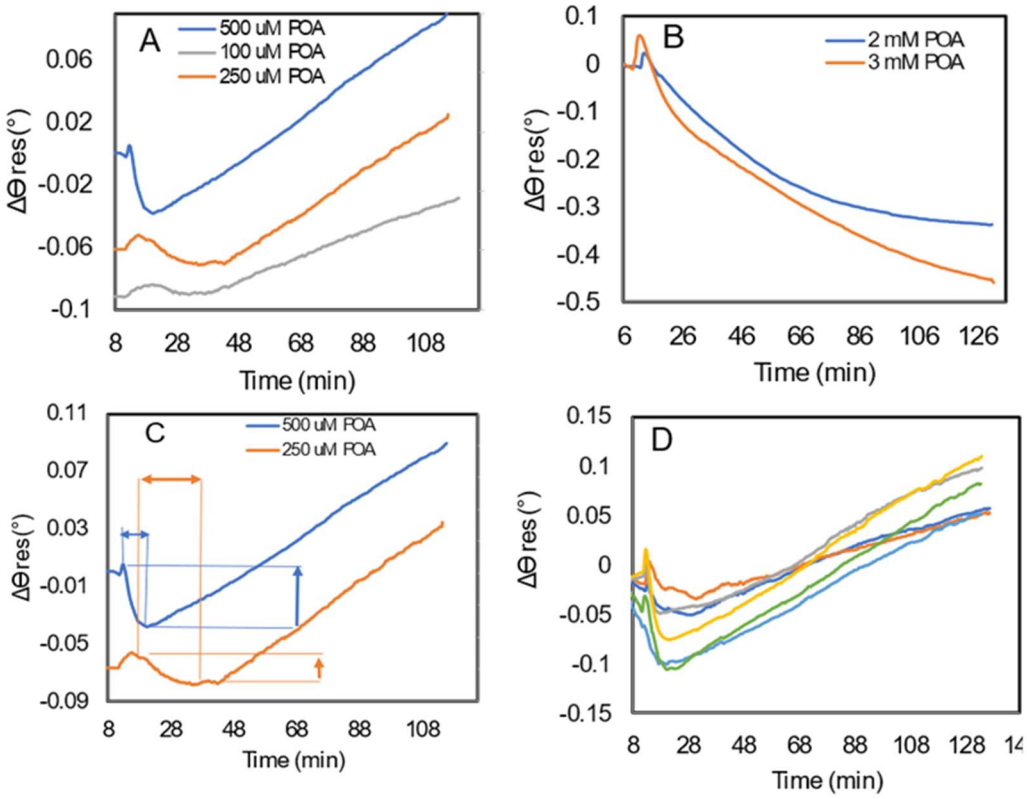

Figure 3. 5 SPR signal responses during propranolol stimulation of HeLa cells: 100, 250, 500µM A) and 2, 3mM B) of POA respectively. C) The dose-dependent PAP response of HeLa cell with micro-molar concentration range of POA. D) six independent experiments showed the reproducibility of the cell response induced by 500 µM POA.

The literature of SPR interaction measurements involving immobilized cells on the sensor surface are quite contradictory; in some cases, the injection of the analyte results in positive SPR responses [11-15] and in other cases negative SPR responses.[9, 16] A widely accepted simplification for the measured SPR signal is that the main SPR peak angular position is linearly proportional to the mass change in the evanescent field. This is also evident from the basic physics of the SPR phenomena.[6] Based on this, it has been suggested that the SPR responses with cells based on measuring the changes in the main SPR peak angular position originates from mass redistribution within the cells.[15, 46] Such a mass

redistribution in cells should lead into changes both in the refractive index, and in the apparent light absorption of cell layers as different cell organelles and structures shift within the cell. However, this mass distribution could induce either negative or positive changes in the SPR responses measured by monitoring only the main SPR peak angular position, depending on if the cytoskeletal mass migration in the cells is in the direction away from or towards the SPR evanescent field region during apoptotic events.[26] This is also supported by the studies by Cuerrier et al., Chabot et al.[9, 16] and Yashunsky et al.[17] Cuerrier et al. and Chabot et al. showed that morphological change in cells, i.e., contraction of cells, induce a negative SPR shift in the reflection intensity measured at a fixed angle, while Yashunsky et al. showed that cell spreading induces an increase in the reflection intensity measured at a fixed angle with mid infrared SPR.

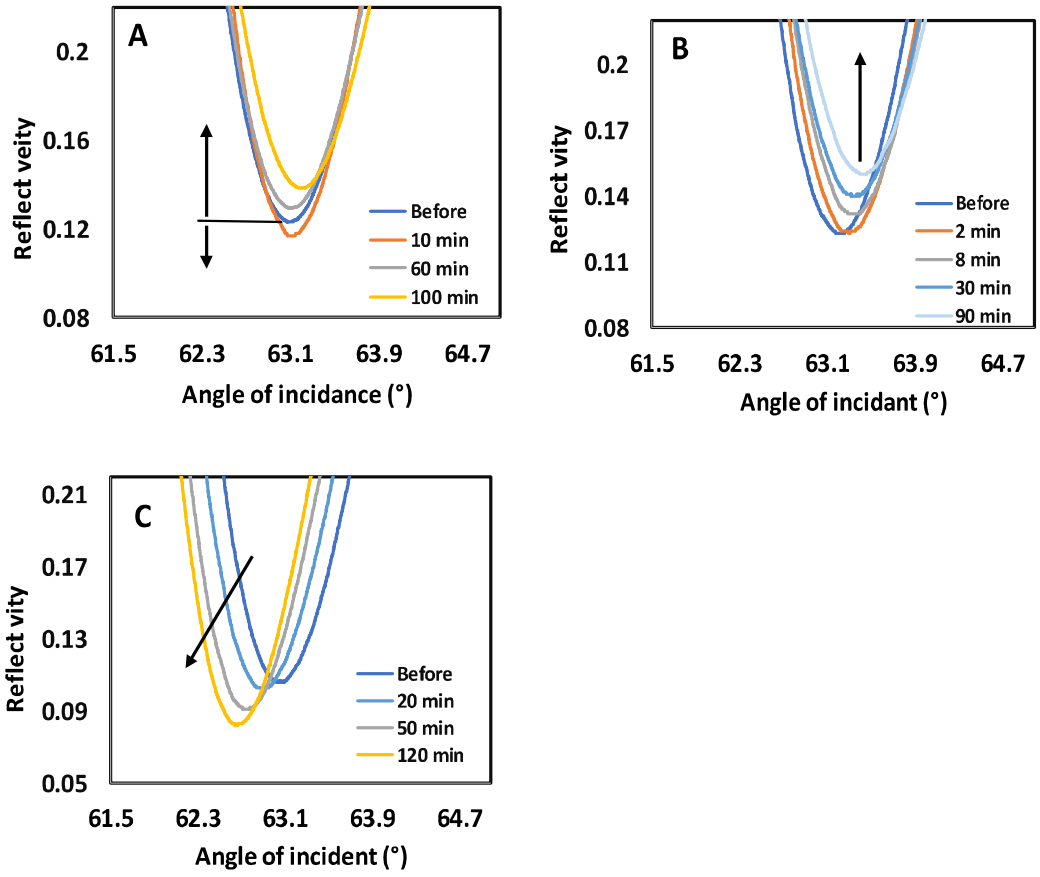

Figure 3. 6 Focused part of full SPR angular spectra showing the main SPR peak minimum intensity when HeLa cells stimulated with 500uM (A) 250uM (B) and 2mM (C) of propranolol. The arrows indicate the evolution of the spectra.

However, none of the studies mentioned above have considered the changes in the main SPR peak angular position together with changes in the main SPR peak minimum intensity. Though, Viitala et al. simulated full SPR angular spectra induced by varying different optical parameters and compared them with actual SPR measurements of drug-MDCK II cell interactions in order to elucidate the signal responses in living cell sensing with SPR.[26] Cell monolayers were divided theoretically into three sections: the lower part within the reach of the evanescent field (EF), the second part representing the rest of the

cell, but outside the evanescent field region, and the bulk medium part. It is clear from the simulated spectra in this study that RI increase, or mass accumulation, at the lower part of the cell (EF region) increases PAP, whereas the same change outside of the evanescent field increases the TIR angle (θ). The increase in the amount of light scattering surfaces within the evanescent field increases PMI and decreases TIR intensity, whereas when this happens outside of the evanescent field, it has no effect on PMI. However, these parameters are not yet widely used in cell sensing assay. Therefore, in this present study we aim to investigate these parameters in terms of HeLa cell apoptotic events in response to different concentrations of POA.

When examining Fig.3.5A and 3.6A in more detail, it is obvious that there is a clear negative shift in both the SPR peak angular position and the SPR peak minimum intensity during cell stimulation with 500 μM of propranolol. After 10 min, both the main SPR peak angular position and the main SPR peak minimum intensity increase to a higher level than before stimulation. These results indicate that a stimulation of HeLa cells with an intermediate concentration of propranolol (i.e., 500 μM) first induces a cell contraction accompanied by a mass redistribution away from the evanescent field region leading to a negative shift in both SPR responses. Thereafter, SPR responses become positive, which is probably a consequence of a mass redistribution towards the evanescent field region. Our result for 500 μM of POA induced apoptosis is almost identical to the SPR signature produced when a G-protein coupled receptor such as angiotensin and thrombin receptors are stimulated.[9, 16] A study by Fang Ye also is in agreement with our result. They activate

β_2-receptor in A431 cells by epinephrine, isoprotenol, and Forskolin which leads to Gs-mediated signaling that proceeds through adenylyl cyclase and protein kinase.[46]

Fig. 3.5D shows six independent experiments indicating the reproducibility of the cell response induced by 500uM POA. Note that the variation in SPR signals is due to the intrinsic spatial variation of the cell-POA interaction rather than errors in measurement. Fig. 5C shows SPR signals resulting from stimulation of HeLa cells with POA in the micromolar concentration range. It is clear that the lower the POA concentration, the lower the negative shift (phase one) of PAP signal, and the longer is the transition time from phase one to phase two. This indicates the concentration dependent response.

There is evidence suggesting that β-Androgenic receptor (β-AR), a family of G-PCR, triggers multiple signaling pathways that could contribute to the induction of apoptosis.[47] In addition, our results indicate that the optical signature induced by apoptotic events of HeLa cells at low concentrations of POA are in agreement with SPR signature produced when G-PCR are simulated.[9, 16, 46] Therefore, we suggest that the POA (β-blocker) in the micromolar concentration range may induce HeLa cell apoptosis via G-PCR signaling pathway.

However, for the SPR responses for lower concentrations of propranolol (100, 250 μM) (Fig. 3.5A, and 3.6B), a slightly negative shift is only seen in the angular position of the SPR peak minimum which is followed by a positive shift during cell stimulation, while the SPR peak minimum intensity showed only positive change with increasing simulation time (Fig. 3.6B). It was surprising to see that the SPR peak angular position resulted in two

phases even though there was only one phase (negative change) in the main SPR peak minimum intensity during stimulation. This could indicate that this concentration of POA indeed induces a slight cell contraction which results in a decline phase of PAP, but not sufficiently large to induce any cell mass redistribution away from the evanescent field within the HeLa cell. However, POA stimulation triggers a diffusion of soluble intracellular molecules toward the bottom portion of the cells and both SPR parameters show increasing signal consequently. It is clear from our results that each SPR parameter is independent and can be used to distinguish between apoptotic cell events induced by cell drug interaction. The same independent effect was observed as MDCK cell line stimulated with D-mannitol showed clear decrease in PAP but not PMI.[26]

It has been suggested that the change in PAP reflects both mass redistribution and cell morphology change and that change in PMI is mainly due to mass redistribution within the cell.[26] Based on this we suggest that simulated HeLa cells with 500uM POA initially show decreased signal caused by cell contraction and mass redistribution away from the evanescent field region. After 10 min, the positive PAP results in a strong contribution of cytoskeleton rearrangement to the SPR response which overlay the signal from morphology change. Same strong contribution of mass redistribution to SPR signal seen with HeLa cell simulated with 250, 100 μM POA (Fig. 3.5A).

In contrast, at higher concentrations (2-3 mM) POA leads to only a rapidly decaying signal of both PAP and PMI (Fig. 3.5B and 3.6C). This is most likely due to rapid cell contraction and intercellular gap formation leading to rapid mass redistribution away from the evanescent field region leading to negative shift in both SPR response (Fig 3.5B, 3.6C)

and even cell detachment. It is clear from that the SPR signal did not follow apoptotic signal that mediated through G-protein coupled receptors. The reason could be the high concentration of POA. As SPR signal can reflect intracellular events and/or morphology change resulting from cell during apoptosis, it is also reflecting the change in cell surface adhesion as well which results in a corresponding change in the refractive index on the sensing surface. Therefore, stimulation of Hela cells with high concentration of POA causes rapid cell shrinking. Thus, the diffusion of cellular macromolecules away from the bottom portion of HeLa cells dominate the both optical responses observed (PAP and PMI), and subsequent cell detachment minimizes the potential effect of any cellular events. Our results are congruent with those of Maltais et al. They also study SPR responses for cell apoptosis and conclude that a decrease in RI as cell died.[19] Their results were confirmed using phase contrast microscopy and covenantal apoptotic assay with annexinV.

As a summary, our results indicate that different POA concentrations cause different cell responses. At high concentration in mM range, POA results in cell detachment, which dominates the optical signal obtained. However, at lower concentration in μM range, the dose is not sufficient to cause cell detachment. Instead, POA activates endogenic G-protein coupled receptors. Similar results have been shown for A431 cells treated with different concentrations of trypsin.[48] Low trypsin concentration mediates G_q-signaling, while higher does results in cell detachment.

Modeling and comparisons between SPR signal and cell confluency.

To quantify the cell confluency and to compare the confluency from microscopic images with our SPR signal, a mathematical SPR model was used. Fig.3.7 shows microscopic images of HeLa cells after POA stimulation. It is clear that the images show a decrease in cell size and an increase in the amount of the intracellular space, due to apoptosis.

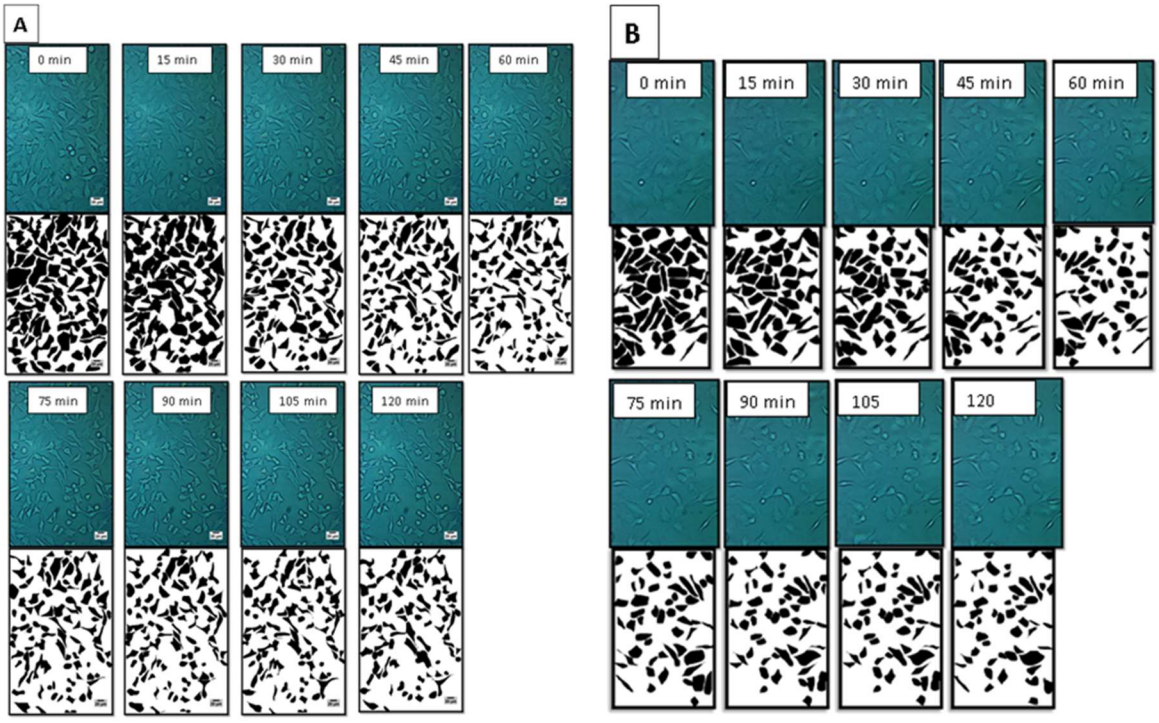

Figure 3. 7 Time-lapse microscopic imaging (25x) of HeLa cells after stimulation with propranolol 2mM A), 500uM B) over 2 h. The upper images are the original images and the lower images show the cellular outline processed by ImageJ.

An equation that enables determination of the refractive index in response to percentage of cell coverage on a sensor slide from the fixed angle SPR sensogram was previously established based on the effective refractive index model.[49] This model allows

quantitative analysis to relate change in cellular attachment area to SPR response expressed in equation below:

$$n\text{eff} = n\text{m} + (nc - n\text{ m})\ \text{ca}' \qquad (1)$$

where the n_{m} and n_{c} is the refractive index of cell culture medium and intracellular fluid respectively. Cell density (c) and its effective spreading area (a`) which is regarded as the cell confluency. Typically, the SPR response ΔR to the effective RI change is approximately linear over a narrow range. Thus, SPR response can be resolved from the cell confluency change (eq.2): Where S is the sensitivity of SPR response in angle shift (ΔΘ)

$$\Delta\text{R} = \text{S}\,(nc - n\text{m})\,\Delta\ \text{ca}' \qquad (2)$$

The NaCl solution exhibits great linearity of RI *versus* concentration and thus can be used as the RI fluid for experiment to determine SPR sensitivity and dynamic range. A gradient concentration of 0.5, 1, 1.5, 2, 2.5, 3, 3.5, 4, 4.5, 5M solutions was sequentially injected to the SPR channel. Each injection lasts for 3 min and is separated by a buffer wash. SPR response and fitted curve are shown in Fig. 3.8. The fitted curve demonstrated that the dynamic range of the SPR system is linear from (1.336) to (1.378) with a sensitivity (S) of 54.47.

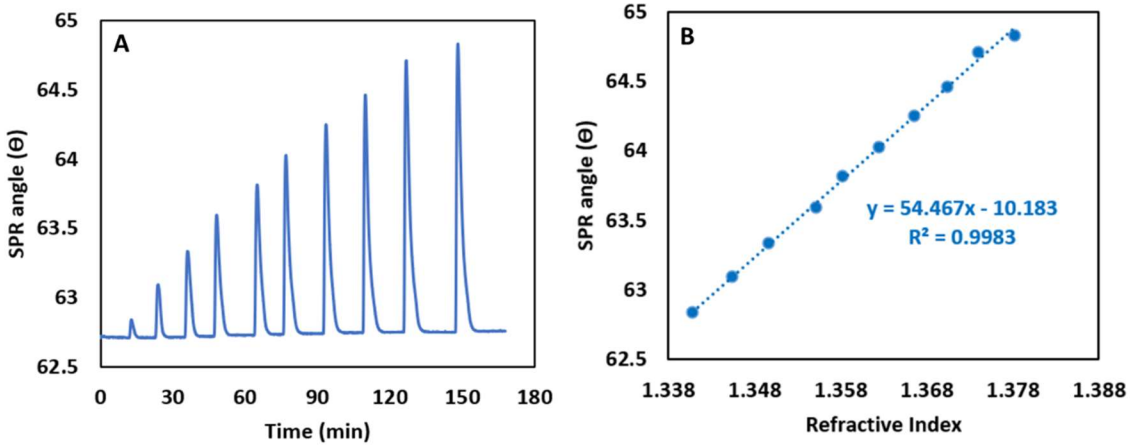

Figure 3. 8 (A) SPR response to a concentration gradient of NaCl solutions. (B) Fitted curve of the SPR angle shift *versus* RI

To investigate the relationship between the behavior of the SPR spectra and cell confluency change during apoptosis process, theoretical curves from averaging models according to equation. 2 were compared to the experimental data. Using the HeLa cell refractive index (n_c) 1.39 ,[49] Buffer refractive index (n_m) 1.338, sensitivity of SPR response 54.47, and cell confluency (Δ ca′) extracted from microscopic image, SPR response in angle shift can be calculated according to equation (2)

Fig 3.9A illustrates results of HeLa cells with 2mM POA stimulation. It is clear that the experimental SPR response (red line) agreed well with that extracted from the microscopic images (blue dots) based on eq (2). In contrast, 500µM of propranolol (Fig. 3.9B) initially shows a similar SPR response in the two methods where both show decreased SPR signal. However, after 10 min SPR signal extracted from microscopic images keeps decreasing, whereas SPR angle shift extracted from the SPR data shows increasing signal.

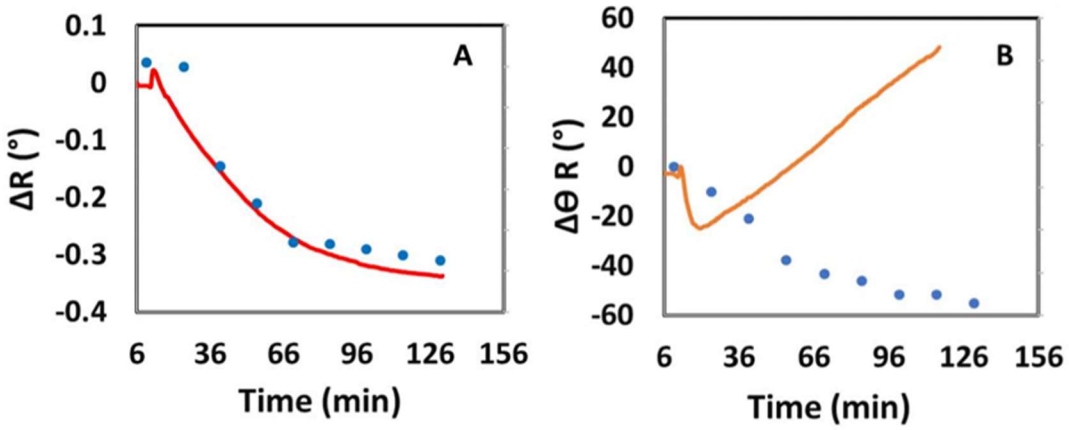

Figure 3. 9 Experimental SPR response (red line) and SPR signal extracted from microscopic image based on eq (2) (blue dots) for 2mM POA (A) and 500uM (B)

Based on our result, SPR signal change reflects more than changes in the size of the area to which cells adhere. It also may detect intracellular events and cytoskeleton rearrangement, since they may also affect the plasma membrane density on the sensor chip. Therefore, SPR response does not agree completely with the cellular morphology change of HeLa cells monitored by microscopic image when stimulated with low concentration of Propranolol, in micromolar range. The reason is that the SPR optical signature of apoptosis is likely to be caused by a unique combination of molecular and morphological events. On the other hand, after stimulation of HeLa cells with high doses of POA, milli-molar range, SPR data agreed with the morphological changes observed by microscopy. Cells shrink quickly and detach from the sensing surface which minimizes the potential effect of any molecular events.

CONCLUSION

It is rather obvious that the origins of the SPR responses are very complex when combining SPR with living cells. In this work, we have presented an attempt to better understand the SPR responses in living cell sensing during apoptosis using HeLa cell monolayers with multiple parameters extracted from full angular SPR spectra recorded in real-time during cell stimulation with different concentrations of Propranolol as a model drug. In addition, SPR detection was compared to the theoretical curve from an averaging model which interprets the SPR response from cell confluency.

This present study indicates that different concentrations of propranolol have different modes of interaction with HeLa cells, which is reflected by both main SPR peak angular position, and the main SPR peak minimum intensity. SPR is a label-free technique that can detect a large range of apoptotic events simultaneously on the same cell population. Our experimental results demonstrate that the change in the area of the cell adhesion to a sensor chip is insufficient to explain the entire SPR response to the activation of living cell

REFERENCES

1. Bauer, J. H.; Helfand, S. L., New tricks of an old molecule: lifespan regulation by p53. *Aging Cell* **2006,** *5* (5), 437-40.

2. Nanda R. et al. p53 mutations in colorectal cancer. *Proc. Natl. Acad. Sci. USA* **1990,** *87*, 7555-7559.

3. Milena Gasco, S. S. a. T. C., The p53 pathway in breast cancer. *Breast Cancer Res* **2002,** *4*, 70-76.

4. Baritaki, S.; Militello, L.; Malaponte, G.; Spandidos, D. A.; Salcedo, M.; Bonavida, B., The anti-CD20 mAb LFB-R603 interrupts the dysregulated NF-kappaB/Snail/RKIP/PTEN resistance loop in B-NHL cells: role in sensitization to TRAIL apoptosis. *Int J Oncol* **2011,** *38* (6), 1683-94.

5. Jensen, M.; Engert, A.; Weissinger, F.; Knauf, W.; Kimby, E.; Poynton, C.; Oliff, I. A.; Rummel, M. J.; Osterborg, A., Phase I study of a novel pro-apoptotic drug R-etodolac in patients with B-cell chronic lymphocytic leukemia. *Invest New Drugs* **2008,** *26* (2), 139-49.

6. Tudos, A. J.; Schasfoort, R. B. M., Chapter 1. Introduction to Surface Plasmon Resonance. In *Handbook of Surface Plasmon Resonance*, 2008; pp 1-14.

7. Keith Burridge, K. F., Thomas Kelly, Glen Nuckolls, and Christopher Turner, FOCAL ADHESIONS: Transmembrane Junctions Between the Extracellular Matrix and the Cytoskeleton. *Ann. Rev. Cell Bioi.* **1988,** *4*, 487-525.

8. K.-F. Giebel, C. B., S. Herminghaus, M. Riedel, P. Leiderer, U. Weiland, and M. Bastmeyer, Imaging of Cell/Substrate Contacts of Living Cells with Surface Plasmon Resonance Microscopy. *Biophysical Journal* **1999,** *76*, 509–516.

9. Chabot, V.; Cuerrier, C. M.; Escher, E.; Aimez, V.; Grandbois, M.; Charette, P. G., Biosensing based on surface plasmon resonance and living cells. *Biosens Bioelectron* **2009,** *24* (6), 1667-73.

10. Ziblat, R.; Lirtsman, V.; Davidov, D.; Aroeti, B., Infrared surface plasmon resonance: a novel tool for real time sensing of variations in living cells. *Biophys J* **2006,** *90* (7), 2592-9.

11. Yanase, Y.; Suzuki, H.; Tsutsui, T.; Uechi, I.; Hiragun, T.; Mihara, S.; Hide, M., Living cell positioning on the surface of gold film for SPR analysis. *Biosens Bioelectron* **2007,** *23* (4), 562-7.

12. Horii, M.; Shinohara, H.; Iribe, Y.; Suzuki, M., Living cell-based allergen sensing using a high resolution two-dimensional surface plasmon resonance imager. *Analyst* **2011,** *136* (13), 2706-11.

13. Golosovsky, M.; Lirtsman, V.; Yashunsky, V.; Davidov, D.; Aroeti, B., Midinfrared surface-plasmon resonance: A novel biophysical tool for studying living cells. *Journal of Applied Physics* **2009,** *105* (10).

14. Hide, M.; Tsutsui, T.; Sato, H.; Nishimura, T.; Morimoto, K.; Yamamoto, S.; Yoshizato, K., Real-time analysis of ligand-induced cell surface and intracellular reactions of living mast cells using a surface plasmon resonance-based biosensor. *Anal Biochem* **2002,** *302* (1), 28-37.

15. Yanase, Y.; Suzuki, H.; Tsutsui, T.; Hiragun, T.; Kameyoshi, Y.; Hide, M., The SPR signal in living cells reflects changes other than the area of adhesion and the formation of cell constructions. *Biosens Bioelectron* **2007,** *22* (6), 1081-6.

16. Cuerrier, C. M.; Chabot, V.; Vigneux, S.; Aimez, V.; Escher, E.; Gobeil, F.; Charette, P. G.; Grandbois, M., Surface Plasmon Resonance Monitoring of Cell Monolayer Integrity: Implication of Signaling Pathways Involved in Actin-Driven Morphological Remodeling. *Cell Mol Bioeng* **2008,** *1* (4), 229-239.

17. Yashunsky, V.; Lirtsman, V.; Golosovsky, M.; Davidov, D.; Aroeti, B., Real-time monitoring of epithelial cell-cell and cell-substrate interactions by infrared surface plasmon spectroscopy. *Biophys J* **2010,** *99* (12), 4028-36.

18. Kosaihira, A.; Ona, T., Rapid and quantitative method for evaluating the personal therapeutic potential of cancer drugs. *Anal Bioanal Chem* **2008,** *391* (5), 1889-97.

19. Maltais, J. S.; Denault, J. B.; Gendron, L.; Grandbois, M., Label-free monitoring of apoptosis by surface plasmon resonance detection of morphological changes. *Apoptosis* **2012,** *17* (8), 916-25.

20. Robelek, R.; Wegener, J., Label-free and time-resolved measurements of cell volume changes by surface plasmon resonance (SPR) spectroscopy. *Biosens Bioelectron* **2010,** *25* (5), 1221-4.

21. Vala, M.; Robelek, R.; Bockova, M.; Wegener, J.; Homola, J., Real-time label-free monitoring of the cellular response to osmotic stress using conventional and long-range surface plasmons. *Biosens Bioelectron* **2013,** *40* (1), 417-21.

22. Baumgarten, S.; Robelek, R., Surface plasmon resonance (SPR) sensors for the rapid, sensitive detection of the cellular response to osmotic stress. *Sensors and Actuators B: Chemical* **2011,** *156* (2), 798-804.

23. Chabot, V.; Miron, Y.; Charette, P. G.; Grandbois, M., Identification of the molecular mechanisms in cellular processes that elicit a surface plasmon resonance (SPR) response using simultaneous surface plasmon-enhanced fluorescence (SPEF) microscopy. *Biosens Bioelectron* **2013,** *50*, 125-31.

24. Michaelis, S.; Wegener, J.; Robelek, R., Label-free monitoring of cell-based assays: combining impedance analysis with SPR for multiparametric cell profiling. *Biosens Bioelectron* **2013,** *49*, 63-70.

25. Lee, J. Y.; Ko, H. J.; Lee, S. H.; Park, T. H., Cell-based measurement of odorant molecules using surface plasmon resonance. *Enzyme and Microbial Technology* **2006,** *39* (3), 375-380.

26. Viitala, T.; Granqvist, N.; Hallila, S.; Ravina, M.; Yliperttula, M., Elucidating the signal responses of multi-parametric surface plasmon resonance living cell sensing: a comparison between optical modeling and drug-MDCKII cell interaction measurements. *PLoS One* **2013,** *8* (8), e72192.

27. Vikholm-Lundin, W. M. A. a. I., Surface Plasmon Resonance on Nanoscale Organic Films In *Nino-Bio-Sensing*, Carrara, S., Ed. Springer Science+Business Media: 2011.

28. Sadowski JW, K. I. J., Peltonenjpk JPK, Characterization of thin films and their structures in surface plasmon resonance measurements. . *Opt Eng.* **1995,** *34*, 2581–6.

29. D. Max Parkin, M. F. B. J. F. P. P., PhD, Global Cancer Statistics, 2002. *CA Cancer J Clin* **2005,** *55*, 74–108.

30. Force, U. S. P. S. T.; Grossman, D. C.; Curry, S. J.; Owens, D. K.; Barry, M. J.; Davidson, K. W.; Doubeni, C. A.; Epling, J. W., Jr.; Kemper, A. R.; Krist, A. H.; Kurth, A. E.; Landefeld, C. S.; Mangione, C. M.; Phipps, M. G.; Silverstein, M.; Simon, M. A.; Tseng, C. W., Screening for Ovarian Cancer: US Preventive Services Task Force Recommendation Statement. *JAMA* **2018,** *319* (6), 588-594.

31. Shapira, I.; Oswald, M.; Lovecchio, J.; Khalili, H.; Menzin, A.; Whyte, J.; Dos Santos, L.; Liang, S.; Bhuiya, T.; Keogh, M.; Mason, C.; Sultan, K.; Budman, D.; Gregersen, P. K.; Lee, A. T., Circulating biomarkers for detection of ovarian cancer and predicting cancer outcomes. *Br J Cancer* **2014,** *110* (4), 976-83.

32. Bianca Marchetti, P. G. S., Martin Plante, Patrick Poyet, Nicole Foll, Georges Pelletier, and Fernand Labrie, Beta-adrenergic receptors in DMBA-induced rat mammary tumors: Correlation with progesterone receptor and tumor growth. *Breast Cancer Research and Treatment* **1989,** *13*, 251-263.

33. G. RE, P. B., A. NOVELLI, C. GIRARDI and F. DI CARLO, EVIDENCE FOR FUNCTIONAL BETA-ADRENOCEPTOR SUBTYPES IN CG-5 BREAST CANCER CELLS. *Pharmacological Research, Vol. 33, No. 4/5, 1996* **1996,** *33*, 255-260.

34. Wang, F.; Liu, H.; Wang, F.; Xu, R.; Wang, P.; Tang, F.; Zhang, X.; Zhu, Z.; Lv, H.; Han, T., Propranolol suppresses the proliferation and induces the apoptosis of liver cancer cells. *Mol Med Rep* **2018,** *17* (4), 5213-5221.

35. Alexa Montoya, T. C., Geri Villanueva, Clarissa N. Amaya, Steven Rains et. al., Use of non-selective β-blockers is associated with decreased tumor proliferative indices in early stage breast cancer. *Oncotarget* **2017,** *8*, 6446-6460.

36. Iseri, O. D.; Sahin, F. I.; Terzi, Y. K.; Yurtcu, E.; Erdem, S. R.; Sarialioglu, F., beta-Adrenoreceptor antagonists reduce cancer cell proliferation, invasion, and migration. *Pharm Biol* **2014,** *52* (11), 1374-81.

37. Eddy Pasquier, J. C., Manon Carre, Sarah Giacometti,et. al., Propranolol potentiates the anti-angiogenic effects and antitumor efficacy of chemotherapy agents: implication in breast cancer treatment. *Oncotarget* **2011,** *2*, 797 - 809.

38. Cole, S. W.; Sood, A. K., Molecular pathways: beta-adrenergic signaling in cancer. *Clin Cancer Res* **2012,** *18* (5), 1201-6.

39. Coelho, M.; Moz, M.; Correia, G.; Teixeira, A.; Medeiros, R.; Ribeiro, L., Antiproliferative effects of beta-blockers on human colorectal cancer cells. *Oncol Rep* **2015,** *33* (5), 2513-20.

40. Akbar, S.; Alsharidah, M. S., Are beta blockers new potential anticancer agents? *Asian Pac J Cancer Prev* **2014,** *15* (22), 9567-74.

41. Coelho, M.; Soares-Silva, C.; Brandao, D.; Marino, F.; Cosentino, M.; Ribeiro, L., beta-Adrenergic modulation of cancer cell proliferation: available evidence and clinical perspectives. *J Cancer Res Clin Oncol* **2017,** *143* (2), 275-291.

42. Chengfang Zhou, X. C., Weiqi Zeng, Cong Peng et. al., Propranolol induced G0/G1/S phase arrest and apoptosis in melanoma cells via AKT/MAPK pathway. *Oncotarget* **2016,** *7*, 68314-27.

43. Zhao, S.; Fan, S.; Shi, Y.; Ren, H.; Hong, H.; Gao, X.; Zhang, M.; Qin, Q.; Li, H., Propranolol induced apoptosis and autophagy via the ROS/JNK signaling pathway in Human Ovarian Cancer. *J Cancer* **2020,** *11* (20), 5900-5910.

44. Moreira, B.; Tuoriniemi, J.; Kouchak Pour, N.; Mihalcikova, L.; Safina, G., Surface Plasmon Resonance for Measuring Exocytosis from Populations of PC12

Cells: Mechanisms of Signal Formation and Assessment of Analytical Capabilities. *Anal Chem* **2017,** *89* (5), 3069-3077.

45. Hinman, S. S.; Ruiz, C. J.; Drakakaki, G.; Wilkop, T. E.; Cheng, Q., On-Demand Formation of Supported Lipid Membrane Arrays by Trehalose-Assisted Vesicle Delivery for SPR Imaging. *ACS Appl Mater Interfaces* **2015,** *7* (31), 17122-30.

46. Fang, Y., Label-Free Cell-Based Assays with Optical Biosensors in Drug Discovery. *ASSAY and Drug Development Technologies* **2006,** *4*, 583-95.

47. Ji, Y.; Chen, S.; Xiao, X.; Zheng, S.; Li, K., beta-blockers: a novel class of antitumor agents. *Onco Targets Ther* **2012,** *5*, 391-401.

48. Fang, Y.; Ferrie, A. M.; Fontaine, N. H.; Mauro, J.; Balakrishnan, J., Resonant waveguide grating biosensor for living cell sensing. *Biophys J* **2006,** *91* (5), 1925-40.

49. Deng, S.; Yu, X.; Wang, P., An irregular-shaped homogeneous refractive index model for interpretation of the surface plasmon resonance response from living cell attachment. *Analytical Methods* **2016,** *8* (16), 3301-3306.

CHAPTER 4: Approach Toward Fundamental Understanding and Smart Design of Sensing Interface for Protein Detection by SPR

ABSTRACT

Protein biomarkers in the blood act as a molecular sign of complex diseases such as cancer, cardiovascular disease, and Alzheimer's disease. Rapid and sensitive detection of the protein facilitates the diagnosis of the disease in an early stage. Usually, increasing the biomarker level in the blood reflect the presence of disease; however, some other protein biomarkers such as amyloid-beta, the Alzheimer's disease biomarker, have a different sign of toxicity: aggregation from monomers to small oligomer structures.

SPR could provide a rapid and convenient method for protein biomarker detection. However, like any other biosensor, developing a proper interface that binds to the target protein is a critical step for the SPR experiment. Therefore, in this work, we investigated protein immobilization on a different kind of interface using two approaches, with IgE was chosen as a target protein. The first approach was a covalent coupling of IgE to MUA SAM-based surface, and the second approach was affinity coupling of IgE to thiolated anti-IgE modified surface. Our results show higher protein binding capacity on the anti-IgE interface compared to the binding capacity on the MUA surface. At the same time, performing SPR signal amplification using an AgNP conjugate represents a higher SPR enhancement signal for IgE that is coupled to the affinity surface. Improper orientation of IgE on the MUA surface results in steric hindrance and less IgE binding capacity on the chip surface. Interestingly, our results demonstrate that even though less IgE is coupled to

the MUA surface, most of them bind to the surface in such a way that the IgE epitope is available and exposed to the solution to facilitate the binding of the aptamer conjugated to AgNP.

In addition, we investigated Aβ (15-27) and Aβ (28-40) conformation change near the lipid bilayer using a molecular dynamic simulation (MDS). Analyzing the simulation results revealed that the helix/coil starting structure in both fragments (N- and C-terminus) adapted to a turn/coil structure at the end of the simulation time. RMSD analysis demonstrated that C-terminus, Aβ (28-40), quickly adapted the turn structure at the beginning of the simulation time while the N-terminus, Aβ (15-27), gradually moved to the turn structure with more fluctuation compared to C-terminus. In addition, the POPC bilayer structure also changed during both simulations performed in this study.

INTRODUCTION

Protein biomarkers in blood serve as molecular signatures of complex diseases such as cancer,[1-3] cardiovascular disorders,[4] and other pathological situations.[5, 6] Hence, sensitive and rapid protein detection provides valuable information about the presence and course of a disease that could improve the survival rate of patients. However, a biomarker may be present at very low levels (e.g., sub-ng/mL) in the blood, which requires a large sample volume and a long processing time for classical biomarker analysis techniques to detect (e.g., enzyme-linked immunosorbent assay (ELISA)).

A suitable detection strategy should offer high throughput, high signal-to-noise ratio, good resolution, reproducible results, and high sensitivity and specificity.[7] The

optimal detection method meeting such criteria is still under consideration; however, surface plasmon resonance (SPR) has been highlighted as a leading technology for the study of real-time protein-protein interaction kinetics, providing feasibility for multichannel biosensing.[8] SPR is advantageous due to its ability to generate quantitative measurements with a lack of labeling variations associated with optical labels such as fluorescent dyes. Additionally, nanoparticle labels on detection antibodies in a sandwich assay format can also be used to enhance the signal.[9, 10]

Protein detection in a solution based on SPR assay typically relay on the immobilization of capture reagent molecules onto a gold surface. The role of the capture reagent is to specifically bind to the target protein molecules. Binding of the target protein to the capture reagent results in a measurable change in the refractive index. In a sandwich assay, a second affinity reagent bind to a different epitope on the target protein, forming a "sandwich". For Surface modification and immobilization techniques, capture reagent molecules have to be immobilized to the metal surface in a way that avoids non-specific adsorption and retains the bioactivity of target proteins.[11] Therefore, developing proper surface chemistry is crucial for a successful SPR experiment. Physical adsorption is simple and has the advantage of immobilizing a large number of biomolecules on the surface. Bovine serum albumin (BSA) is attached on gold surface via direct physical adsorption and stays immobilized under mild rinsing conditions. Then, antibodies can be immobilized on gold surfaces through antibody-BSA conjugates; this method has been applied in detection of low molecular weight analytes such as TNT[12]. In addition, avidin has been used as a bridge to connect biotin-antibody to biotin-BSA adsorbed surface.[13]

More often, proteins are covalently bound to the immobilization support through accessible functional groups of exposed amino acids. Covalent bonds are mostly formed between side-chain-exposed functional groups of proteins with suitably modified supports, resulting in an irreversible binding and producing a high surface coverage. The amine groups of proteins are the most used moieties for covalent immobilization. Lysines are present in most proteins, and can make up 6%[14] to over 10%[15] of the overall amino acid sequence and are frequently located on the surface of the protein. Lysines are very reactive toward electrophilic agents without the need to be activated and provide good stability.[16-18] The immobilization of proteins using the carboxylic side chains is also interesting since glutamic and aspartic acid constitute a major fraction of the surface exposed amino acids.[7] The carboxylic acid function of these amino acids, along with the C-terminus, can react with amines using the routine coupling chemistry also used for solid phase peptide synthesis. This coupling reaction is activated by a carbodiimide like N, N′-dicyclohexyl carbodiimide (DCC), or EDC and results in a rapid and quantitative formation of a peptide bond.

A commonly used interface method to selectively modify surfaces toward covalent protein coupling is the use of a self-assembled monolayer (SAM) on the gold surface, which increases the degree of freedom of the protein molecules. The surface density of protein molecules can be conveniently controlled with this method. In addition, it helps in minimization of nonspecific protein sorption on the SPR chip.[19] Furthermore, SAM-based technology provides good stability under extreme pH and temperature.[20] Usually proteins are covalently attached via alkanethiols containing carboxylic[21] or amine functional[22]

groups among other SAM1`s functional groups. Carboxylic acid groups can be activated by 3-(3-dimethylaminopropyl)-carbodiimide (EDC) and N-hydroxysuccinimide (NHS) to form a semi-stable NHS ester, which reacts with an amine in the following reaction to form the amide bond.

Other reagents can be used as well; however, the experimental condition has to be optimized. Pei et al.[23] study the effect of activation reagents on immobilizing antibodies on a carboxyl-functionalized surface. The carboxylic acids were activated with 1-ethyl-3-(3-dimethylaminopropyl) carbodiimide (EDC), EDC/NHS, or EDC/sulfo-NHS toward the coupling of a monoclonal antimyoglobin antibody at pH 4.0. The results showed that the immobilization was most effective for EDC/sulfo-NHS activation. This difference can be explained by electrostatic attraction versus repulsion forces between the activated interface and the protein at these reaction conditions. Since the antibody has a pI of 7−8, it will be positively charged at pH4.0, while the surface charge is positive, neutral, and negative for EDC, NHS, and sulfo-NHS, respectively. EDC esters are, however, also considered to be rather unstable in aqueous solutions, so deactivation before the introduction of sample is possible. This study clearly shows that electrostatic attraction can be essential for successful immobilization and that this is highly dependent on the pKa of the surface functional groups, the protein pI, and the pH of the reaction buffer.

Covalent binding of protein via side chains of amino acids is often random, since it is based upon residues typically present on the exterior of the protein. Therefore, the attachment may occur simultaneously through many residues, enhancing heterogeneity of immobilized proteins. This was investigated by Wang et al.[24] who immobilized ricin (a

highly toxic protein that is an inhibitor in protein synthesis) on a gold surface using an NHS ester. Ricin has nine lysine residues on its surface, which, by reacting with NHS, were supposed to determine which side of the ricin structure is in contact with the interface and which side is exposed to the solution. The authors then visualized single ricin molecules in situ by using an AFM tip modified with an antiricin aptamer and observed different conformations due to the covalent coupling of the different lysines. This confirms that variable orientations of the protein on the substrate surface appear when multiple and accessible lysine residues are present in the protein structure.

However, covalent immobilization of proteins based on endogenous amino acid chemistry is not necessarily entirely random but can result in surface coatings in which the majority of the proteins have a similar or even unique orientation. This is illustrated by Fuentes et al.[25] who immobilized horseradish peroxidase (HRP) on agarose which was functionalized with glyoxyl, glutaraldehyde, or cyanogen bromide (BrCN), functional groups that can react with the present amino groups in the protein.

Glyoxyl-agarose has a dense layer of linear aldehyde groups, which reacts with primary amino groups in the protein[18, 25] to form a Schiff's base.[26] This Schiff's base has to be reduced to transform them into stable covalent bonds. This immobilization stables at Alkaline pH (around pH 10.0) which leads to a multipoint immobilization. Functional groups in glutaraldehyde-agarose and Br-CN-agarose are able to immobilize a protein at pH (7-8.5). Therefore, only the terminal amino group will preferentially react and multipoint covalent immobilization may not be very high.[27] This means that at neutral pH, the reactivity of the terminal amine group will be significantly higher than the reactivity of

the protonated ε-amine group and proteins will first be immobilized with this terminal amine group, provided it is accessible. In other words, the orientation is determined by the reaction procedure and conditions.[18] Although the ε-amino group of lysine is probably the most abundant primary amino group at the surface of a protein, only nonprotonated amino groups will be nucleophilic enough to react. The pKa of a surface exposed ε-amine group of lysine is typically that of the free amino acid, around 10.5, while the terminal amine group has a pKa value of 7−8.[18, 28] Although there may be other lysine residues with altered pKa values present, these are likely to be located at internal pockets in microenvironments not accessible for immobilization reactions.[18] Therefore, chemical attachment can also be guided in an orderly manner to attain oriented immobilization.[17]

Biochemical affinity reactions offer a gentle oriented immobilization of proteins, providing an important advantage over other immobilization techniques. Moreover, not only oriented and homogeneous attachment is obtained.[7, 29, 30], but it is also possible to detach proteins and make repeated use of the same surface using chemical treatment, pH change, or heat treatment.[31, 32] In most of cases, bioaffinity interactions are used in conjunction with other immobilization mechanisms (i.e., physisorption and covalent bonding) with the bioaffinity reagent used as an intermediate binding molecule between the surface and proteins.

Antibodies have an exceptional specificity toward binding partner. Due to their high affinity and specificity, they are key reagents for protein detection.[33] Antibodies have multiple reactive side chains that can serve as attachment sites for conjugation to solid supports, such as gold surface or nanoparticles, or labels that act as signal enhancer.

Antibodies are usually covalently attached to surfaces or detection labels. However, covalent conjugation may affect interaction with the target protein. Modifying a molecule that can interact with the antibody such as protein A may overcome this challenge. Protein A has a strong affinity for the constant region (Fc) of various antibodies (goat and human among other species).[34] Thus, the variable Fab region of the antibody is accessible to antigen binding.[29]

Given that thiol moieties have a high affinity to conjugate with gold surfaces via Au–S bonds, chemically modifying biological molecules such as antibodies which anchor them to the gold surface through Au–S interaction, is regarded as attractive. Wang et al.[35] used Traut`s reagent to anchor thiol groups into antibodies. However, this does not control the linking orientation of the antibodies to the nanoparticle. Therefore, using a heteriofunctional linker such as (PEG6-$CONHNH_2$) and (SH-PEG-NH_2) by specifically reacting with the carbohydrate moiety and carboxyl group respectively in the Fc portion of the antibody can direct the conjugation orientation as they describe.

Aptamers are single-stranded DNA or RNA oligonucleotides bioaffinity capture reagents that have drawn significant attention. They can bind to proteins with high affinity and specificity.[36, 37] First described in 1990,[38, 39] aptamers are created by an *in vitro* process known as SELEX, systemic evolution of ligands by exponential enrichment. Aptamers have several advantages for use as affinity reagents such as low cost, high stability, and high specificity, with dissociation constants in the femtomolar to picomolar range. [40-42] Additionally, DNA aptamers are highly stable reagents such that bound proteins can be removed either chemically or thermally to regenerate the free aptamer for another round of

binding. Aptamers can be easily integrated into many protein assay formats by substituting for antibodies and are easily labeled and modified with various molecules and functional groups.

Generally, Affinity interfaces used for protein immobilization and detection provide oriented and homogenous attachment of protein and surface regeneration. One potential drawback, however, is that affinity immobilized protein may not be tethered to the surface as strongly as covalently immobilized protein, and there is a risk that the protein could be washed off during an experiment or upon regeneration of the surface. [43] On the other hand, covalently immobilized proteins are attached stably to the surface, but oriented randomly via any free amine, so only a subset of the probes may be oriented for optimal binding. However, oriented immobilization could be achieved.

Consequently, choosing a proper interface for protein immobilization and detection is critical for successful SPR experiments. The main issue addressed in the present work is therefore, strategies for coupling protein molecules to gold surface for detection using two approaches: covalent coupling and affinity coupling. IgE was chosen as the target protein biomarker molecule.

Immunoglobulin E (IgE) is a glycoprotein with an average molecular mass of 188 kDa, the shortest half-life, and the lowest concentration in serum of all the immunoglobulins (IgG, IgA, IgM, IgD, IgE).[44] For several decades, much attention has been paid to IgE because it plays a very important role in the development of allergies and parasitic diseases. An allergy is an abnormal immunological response due to sensitization

to some components from the environment or food for example. It today represents a major health problem, affecting 10-20% of the general population worldwide, especially in industrialized countries.[45]

Briefly, the mechanism of IgE-mediated allergic reaction involves antigen presentation, IgE production, mast cell activation, mediator release, and symptom exhibition.[46] Typical IgE concentration in a newborn child is extremely low (<1.3 KIU/L where 1 IU = 2.4 ng). It then increases steadily during childhood, reaching its highest level between the age of 15 and 35, and thereafter it remains constant until the age of 60, when a slow decrease begins.[47] The average total IgE concentration in a healthy adult is about 90 kIU/L.[48] Higher levels usually reflect the presence of allergy. Consequently, investigation of a proper interface for IgE detection as an allergic biomarker is important for disease diagnosis.

Some other protein biomarkers such as in Neurodegenerative disorders, including Alzheimer's disease, have a different mechanism of toxicity namely, aggregation of unfolded peptides into oligomers that coalesce to form an ordered fibril.[49, 50]

The actual folding fate of amyloid-beta (Aβ) in situ is critically dependent not only on its concentration but also on its immediate biochemical or possible pathologically altered environment. [51-53] In this aggregation process, the steps involved in the initiation of aggregation from monomers to small oligomer structures are not well determined. There are many aspects of cellular function that may play a significant role in the early stages of Aβ aggregation, such as cellular pH,[54] salt concentration,[55] and interactions of Aβ with

metal ions.[56] However, one hypothesis that shows promise for explaining both the early steps of aggregation and the effect of certain risk factors in Alzheimer's disease is the interaction between Aβ and cellular membranes.[57-59] This hypothesis postulates that Biological membranes potentially modulate the pathological conversion of structurally and functionally proteins into amyloidogenic assemblies. To this end, we aim to use a bilayer cell membrane as an interface to investigate Aβ conformation change near lipid bilayer using MD simulation.

Molecular dynamics (MD) simulations predict how every atom in a protein or other molecular system will move over time based on a general model of the physics governing interatomic interactions.[60] These simulations can capture a wide variety of important biomolecular processes, including conformational change, ligand binding, and protein folding. This reveals the positions of all of the atoms at femtosecond temporal resolution,[61] which is very difficult for any experimental techniques. In addition, the simulation conditions are precisely known and can be carefully controlled: the initial conformation of a protein, which ligands are bound to it, whether it has any mutations, which other molecules are present in its environment, its protonation state, the temperature, the voltage across a membrane, and so on.[61] By comparing simulations performed under different conditions, one can identify the effects of a wide variety of molecular perturbations.

More frequently, simulations are used to generate a qualitative understanding of how a biomolecule or drug works. Usually, in such cases, no experiment is available that could provide all of the same information as the simulations. Experiments can, however, be designed to test specific predictions from these simulations to more broadly validate the

simulation results.[60, 61] Perhaps even more importantly, simulations can generate hypotheses that lead to new experimental work. [61]

EXPERIMENTAL

Materials

Human IgE and goat anti-human IgE were purchased from Sigma Millipore, Human IgE aptamer was purchased from Integrated DNA Technologies (IDT), Bis[2-(2-bromoisobutyryloxy)undecyl] disulfide, 11-mercaptoundecanoic acid (MUA), 2-hydroxyethyl methacrylate (HEMA), CuBr, 2,2'-bipyridyl (bpy), L-ascorbic acid (AA), N-hydroxysuccinimide (NHS), 1-(3-dimethylaminopropyl) -3-ethylcarbodiimide hydrochloride (EDC), silver nitrate ($AgNO_3$), trisodium citrate (TSC), tannic acid (TA), Tris (2-carboxyethyl) phosphine (TCEP) were obtained from Sigma-Aldrich. All proteins solutions were prepared in 20 mM phosphate buffered saline (containing 150 mM NaCl, pH 7.4). Amicon centrifugal filter devices, MWCO 10 kDa was purchased from Sigma-Aldrich. Crystal structure of Amyloid-beta protein was obtained from Protein Data Bank (PDB ID: 1AML) (https://www.rcsb.org/). Coordinate and topology files of Phospholipid bilayer POPC were built using VMD software. Molecular Dynamic calculation was performed using NAMD software. VMD software is used to visualize and analyze the MDS output

Surface Plasmon Resonance Measurements

A dual-channel SPR spectrometer NanoSPR-321 (NanoSPR, Addison, IL) with a GaAs semiconductor laser light source (λ = 670 nm) was used for all SPR measurements. The device comes with a high-refractive index prism (n = 1.61) and a 30 μL flow cell. SPR gold chips were fabricated with a 2 nm thick chromium adhesion layer, followed by deposition of a 46 nm thick gold layer via e-beam evaporation onto cleaned BK-7 glass slides based on previously published procedures.[62]

Thiolation of anti-IgE by Cysteamine ($HS\text{-}CH_2\text{-}CH_2\text{-}NH_2$)

The procedure follows a protocol previously reported [35] with some modification. First, carboxyl groups on anti-IgE were activated by incubation of 0.25 mg/ml of anti-IgE with EDC/NHS (1:4) molar ratio, and the extra reagent was removed by centrifugal filtration (Amicon, MWCO 10 KDa). After activation of the carboxyl groups, anti-IgE was incubated with cysteamine to form amide linkage between the carboxyl groups of anti-IgE and the amine group of $HS\text{-}CH_2\text{-}CH_2\text{-}NH_2$. Again, thiolated antibodies were cleaned up from excess reagent through centrifugal filtration (Amicon, MWCO 10 kDa).

Immobilization of thiolated anti-IgE

Prior to immobilization, a mixture of thiolated anti-IgE and cysteamine (1:10 molar ratio) in PBS buffer was mixed with 100 mM DTT. The gold substrate was extensively rinsed with copious ethanol and DI water. After that, the chip was dried under an N2 stream and clamped to a flow cell on a prism. After flowing the buffer to reach a steady state, 30 μL thiolated anti-IgE/cysteamine immobilization solutions were injected into the flow cell.

They were then incubated for 1 h. Our group previously described this protocol for immobilization of thiolated aptamer on a gold surface.[63]

Preparation of AgNP

Silver nanoparticles were prepared according to the previous report [64] with some modifications. Briefly, 100 mL volume of an aqueous solution containing trisodium citrate (TSC) (5 mM) and tannic acid (TA) (0.1 mM) was prepared in glassware previously cleaned with aqua regia (3:1 HCl to HNO3). This solution was heated to 90°C under vigorous stirring. Then, 1 mL of AgNO3 (25 mM) was added with continued heating and stirring for about 15 min or until a dark yellow solution formed. Next, the solution was allowed to cool to room temperate and stored at 4°C in a dark glass bottle. AgNP were purified by centrifugation (15000 xg/ 20 min) in order to remove excess TA and further redispersed in Milli-Q-water before sample characterization and conjugation.

Preparation of AgNP-aptamer-initiator

AgNP were conjugated with a thiolated IgE-aptamer and initiator in a 1:1 ratio according to a protocol previously reported [65] with some modification. First, the disulfide bond of the aptamer and the initiator were reduced by TCEP (25 µl 100µM of aptamer or the initiator were incubated with 25 µl 20 mM TCEP in dark for 1h). Then, the purified AgNP were concentrated by a factor of 3 and 1 ml of concentrated AgNP, deprotected aptamer (100µl, 10µM) and deprotected initiator (100µl, 10µM) were mixed at room temperature. After standing for at least 18 h, the pH value of the solution was adjusted by adding 122µl of 1 x PBS and reacting for 6 h. Then 21 µl of 2M NaCl solution was added.

This operation was repeated 3 times at the interval of 3h to make sure that the concentration of NaCl would grow gradually. After an additional incubation of at least 48 h, excess reagents were removed by centrifugation (15 min, 15000 Xg, for 3 times). The resulting precipitate of AgNP-aptamer-initiator was washed and recentrifuged in 0.1 PBS and resuspended in 1ml of 0.1 PBS.

Membrane/peptide preparation

Amyloid beta-peptide ($A\beta_{40}$) was retrieved from Protein Database (PDB) ID:1AML which has the following sequence [Asp - Ala - Glu - Phe - Arg - His - Asp - Ser - Gly - Tyr - Glu - Val - His - His - Gln - Lys - Leu - Val - Phe - Phe - Ala - Glu - Asp - Val - Gly - Ser - Asn - Lys - Gly - Ala - Ile - Ile - Gly - Leu - Met - Val - Gly - Gly - Val – Val] and then the two fragments were taken from the same structure. The first fragment is the amino acid sequence from 28 to 40, which represents the hydrophobic C-terminus of Amyloid-beta. The second fragment is sequenced from 15 to 27 which represents charged N-terminus. They are abbreviated Aβ (28-40) and Aβ (15-27), respectively. All structures from the PDB were edited using VEGA ZZ software to add missing hydrogen, assign force field parameters and convert the structures to a united atom format described by the Charmm force field. Gasteiger partial charges were assigned as well. Topology and coordinate files for each fragment were built using VMD before the minimization step, which was performed to get rid of any possible bad contacts.

Phospholipid bilayer zwitterions POPC were used as a model of cell membranes. The coordinates and topology files for the hydrated POPC bilayer were built using VMD.

The membrane was built in the XY plane where X=30 and Y=30. Water molecules, lipid, and then the whole system (lipid with water) were minimized using 2000 steps, respectively. After that, both membrane psf/pdb and Aβ (28-40) fragment psf/pdb were loaded in VMD. First, the membrane was aligned with its center of mass using TK Console Window and then the Aβ (28-40) fragment was moved above the membrane. This easily can be done by hitting the "8" key to switch VMD in the "move molecule" mode. The following step was to combine the membrane/Aβ (28-40) files into one set of PSF and PDB files using TK Console Window. The same steps were done to combine the membrane/ Aβ (15-27) files into one set of PSF and PDB files as well. Each system POPC/Aβ (28-40) and POPC/Aβ (15-27) were subjected to whole system minimization.

Molecular Dynamic Simulation

The two systems (POPC/Aβ 15-27, and POPC/Aβ 28-40) were subjected to an equilibrium process in which temperature raised gradually from 50 to 250 K. Then simulations were run for each system for 250 ps with 1fs time step. The MD simulations were carried out with NVT ensemble, i.e., a constant number of particle (N), volume (V), and temperature (T), and periodic boundary condition was used as well. The temperature was held constant at 300 K using Langevin thermostat (NAMD) and a distance cutoff of 12 Å was used as a switching cutoff function.

RESULTS AND DISCUSSION

Protein biomarkers in blood serve as a molecular sign of complex diseases such as cancer[1-3], and other pathological situations such as Alzheimer's disease[6]. Sensitive and

rapid protein detection facilitates the diagnosis and treatment of diseases in the early stages. Classical biomarker analysis techniques (e.g., enzyme-linked immunosorbent assay (ELISA)) require large sample volumes and long processing times. Biosensors such as SPR could provide a rapid and convenient alternative to conventional analytical methods. In general, biosensors consist of two parts, i.e., a transducer and a biological (or chemical) interface, which lead to the variation of a physical quantity when the protein of interest binds to the sensor system. The biological interface in immunosensors consists of antibodies that need a linker layer to be attached to the transducer surface (gold surface). Other biological interfaces that can be used for protein detection are an aptamer and a lipid bilayer assembling cell membrane. A chemical interface such as a self-assembled monolayer (SAM) can be used as well, where the exterior amino acid of the target protein is covalently attached to the SAM surface. Afterward, target proteins are recognized by an affinity reagent.

There are two common formats for protein assays, label-free assays, and sandwich assays. Both label-free and sandwich assays require the biological or chemical interface that binds to the target protein. In the label-free assay, binding of the target protein to the interface results in a measurable change in SPR angle. In the sandwich assay, a second affinity reagent binds to a different epitope on the target protein, forming a "sandwich." Additionally, nanoparticle labels on detection antibodies or aptamer can also be used to enhance the SPR signal.[66, 67]

Developing a proper interface for protein detection is important for a successful SPR experiment. Therefore, in this work we aim to investigate the protein immobilization

on different kinds of interfaces; IgE was chosen as a target protein. The first approach was a covalent coupling of IgE to MUA SAM-based surface; the second approach was affinity coupling of IgE to a thiolated anti-IgE modified surface. Thereafter, we investigated the SPR signal enhancement with IgE-aptamer/initiator coated silver nanoparticles using the two approaches. Moreover, we investigated amyloid-beta protein structure change near the lipid bilayer using molecular dynamic study.

Characterization of AgNP and AgNP-apt-init conjugate.

The functionalization of AgNP is characterized by UV spectroscopy as the position of the surface plasmon (SP) band of AgNP is sensitive to the local chemical environment and that the SP bandwidth is associated with particle size distribution. Therefore, the absorption spectra of AgNP were used to monitor AgNP conjugation and polymerization. After the modification of aptamer and initiator molecules, a shift from 408nm (AgNP) to 413 nm (AgNP-apt-init) was observed (Fig.4.1). According to previous studies [68], the poly-adenine (poly-A) sequence could be used to prevent the aggregation of silver nanoparticles, so the polyadenine (A15) at the attaching side of the aptamer was selected to stabilize the nanoparticles and increase the efficiency of modification. A thiolated initiator with ten methyl groups as a spacer was chosen to give the accessibility for the polymerization step to take place.

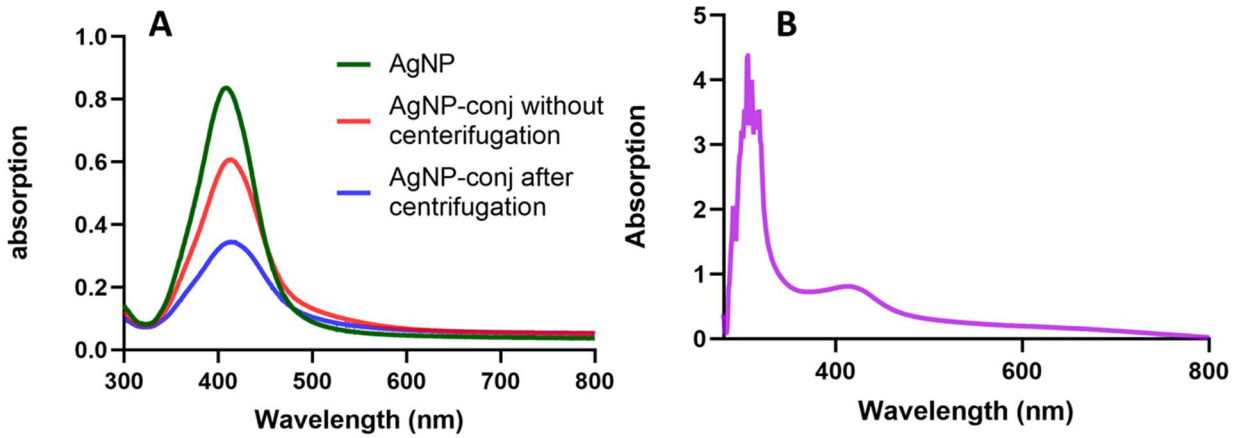

Figure 4. 1 UV-VIS characterization of AgNP surface modification (A) AgNP, green curve, AgNP conjugate without centrifugation, red line, and AgNP conjugate with centrifugation, blue curve. (B) PHEMA grew on AgNP.

The maximum absorbance (OD) of AgNP was 1.03, and that of the AgNP conjugate after centrifugation was 0.494 (Fig. 4.1). Herein, according to the Beer-Lambert law, the average yield of the AgNP-conjugate was estimated to be 48% by the ratio of OD.

To confirm the attachment of the initiator to the AgNP surface, solution-phase ATRP was conducted by mixing AgNP-apt-init with HEMA in the presence of the catalyst under nitrogen protection. The formation of poly (2-hydroxyethyl methacrylate) (PHEMA) on the AgNP-apt-init surface in 30 min shifted the surface plasmon band of particles to 435 nm (Fig. 4.1B). This peak shift was attributed to the increased local dielectric constant surrounding particles upon polymer formation. In addition, an absorption peak was observed around 300 nm, which is identified as a characteristic peak for UV spectrum pf PHEMA.[69]

The successful polymer coating on AgNP was also characterized by Nanoparticle Tracking Analysis (NTA) (Fig. 4.2). The hydrated diameter of the particle increased after the ATRP reaction. Increasing particle size distribution after polymer growth has been reported[69, 70]

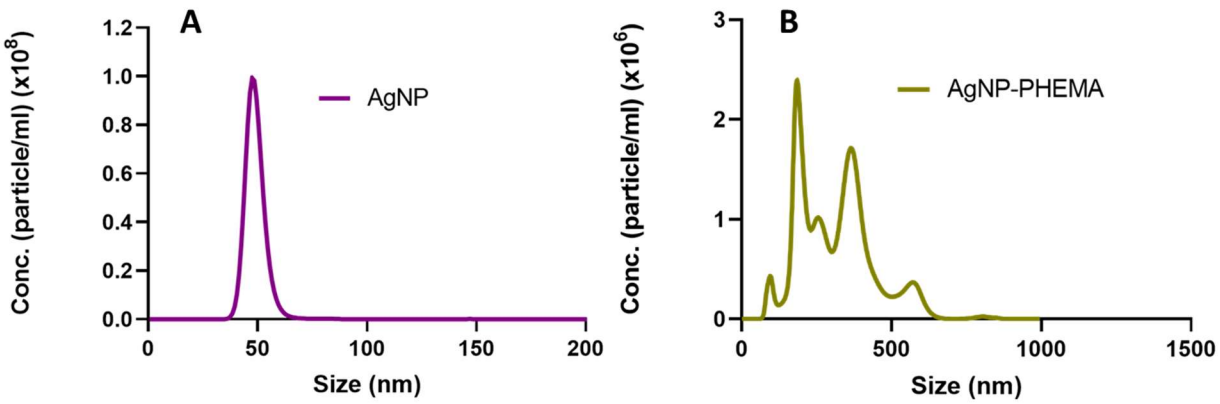

Figure 4. 2 Nanoparticle tracking analysis (NTA) of AgNP (left figure) and AgNP coated with initiator and aptamer after ATRP reaction (right figure).

SPR analysis of IgE immobilization by covalent and affinity interface

The foundation of most covalent attachment chemistries on gold is a self-assembled monolayer (SAM) of alkane-thiols terminating in a functional group such as a free carboxyl group. This foundation exploits three characteristics of alkanethiols: (i) the thiol sulfur interacts with gold to form a strong, stable bond [71]; (ii) the methylene chains stack via van der Waals forces to drive the spontaneous organization into SAMs [72]; and (iii) the tail group is available to form an irreversible linkage with amino acid residue on the protein exterior. SAM of 11-mercapto undecanoic acid was used for this study to attach IgE covalently to the gold surface.

Due to high antibody affinity and specificity, antibodies are key reagents for protein detection.[33] Therefore, anti-IgE was used as a capture reagent for IgE detection. Anti-IgE as any other antibodies have multiple reactive side chains that can serve as attachment sites for conjugation to solid supports. The immobilization of antibodies on gold supports is carried out using bifunctional reagents containing thiol groups, which bind strongly to the gold surface.[73] On the other hand, the biomolecule itself can be modified with a sulfhydryl group that enables direct immobilization on gold.[35] Therefore, in this work, anti-IgE was chemically modified to anchor thiol groups into them through the reaction of amine groups of cysteamine with carboxyl groups in the anti-IgE by using EDC/NHS.

Influence of each immobilization technique used in this study on surface concentration of immobilized IgE and observed binding kinetics

The red line in Figure 4.3B represents SPR data for IgE immobilization by covalent coupling over the MUA monolayer. The gold substrate was incubated in 1mM MUA ethanol solution for 18 hours to form a self-assembled monolayer with carboxyl functional groups on the surface. After extensive rinsing with copious ethanol and DI water, the chip was dried under an N2 stream. The gold substrate was then clamped to a flow cell on a prism. To activate the carboxylic acid group, EDC (0.4M)/NHS (0.1M) solution was injected into the flow cell and incubated for 30 min. After rinsing with PBS buffer, 40 μg/ml IgE in PBS was injected and incubated for 30 min to allow formation of covalent amide linkage. Passivation of the unused activated carboxyl groups (N-hydroxysuccinimide ester) was performed by incubation with blocking buffer solution

(PBS with1% BSA and 0.1% tween 20) for 1h (data not shown), which was followed by 10 min rinsing.

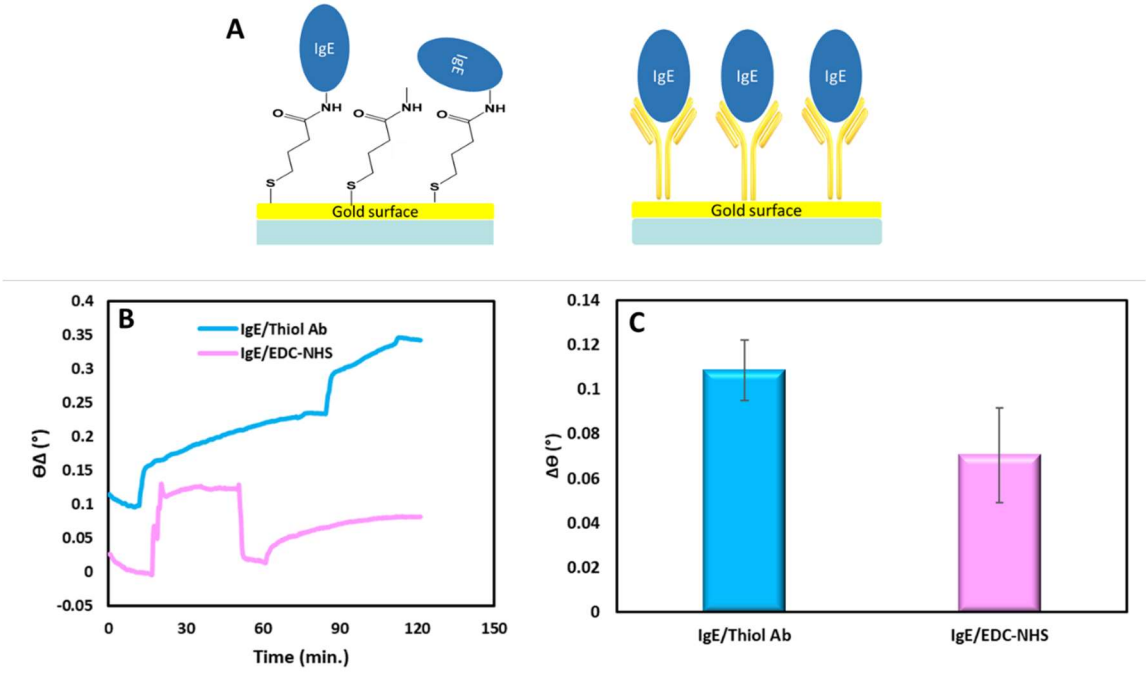

Figure 4. 3 (A) cartoon representation of IgE coupled to MUA and anti-IgE surface. (B) SPR signals obtained by different modified SPR chips for IgE detection. (C) The column chart represents the surface concentration of immobilized IgE.

SPR data for IgE immobilized by affinity coupling over the thiolated anti-IgE surface are shown in Figure 4.3B's blue line. Gold substrate was extensively rinsed with absolute ethanol and DI-water before drying under an N2 stream. Then the gold substrate was clamped to a flow cell on a prism. After flowing the buffer for some time, 30 µL thiolated anti-IgE/cysteamine immobilization solutions were injected into the flow cell. They were then incubated for 1 h to facilitate the direct coupling of thiolated anti-IgE to Au surface. After the rinsing step, 40 µg/ml IgE in PBS buffer was injected and incubated for 30 min.

Figure 4.3C shows the influence of different immobilization techniques used in this study on the surface concentration of immobilized IgE. We found that SPR-angle shifts caused by the covalent immobilization of IgE are 0.07° and 0.1085° for the SPR-chip based on IgE immobilization using affinity coupling via thiolated anti-IgE modified surface. From the shift of SPR-angle, the surface concentration of the IgE was calculated as 0.583 and 0.904 ng/mm2 for MUA and thiolated anti-IgE modified SPR-chips respectively; the shift of SPR-angle by 0.12° corresponds to the change of surface concentration of protein by 1 ng/mm2.[74, 75] It is clear that IgE immobilized by affinity interface shows a higher binding capacity level than IgE immobilized through covalent coupling. This confirms the affinity of antibodies (anti-IgE) toward a binding partner protein (IgE) and that the immobilization technique of anti-IgE interface through direct self-assembled onto hydrophilic gold via thiol functional group provides proper orientation of anti-IgE immobilization which result in more IgE binding capacity over the modified surface.

Covalent immobilization of IgE shows less protein binding capacity. The reason could be the disordered IgE orientation. It has been reported that disordered protein orientation results in loss of binding capacity.[76, 77] The main reason for the reduction of binding capacity is based on the random orientation of the protein molecules and steric-hindrance induced by the improper orientation of the protein toward the surface of solid substrate.[78]

Observing the IgE binding sensograme (Fig. 4.3B) indicates that the binding of IgE to anti-IgE surface shows less convex binding kinetics (more linear) in the association phase, whereas binding of IgE to EDC/NHS surface cause more convex traces in the

association phase. This observation indicates that the binding of IgE/anti-IgE is limited by mass transfer limitation (MTL).

In SPR, the analyte in a solution must first diffuse from the bulk to the surface to interact with the immobilized ligand. The MTL condition causes both the association and dissociation phase to exhibit slower kinetics. In the association phase, the local concentration (surface concentration) of the analyte is lower than the analyte in the bulk solution; whereas, in the dissociation phase, dissociated analyte molecules rebind to empty surface site before they can escape to the bulk solution. This slow association kinetics led to deviate the binding process from the exponential toward the initially more linear sinsogame.

The bivalent nature of the IgE binding will most likely induce “forced proximity” that is, the binding of one site of the IgE is expected to force the second binding site to stay close to its corresponding site. The first binding event will produce an increase in response while the subsequent binding events will not change the signal because the proteins are already within the reach of the sensor and will not cause any mass increase. However, this will create a shortage of analytes at the interaction surface and MTL condition. In the other hand, the binding of IgE to the EDC/NHS surface is mediated through an amide linkage. This chemical interaction lacks the bivalent binding nature and follows the single exponential binding curve. This could reveal how multivalency triggers sensograme shape deformation and how the study of the kinetics binding provides more information on protein-protein interaction and function.

A previous study shows how the capability of SPR to study the protein binding kinetics contributes to an explanation of the difference of *in vivo* functions of SH2 domain-containing inositol 5-phosphatase 1 (SHIP1) and 2 (SHIP2).[79] These domains are structurally similar proteins that catalyze the degradation of lipid messenger phosphatidylinositol 3,4,5-triphosphate to produce phosphatidylinositol 3,4-diphosphate. Analyzing their interaction with pY peptides using SPR indicates that the two domains have similar binding affinities but dramatically different binding kinetics. SHIP2 domain presented both very slow association and dissociation rates. This slow kinetics is attributed to MTL as the SHIP2 exists in a mixture of active and inactive isomers, and binding of the active form generates force to convert the inactive isomer to the active form. The SHIP1 domain showed faster binding behavior, immediately binding to the receptor. At the same time, its fast dissociation allows rapid exposure of the pY motif for dephosphorylation or binding to other proteins. In contrast, SHIP2 takes a longer time to bind to these receptors; once bound, however, SHIP2 stays bound to the pY proteins for a much longer period of time, preventing their dephosphorylation or exchange with other protein partners.

Investigation of SPR signal amplification of IgE detection using the two approaches demonstrated in this study.

Previously, we report an application of AuNP-PEMA to SPR signal enhancement with a bacterial cholera toxin and GM1 incorporated in supported PC bilayer membranes that were formed by direct fusion on the calcinated gold surface. [21] The surface-bound CT was recognized by biotinylated anti-CT, which provides a handle to link initiator-bearing nanoparticles to the analyte via an avidin bridge. Two consecutive steps contribute to SPR

signal amplification: AuNP-initiator-biotin binding and localized ATRP polymer growth on the AuNP surface.

In this current work, we aim to investigate SPR signal enhancement induced by AgNp-aptamer-initiator conjugate (AgNP-apt-init) using the two approaches. In the first approach, AgNP-apt-init is used to recognize IgE bound to MUA-based SAM surface by aptamer link. At the same time, this nanoparticle (AgNP) will induce SPR signal amplification. While in the second approach, the AgNP-apt-init conjugate forms a sandwich assay for protein detection and signal amplification given that IgE has two different binding sites for anti-IgE and IgE specific aptamer.[80] This means that IgE can bind to both a thiolated anti-IgE interface and aptamer conjugated to AgNP at the same time.

SPR signals induced by AgNP-apt-init binding to the SPR chip based on covalent immobilization and affinity immobilization of IgE were 0.176 and 0.259 degrees, respectively (Fig. 4.4). Higher signal enhancement of IgE immobilized over antibodies modified surface is expected. This is based on the result shown in Figure 4.3 that there is more IgE binding capacity over the thiolated anti-IgE interface compared to MUA interface.

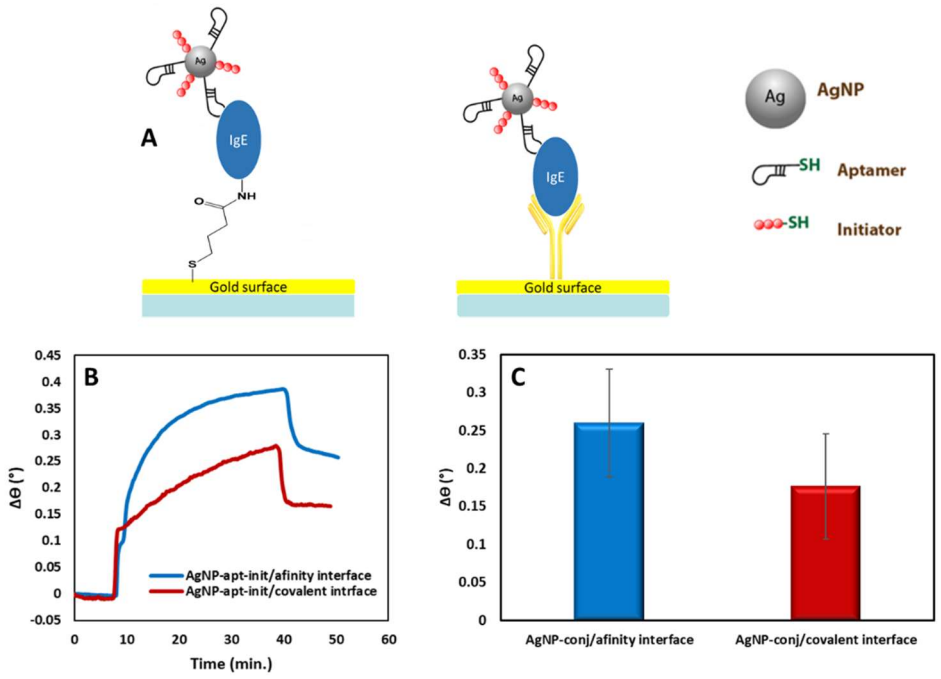

Figure 4. 4 (A) cartoon representation for SPR signal amplification in IgE detection. (B) SPR sensograme of signals amplification with AgNP conjugate. (C) Column chart represents a comparison of signal enhancement with a different interface.

However, surprisingly the two approaches show comparable signal enhancement if compared with SPR signal before amplification. The SPR signals enhancement were 2.5 and 2.3 times higher than the signal observed before amplification for covalent and affinity coupling of IgE to the SPR chip, respectively. These results could mean that majority of the IgE immobilized on the MUA surface was in the orientation which facilitates the affinity binding of the aptamer nanoparticle conjugate on the other end of the protein (IgE). Our result is in alignment with a previous report[25] which concludes that covalent immobilization of protein is not necessarily entirely random but can result in surface coatings in which the majority of the proteins have a similar or even unique orientation.

Nevertheless, the immobilization technique based on interaction between the thiolated anti-IgE and gold surface is advantageous as it provides proper orientation of the anti-IgE modified thiol group and a higher protein binding capacity in respect to covalent immobilization techniques presented in this study. In addition, it is carried out by simple adsorption of the thiol group modified anti-IgE onto a gold surface.

Moreover, investigating the binding kinetics of SPR signal amplification using both interface approaches (Fig. 4.4B) indicates that both binding sensograms show ideal binding kinetics association curves. However, the blue curve which represents SPR signal amplification using biological interface (anti-IgE) exhibits a more ideal curvature association phase.

Investigation of amyloid-beta conformation change near lipid bilayers using molecular dynamic simulation

MD simulation studies aim to observe biomolecular processes in action, particularly important functional processes such as protein folding, or membrane protein interaction. Observing these processes in action helps answer questions about the structural basis for events that are difficult to address experimentally. For example: In what order do substructures form during protein folding? [81, 82] How does an anchoring of proteins to membranes lead to their aggregation?[53, 83]

A membrane is a biological interface that promotes pathological aggregation of an amyloidogenic protein. A lipid bilayer, the basic structural element of biological membranes, is commonly regarded as a two-dimensional liquid providing a variety of

environments, which can affect structure and dynamics of the protein. A number of studies provide evidence for substantial enhancement of protein and peptide aggregation in a membrane environment.[51-53]

Aβ is a cleavage product of the single transmembrane protein APP. β-secretase cleaves the extracellular domain of APP to generate the N terminus of Aβ, and then γ-secretase performs unusual proteolysis in the middle of the transmembrane domain of APP to produce the C terminus of Aβ.[84] Residues 29–40 of Aβ40 are from the transmembrane domain of APP. A discrete molecular dynamics study shows that the C-terminal region of Aβ42 plays an important role in its aggregation process.[85] Therefore, we aim to investigate amyloid-beta conformation change near the POPC lipid bilayer.

Two independent molecular dynamic simulations (250ps long) were performed. The first system was a simulation of hydrophobic C-terminus Amyloid-beta Aβ (28-40) fragment near the POPC bilayer. The second system was a simulation of charged N-terminus Aβ (15-27) also near POPC as a membrane model. Initially, the Aβ residues were arranged on the surface of the membrane for each system. Looking to the simulation snapshots (Fig. 4.5), Aβ fragments in both systems stay near the membrane surface during the majority of the simulation time. Although it was possible for hydrophobic Aβ residues (28-40) to pass through the upper periodic boundary and interact with the bottom leaflet of the bilayer, this did not occur with any residues during the chosen simulation setup. Snapshot structure demonstrates that 15-27 residues gradually lie down parallel to the membrane surface. This orientation maximizes the interaction with the bilayer without burying any residue. While the 28-40 residues form a curved structure on top of the POPC

bilayer with some contact residues at the beginning of the simulation time. This result aligns with previous studies. In one study, they examine the conformational dynamics of $A\beta_{40}$ in the membrane by inserting residues 29-40 of $A\beta_{40}$ into a DPPC lipid bilayer.[86] During the simulation time, $A\beta_{40}$ moves to the interface between the DPPC lipids and the water molecules, and part of the peptide lies down on the surface of the lipid bilayer. Then as the simulation goes on, $A\beta_{40}$ tends to totally exit the lipid bilayer. Another study using SPR reported binding of Aβ to the POPC bilayer.[87]

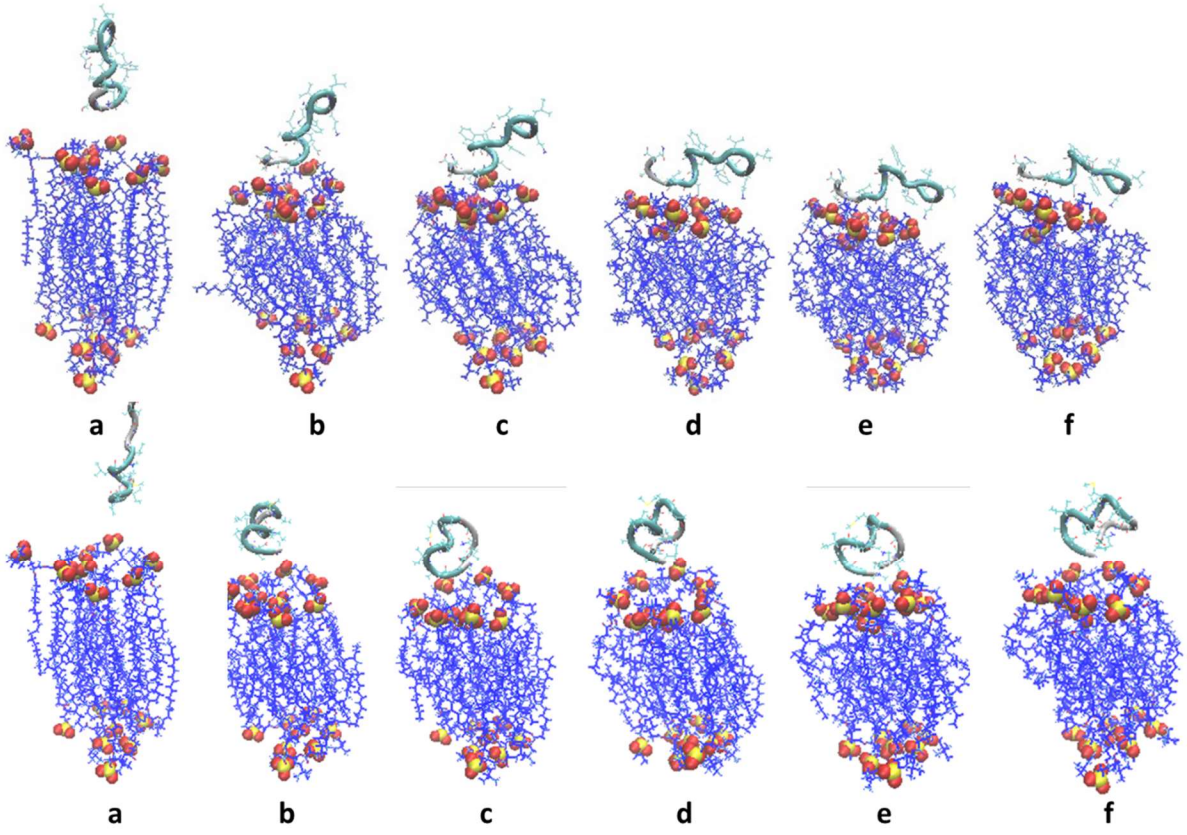

Figure 4. 5 Simulation snapshots from the MD simulation of Aβ (15-27)/POPC (top picture) and Aβ (28-40)/POPC (bottom one) at different timestep a) 0, b)50, c)100, d)150, e)200, f) 250ps

In attempts to study the two Aβ fragments conformation change during the MD simulation, our results show that helix/coil starting structures in both fragments adapted turn/coil structures at the end of the simulation time (Fig. 4.6). Xu et al.[86] previously reported that some of $A\beta_{40}$ residues switched to turn structures then recovered to the helix structures at the end of the simulation time which was 100 ns. Based on Xu et al. result, the turn is a transit structure during the nanosecond simulation period; however, our simulation time is much lower (250 ps).

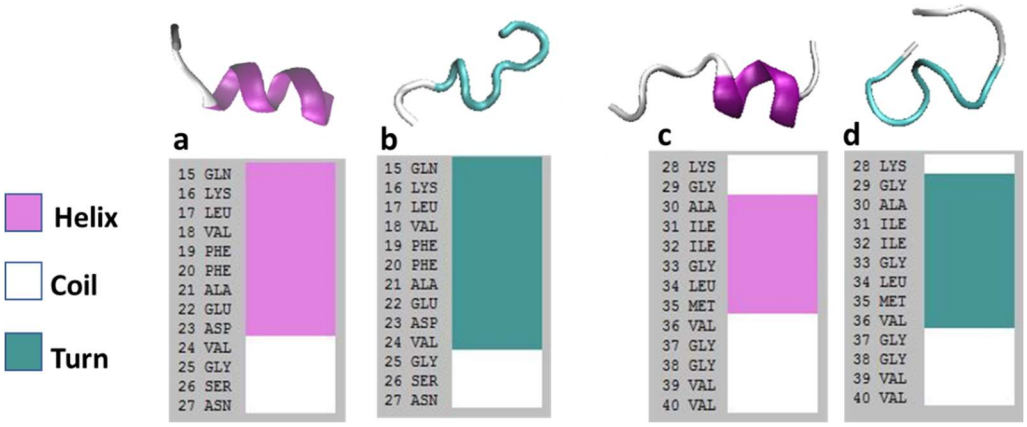

Figure 4. 6 secondary structure of Aβ fragments: on the right Aβ (28-40) a) before b) after simulation on the left Aβ (15-27) a) before b) after simulation

The root mean square deviation (RMSD) for C-terminus Aβ (28-40) (Fig. 4.7) increases rapidly within 15ps and then it remains stable at around 5A° over the whole simulation period. On the other hand, the RMSD for N-terminus of the peptide gradually increases until it reaches 3.7A° after 200ps of simulation time with respect to the starting structure. RMSD analysis demonstrates that the C-terminus quickly adapted to turn structure at the beginning of the simulation while N-terminus gradually moved to turn structure with more fluctuation compared to C-terminus. That may be interperted as the C-

terminus have a higher affinity for the POPC bilayer. Discrete molecular dynamics study also shows that the C-terminal region of Aβ42 plays an important role in its aggregation process.[85]

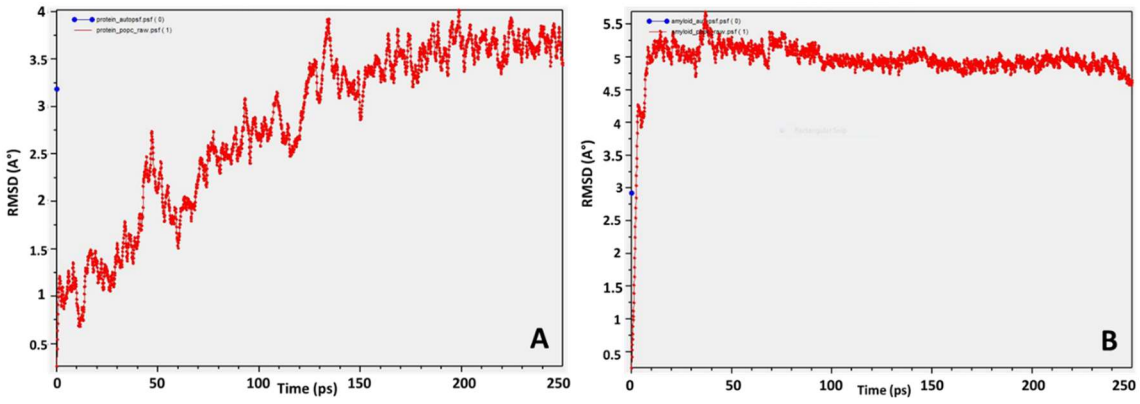

Figure 4. 7 RMSD vs Time plot of Aβ (15-27) (on right) and Aβ (28-30) (on left) during simulation time.

Figure 4.8 demonstrates that the POPC bilayer structure also changed during both conducted simulations. It appears from the figure that the membrane shrinks after MD simulation, which may lead to a change in the membrane properties. The RMSD curve also shows the deviation of the membrane in respect to the starting structure. ^{31}P-NMR[88] and x-ray reflectivity[89] results have shown that Aβ peptides interact with lipids and lead to significant alteration of the properties of the bilayer itself. Other studies also reported that Amyloid-beta induces membrane permeabilization, resulting from alterations in bilayer structure.[90, 91] These results, including ours, provide a clear demonstration that lipids can fundamentally impact the aggregation pathway for Aβ.

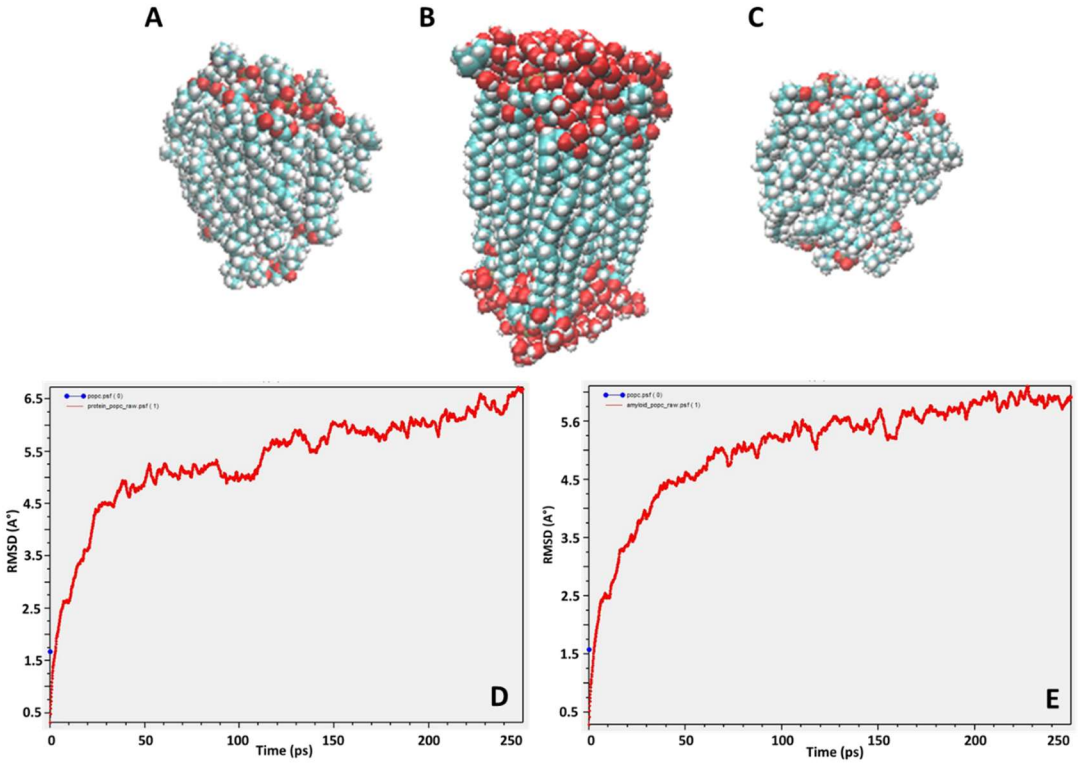

Figure 4. 8 POPC bilayer structure A) after MD simulation with Aβ (28-40) B) before MD simulation C) after MD simulation with Aβ (15-27) D and C RMSD vs Time plot of Aβ (15-27)/POPC (on right) and Aβ (28-30)/POPC (on left) during simulation time.

CONCLUSION

In this work, two interface designs for protein immobilization and detection were investigated. IgE was chosen as a target protein biomarker molecule which was attached to a gold surface using covalent coupling (MUA interface) and affinity coupling (thiolated anti-IgE interface). Results indicate that IgE immobilized by affinity interface shows a higher binding capacity level than IgE coupled through a covalent interface. This could be explained by the steric hindrance induced by improper orientation of IgE on the MUA surface. Observing the binding kinetics of the SPR sensograme indicates a slow association

rate of IgE/anti-IgE binding while IgE/MUA binding represents an ideal curvature association phase.

In addition, we studied SPR signal amplification of IgE induced by a AgNP conjugate using the two interface approaches. Our results demonstrate higher signal enhancement induced by AgNP conjugate binding to SPR surface based on affinity interface compared to the signal based on covalent interface. This result is reasonable as we see more IgE attached to the thiolated IgE interface than MUA interface. However, comparing the signal enhancement with the signal before amplification of each approach shows rival results. This could mean, even there are less IgE coupled to MUA surface; however, most of them bind to the surface in such a way that the IgE epitope is available and exposed to the solution to facilitate the binding of the aptamer conjugated to AgNP.

Moreover, we investigated Aβ (15-27) and Aβ (28-40) confirmation change near the lipid bilayer using a molecular dynamic simulation (MDS). Analyzing the simulation results revealed that both amyloid-beta fragments and the POPC bilayer undergo conformation change in respect to the starting structure. It is worth noting that N-terminus fragment takes more time to adapt the turn structure with more fluctuation compared to the C-terminus, which could indicate the higher affinity of C-terminus toward the POPC bilayer.

REFERENCES

1. Lam, S. W.; Jimenez, C. R.; Boven, E., Breast cancer classification by proteomic technologies: current state of knowledge. *Cancer Treat Rev* 2014, *40* (1), 129-38.

2. G, K., Diagnostic and prognostic molecular biomarkers for prostate cancer. *Histopathology.* 2012, *60* (1), 125-141.

3. Tran HT, L. Y., Zurita AJ, Lin Y, Baker-Neblett KL, Martin AM, Figlin RA, Hutson TE, Sternberg CN, Amado RG, Pandite LN, Heymach JV, Prognostic or predictive plasma cytokines and angiogenic factors for patients treated with pazopanib for metastatic renal-cell cancer: a retrospective analysis of phase 2 and phase 3 trials. *Lancet Oncol.* 2012, *13* (8), 827-837.

4. Signorelli, S. S.; Fiore, V.; Malaponte, G., Inflammation and peripheral arterial disease: the value of circulating biomarkers (Review). *Int J Mol Med* 2014, *33* (4), 777-83.

5. Araujo, M.; Doi, S. Q., Editorial: Biomarkers in CKD. *Front Med (Lausanne)* 2017, *4*, 168.

6. Blennow, K.; Zetterberg, H., The past and the future of Alzheimer's disease CSF biomarkers-a journey toward validated biochemical tests covering the whole spectrum of molecular events. *Front Neurosci* 2015, *9*, 345.

7. Federica Rusmini, Z. Z., and Jan Feijen, Protein Immobilization Strategies for Protein Biochips *Biomacromolecules* 2007, *8*, 1775-1789.

8. R., K., SPR for molecular interaction analysis: a review of emerging application areas. *J Mol Recognit* 2004, *17* (3), 151-161.

9. Uludag, Y.; Tothill, I. E., Cancer biomarker detection in serum samples using surface plasmon resonance and quartz crystal microbalance sensors with nanoparticle signal amplification. *Anal Chem* 2012, *84* (14), 5898-904.

10. Cao, C.; Sim, S. J., Signal enhancement of surface plasmon resonance immunoassay using enzyme precipitation-functionalized gold nanoparticles: a femto molar level measurement of anti-glutamic acid decarboxylase antibody. *Biosens Bioelectron* 2007, *22* (9-10), 1874-80.

11. Campbell, C. T.; Kim, G., SPR microscopy and its applications to high-throughput analyses of biomolecular binding events and their kinetics. *Biomaterials* 2007, *28* (15), 2380-92.

12. Charles, P. T.; Adams, A. A.; Howell, P. B., Jr.; Trammell, S. A.; Deschamps, J. R.; Kusterbeck, A. W., Fluorescence-based sensing of 2,4,6-trinitrotoluene (TNT) using a multi-channeled poly(methyl methacrylate) (PMMA) microimmunosensor. *Sensors (Basel)* 2010, *10* (1), 876-89.

13. Linman, M. J.; Taylor, J. D.; Yu, H.; Chen, X.; Cheng, Q., Surface plasmon resonance study of protein-carbohydrate interactions using biotinylated sialosides. *Anal Chem* 2008, *80* (11), 4007-13.

14. Klok, M. A. G. a. H.-A., Peptide/proteinpolymer conjugates: synthetic strategies and design concepts. *Chem. Commun* 2008, *23* (23), 2591-2611.

15. Jonkheijm, P.; Weinrich, D.; Schroder, H.; Niemeyer, C. M.; Waldmann, H., Chemical strategies for generating protein biochips. *Angew Chem Int Ed Engl* 2008, *47* (50), 9618-47.

16. Brady, D.; Jordaan, J., Advances in enzyme immobilisation. *Biotechnol Lett* 2009, *31* (11), 1639-50.

17. Srivatsa V. Rao l, K. W. A., and Leonidas G. Bachas Oriented Immobilization of Proteins. *Mikrochim. Acta* 1998, *128*, 127-143.

18. Mateo, C.; Abian, O.; Bernedo, M.; Cuenca, E.; Fuentes, M.; Fernandez-Lorente, G.; Palomo, J. M.; Grazu, V.; Pessela, B. C. C.; Giacomini, C.; Irazoqui, G.; Villarino, A.; Ovsejevi, K.; Batista-Viera, F.; Fernandez-Lafuente, R.; Guisán, J. M., Some special features of glyoxyl supports to immobilize proteins. *Enzyme and Microbial Technology* 2005, *37* (4), 456-462.

19. Katsumi Uchida, H. O., Mitsuhiro Kaneko, Kazunori Kataoka, and Yukio Nagasaki, A Reactive Poly(ethylene glycol) Layer To Achieve Specific Surface Plasmon Resonance Sensing with a High S/N Ratio: The Substantial Role of a Short Underbrushed PEG Layer in Minimizing Nonspecific Adsorption. *Anal. Chem.* 2005, *77*, 1075-1080.

20. Kawaguchi, T.; Shankaran, D. R.; Kim, S. J.; Gobi, K. V.; Matsumoto, K.; Toko, K.; Miura, N., Fabrication of a novel immunosensor using functionalized self-

assembled monolayer for trace level detection of TNT by surface plasmon resonance. *Talanta* 2007, *72* (2), 554-60.

21. Ying Liu, Y. D., Jessica Jauw, Matthew J. Linman, and Quan Cheng, Highly Sensitive Detection of Protein Toxins by Surface Plasmon Resonance with Biotinylation-Based Inline Atom Transfer Radical Polymerization Amplification. *Anal. Chem.* 2010, *82*, 3679–3685.

22. Hye Jin Lee, A. W. W., Yuan Li, and Robert M. Corn, Fabricating RNA Microarrays with RNA-DNA Surface Ligation Chemistry. *Anal. Chem.* 2005, *77*, 7832-7837.

23. Pei, Z.; Anderson, H.; Myrskog, A.; Duner, G.; Ingemarsson, B.; Aastrup, T., Optimizing immobilization on two-dimensional carboxyl surface: pH dependence of antibody orientation and antigen binding capacity. *Anal Biochem* 2010, *398* (2), 161-8.

24. Wang, B.; Guo, C.; Zhang, M.; Park, B.; Xu, B., High-resolution single-molecule recognition imaging of the molecular details of ricin-aptamer interaction. *J Phys Chem B* 2012, *116* (17), 5316-22.

25. Manuel Fuentes, C. M., Roberto Ferna´ndez-Lafuente, and J. M. Guisa´n, Detection of Polyclonal Antibody Against Any Area of the Protein-Antigen Using Immobilized Protein-Antigens: The Critical Role of the Immobilization Protocol. *Biomacromolecules* 2006, *7*, 540-544.

26. Mendes, A. A.; Giordano, R. C.; Giordano, R. d. L. C.; de Castro, H. F., Immobilization and stabilization of microbial lipases by multipoint covalent attachment on aldehyde-resin affinity: Application of the biocatalysts in biodiesel synthesis. *Journal of Molecular Catalysis B: Enzymatic* 2011, *68* (1), 109-115.

27. Lopez-Gallego, F.; Betancor, L.; Mateo, C.; Hidalgo, A.; Alonso-Morales, N.; Dellamora-Ortiz, G.; Guisan, J. M.; Fernandez-Lafuente, R., Enzyme stabilization by glutaraldehyde crosslinking of adsorbed proteins on aminated supports. *J Biotechnol* 2005, *119* (1), 70-5.

28. Hernandez, K.; Fernandez-Lafuente, R., Control of protein immobilization: coupling immobilization and site-directed mutagenesis to improve biocatalyst or biosensor performance. *Enzyme Microb Technol* 2011, *48* (2), 107-22.

29. Asanomi, Y.; Yamaguchi, H.; Miyazaki, M.; Maeda, H., Enzyme-immobilized microfluidic process reactors. *Molecules* 2011, *16* (7), 6041-59.

30. Kazuhiro Nakanishi, T. S., Yoichi Kumada , Koreyoshi Imamura, and Hiroyuki Imanaka, Recent Advances in Controlled Immobilization of Proteins onto the Surface of the Solid Substrate and Its Possible Application to Proteomics. *Current Proteomics* 2008, *5*, 161-175.

31. MacCraith, S. L. a. B. D., Immobilization of Biomolecules on Cycloolefin Polymer Supports *Anal. Chem.* 2007, *79*, 6264-6270.

32. Yakovleva, J.; Davidsson, R.; Bengtsson, M.; Laurell, T.; Emnéus, J., Microfluidic enzyme immunosensors with immobilised protein A and G using chemiluminescence detection. *Biosensors and Bioelectronics* 2003, *19* (1), 21-34.

33. Byrne, B.; Stack, E.; Gilmartin, N.; O'Kennedy, R., Antibody-based sensors: principles, problems and potential for detection of pathogens and associated toxins. *Sensors (Basel)* 2009, *9* (6), 4407-45.

34. Iijima, M.; Kadoya, H.; Hatahira, S.; Hiramatsu, S.; Jung, G.; Martin, A.; Quinn, J.; Jung, J.; Jeong, S. Y.; Choi, E. K.; Arakawa, T.; Hinako, F.; Kusunoki, M.; Yoshimoto, N.; Niimi, T.; Tanizawa, K.; Kuroda, S., Nanocapsules incorporating IgG Fc-binding domain derived from Staphylococcus aureus protein A for displaying IgGs on immunosensor chips. *Biomaterials* 2011, *32* (6), 1455-64.

35. Wang, X.; Mei, Z.; Wang, Y.; Tang, L., Comparison of four methods for the biofunctionalization of gold nanorods by the introduction of sulfhydryl groups to antibodies. *Beilstein J Nanotechnol* 2017, *8*, 372-380.

36. Hermann T, P. D., Adaptive recognition by nucleic acid aptamers. *Science.* 2000, *287* (5454), 820-825.

37. Jayasena, S. D., Aptamers: An Emerging Class of Molecules That Rival Antibodies in Diagnostics *Clinical Chemistry* 1999, *54* (9), 1628–1650.

38. Szostak, A. D. E. J. W., In vitro selection of RNA molecules that bind specific ligands *Nature* 1990, *346*, 818.

39. Tuerk C, G. L., Systematic evolution of ligands by exponential enrichment: RNA ligands to bacteriophage T4 DNA polymerase. *Science* 1990, *249* (4968), 505-510.

40. Cho, E. J.; Lee, J. W.; Ellington, A. D., Applications of aptamers as sensors. *Annu Rev Anal Chem (Palo Alto Calif)* 2009, *2*, 241-64.

41. Toh, S. Y.; Citartan, M.; Gopinath, S. C.; Tang, T. H., Aptamers as a replacement for antibodies in enzyme-linked immunosorbent assay. *Biosens Bioelectron* 2015, *64*, 392-403.

42. Darmostuk, M.; Rimpelova, S.; Gbelcova, H.; Ruml, T., Current approaches in SELEX: An update to aptamer selection technology. *Biotechnol Adv* 2015, *33* (6 Pt 2), 1141-61.

43. Kodoyianni, V., Label-free analysis of biomolecular interactions using SPR imaging. *Biotechniques* 2011, *50* (1), 32-40.

44. Harlow, E. L., D., *Using antibodies: a laboratory manual*. Cold Spring: Harbor Laboratory Press: New York, 1999.

45. Su, X.; Zhang, J., Comparison of surface plasmon resonance spectroscopy and quartz crystal microbalance for human IgE quantification. *Sensors and Actuators B: Chemical* 2004, *100* (3), 309-314.

46. Hsiao-Wei Wen, W. B.-W., Thomas R. DeCory, and Richard A. Durst, Peanut Allergy,Peanut Allergens, and Methods for the Detection of Peanut Contamination in Food Products. *Compr. Rev. Food Sci. Food Saf* 2007, *6*, 47–58.

47. Papamichael, K.; Kreuzer, M.; Guilbault, G., Viability of allergy (IgE) detection using an alternative aptamer receptor and electrochemical means. *Sensors and Actuators B: Chemical* 2007, *121* (1), 178-186.

48. Peuravuori H, K. T., Pyrophosphatase-based enzyme-linked immunosorbent assay of total IgE in serum. . *Clin Chem.* 1993, *39*, 846-51.

49. Thirumalai, D., Emerging ideas on the molecular basis of protein and peptide aggregation. *Current Opinion in Structural Biology* 2003, *13* (2), 146-159.

50. Stefani, M., Protein misfolding and aggregation: new examples in medicine and biology of the dark side of the protein world. *Biochim Biophys Acta* 2004, *1739* (1), 5-25.

51. CHAKRABARTTY, J. M. a. A., Characterization of the interactions of Alzheimer P-amyloid peptides with phospholipid membranes. *Eur. J. Biochem.* 1997, *245*, 355-363

52. SELKOE, D. J., Alzheimer's Disease: Genes, Proteins, and Therapy. *HYSIOLOGICAL REVIEWS* 2001, *81*, 741-766.

53. Hongxia Zhao, E. K. J. T., and Paavo K. J. Kinnunen, Formation of Amyloid Fibers Triggered by Phosphatidylserine-Containing Membranes. *Biochemistry* 2004, *43*, 10302-10307.

54. Kirkitadze, M. D.; Condron, M. M.; Teplow, D. B., Identification and characterization of key kinetic intermediates in amyloid beta-protein fibrillogenesis. *J Mol Biol* 2001, *312* (5), 1103-19.

55. Klement, K.; Wieligmann, K.; Meinhardt, J.; Hortschansky, P.; Richter, W.; Fandrich, M., Effect of different salt ions on the propensity of aggregation and on the structure of Alzheimer's abeta(1-40) amyloid fibrils. *J Mol Biol* 2007, *373* (5), 1321-33.

56. Smith, D. G.; Cappai, R.; Barnham, K. J., The redox chemistry of the Alzheimer's disease amyloid beta peptide. *Biochim Biophys Acta* 2007, *1768* (8), 1976-90.

57. Aisenbrey, C.; Borowik, T.; Bystrom, R.; Bokvist, M.; Lindstrom, F.; Misiak, H.; Sani, M. A.; Grobner, G., How is protein aggregation in amyloidogenic diseases modulated by biological membranes? *Eur Biophys J* 2008, *37* (3), 247-55.

58. Matsuzaki, K., Physicochemical interactions of amyloid beta-peptide with lipid bilayers. *Biochim Biophys Acta* 2007, *1768* (8), 1935-42.

59. Gorbenko, G. P.; Kinnunen, P. K., The role of lipid-protein interactions in amyloid-type protein fibril formation. *Chem Phys Lipids* 2006, *141* (1-2), 72-82.

60. McCammon, M. K. a. J. A., Molecular dynamics simulations of biomolecules. *nature structural biology* 2002, *9*, 646-652.

61. Hollingsworth, S. A.; Dror, R. O., Molecular Dynamics Simulation for All. *Neuron* 2018, *99* (6), 1129-1143.

62. Hinman, S. S.; Ruiz, C. J.; Drakakaki, G.; Wilkop, T. E.; Cheng, Q., On-Demand Formation of Supported Lipid Membrane Arrays by Trehalose-Assisted Vesicle Delivery for SPR Imaging. *ACS Appl Mater Interfaces* 2015, *7* (31), 17122-30.

63. Wang, Z.; Wilkop, T.; Xu, D.; Dong, Y.; Ma, G.; Cheng, Q., Surface plasmon resonance imaging for affinity analysis of aptamer-protein interactions with PDMS microfluidic chips. *Anal Bioanal Chem* 2007, *389* (3), 819-25.

64. Bastús, N. G.; Merkoçi, F.; Piella, J.; Puntes, V., Synthesis of Highly Monodisperse Citrate-Stabilized Silver Nanoparticles of up to 200 nm: Kinetic Control and Catalytic Properties. *Chemistry of Materials* 2014, *26* (9), 2836-2846.

65. Hui Li, Z. S., Wenying Zhong, Nan Hao, Danke Xu, and Hong-Yuan Chen, Ultrasensitive Electrochemical Detection For DNA Arrays Based on Silver Nanoparticle Aggregates. *Anal. Chem.* 2010, *82*, 5477–5483.

66. Sepúlveda, B.; Angelomé, P. C.; Lechuga, L. M.; Liz-Marzán, L. M., LSPR-based nanobiosensors. *Nano Today* 2009, *4* (3), 244-251.

67. Alastair W. Wark, H. J. L., Abraham J. Qavi, and Robert M. Corn, Nanoparticle-Enhanced Diffraction Gratings for Ultrasensitive Surface Plasmon Biosensing. *Anal. Chem. 2007, 79, 6697-6701* 2007, *79*, 6697-6701.

68. Hu, H.; Li, H.; Zhao, Y.; Dong, S.; Li, W.; Qiang, W.; Xu, D., Aptamer-functionalized silver nanoparticles for scanometric detection of platelet-derived growth factor-BB. *Anal Chim Acta* 2014, *812*, 152-60.

69. Liu, Y.; Cheng, Q., Detection of membrane-binding proteins by surface plasmon resonance with an all-aqueous amplification scheme. *Anal Chem* 2012, *84* (7), 3179-86.

70. Xinhui Lou, C. W., and Lin He, Core-Shell Au Nanoparticle Formation with DNA-Polymer Hybrid Coatings Using Aqueous ATRP. *Biomacromolecules* 2007, *8*, 1385-1390.

71. Ralph G. Nuzzo, F. A. F., and David L. Allara, Spontaneously Organized Molecular Assemblies. Preparation and Properties of Solution Adsorbed Monolayers of Organic Disulfides on Gold Surfaces. *J. Am. Chem. Soc.* 1987, *109*, 2358-2368.

72. Christopher Love, L. A. E., † Jennah K. Kriebel,† Ralph G. Nuzzo,*,‡ and George M. Whitesides, Self-Assembled Monolayers of Thiolates on Metals as a Form of Nanotechnology. *Chem. Rev.* 2005, *105*, 1103−1169.

73. Lee, W.; Oh, B. K.; Lee, W. H.; Choi, J. W., Immobilization of antibody fragment for immunosensor application based on surface plasmon resonance. *Colloids Surf B Biointerfaces* 2005, *40* (3-4), 143-8.

74. A. Kausaite-Minkstimiene, A. R., J. Kirlyte, and A. Ramanavicius, Comparative Study of Random and Oriented Antibody Immobilization Techniques on the Binding Capacity of Immunosensor. *Anal. Chem.* 2010, *82*, 6401–6408.

75. Karlsson, R. S., R., Surface Plasmon Resonance Detection and Multispot Sensing for Direct Monitoring of Interactions Involving Low-Molecular-Weight Analytes and for Determination of Low Affinities. *Analytical Biochemistry* 1995, *228* (2), 274-28.

76. Jyoung, J. Y.; Hong, S.; Lee, W.; Choi, J. W., Immunosensor for the detection of Vibrio cholerae O1 using surface plasmon resonance. *Biosens Bioelectron* 2006, *21* (12), 2315-9.

77. Nikin Patel D. et al. MImmobilization of Protein Molecules onto Homogeneous and Mixed Carboxylate-Terminated Self-Assembled Monolayers. *Langmuir* 1997, *13*, 6485-6490

78. Tang, D. Q.; Zhang, D. J.; Tang, D. Y.; Ai, H., Amplification of the antigen-antibody interaction from quartz crystal microbalance immunosensors via back-filling immobilization of nanogold on biorecognition surface. *J Immunol Methods* 2006, *316* (1-2), 144-52.

79. Zhang, Y.; Wavreille, A. S.; Kunys, A. R.; Pei, D., The SH2 domains of inositol polyphosphate 5-phosphatases SHIP1 and SHIP2 have similar ligand specificity but different binding kinetics. *Biochemistry* 2009, *48* (46), 11075-83.

80. Kim, S.; Lee, J.; Lee, S. J.; Lee, H. J., Ultra-sensitive detection of IgE using biofunctionalized nanoparticle-enhanced SPR. *Talanta* 2010, *81* (4-5), 1755-9.

81. Castellani, F.; van Rossum, B.; Diehl, A.; Schubert, M.; Rehbein, K.; Oschkinat, H., Structure of a protein determined by solid-state magic-angle-spinning NMR spectroscopy. *Nature* 2002, *420* (6911), 98-102.

82. Kresten Lindorff-Larsen, S. P., Ron O. Dror, David E. Shaw, How Fast-Folding Proteins Fold. *SCIENCE* 2011, *334*, 517-20.

83. Kubo, S.; Nemani, V. M.; Chalkley, R. J.; Anthony, M. D.; Hattori, N.; Mizuno, Y.; Edwards, R. H.; Fortin, D. L., A combinatorial code for the interaction of alpha-synuclein with membranes. *J Biol Chem* 2005, *280* (36), 31664-72.

84. Esler WP, W. M., A portrait of Alzheimer secretases--new features and familiar faces. . *Science* 2001, *293*, 1449-1454.

85. B. Urbanc, M. B., L. Cruz, G. Bitan, and D. B. Teplow, Elucidation of Amyloid □-Protein Oligomerization Mechanisms: Discrete Molecular Dynamics Study. *JAM. CHEM.* 2010, *132*, 4266–4280.

86. Yechun Xu, J. S., Xiaomin Luo, Weiliang Zhu, Kaixian Chen, Jianpeng Ma, and Hualiang Jiang, Conformational transition of amyloid ␣-peptide. *Proc Natl Acad Sci U S A.* 2005, *15*, 5403-4507.

87. Kremer, J. J.; Murphy, R. M., Kinetics of adsorption of β-amyloid peptide Aβ(1–40) to lipid bilayers. *Journal of Biochemical and Biophysical Methods* 2003, *57* (2), 159-169.

88. Bokvist, M.; Lindstrom, F.; Watts, A.; Grobner, G., Two types of Alzheimer's beta-amyloid (1-40) peptide membrane interactions: aggregation preventing transmembrane anchoring versus accelerated surface fibril formation. *J Mol Biol* 2004, *335* (4), 1039-49.

89. Ege, C.; Majewski, J.; Wu, G.; Kjaer, K.; Lee, K. Y., Templating effect of lipid membranes on Alzheimer's amyloid beta peptide. *Chemphyschem* 2005, *6* (2), 226-9.

90. Hai Lin, R. B., The FASEB Journal AND RATNESHWAR LAL, Amyloid ␣ protein forms ion channels: implications for Alzheimer’s disease pathophysiology. *The FASEB Journal* 2001, *15*, 2433-2444.

91. Sparr, E.; Engel, M. F.; Sakharov, D. V.; Sprong, M.; Jacobs, J.; de Kruijff, B.; Hoppener, J. W.; Killian, J. A., Islet amyloid polypeptide-induced membrane leakage involves uptake of lipids by forming amyloid fibers. *FEBS Lett* 2004, *577* (1-2), 117-20.

CHAPTER 5: Conclusions and Future Outlook

Optical biosensors such as SPR and SPR imaging are usually used for routine biomolecular interaction analysis because they provide detailed information on binding affinity and kinetics.[1] Thus, these technologies are often referred to as affinity-based biosensors. Significant improvements in instrumentation and assay design[2] have allowed a wider variety of interactions to be analyzed in more detail. In particular, the ability to directly detect the binding of small molecules to immobilized receptors has dramatically increased the application of SPR not only in biomarker detection and analysis [3, 4] but also in drug screening and discovery.[5] More recently, SPR has seen rising use in cell-based assays, therefore increasing their potential impact on drug discovery.

The goal of this dissertation has focused on addressing the challenges of advanced and practical biomedical application of SPR techniques, particularly towards drug discovery, cell-drug interaction, and biomarker analysis and detection. Chapter 2 of this dissertation describes the development of a potential peptide inhibitor against the SARS-CoV-2 virus based on disrupting PPI. Two peptides were synthesized and studied as an inhibitor for SARS-CoV-2 spike protein from binding to ACE2 receptor with a competition assay format. The two peptides inhibitor are of increasing sequence length based on α-helix of ACE2 PD [22-44], [30-42] peptides, respectively. We observed a progressive reduction of the SPR binding signal as a function of the concentration confirming specific inhibition. SPR results provide direct evidence that the peptides under study are strong candidates to potentially inhibit SARS-CoV-2 binding to the ACE2 receptor. They inhibited spike-mediated infection with comparable efficiency, highlighting that adding extra amino acid

residues does not necessarily increase binding efficiency or inhibition of the peptide toward the spike protein. In fact, the shorter peptide was found to reach maximal inhibition at lower concentrations (0.65 μg/ml) than the longer peptide (2.00 μg/ml). In addition, we identified the critical amino acid residues of the RBD/ACE2 derived peptide using molecular docking software, PatchDock. Both peptides were found to block most of the RBD residues that are known to bind to the original ACE2 PD, as predicted by analyzing the crystal structure of the ACE2/RBD complex. The results of our molecular docking and experimental inhibition assay are in good agreement, indicating that small inhibitory peptides can be utilized to inhibit the ACE/SARS-CoV-2 spike protein complex. This may be developed into an anti-SARS-CoV-2 treatment of the viral infection without the adverse side effects for small molecules or recombinant proteins.

Drug discovery paradigms can benefit from target-directed approach [6, 7] and cell systems biology;[8, 9] Future experiments are needed to pursue peptides as inhibitors using cell-based assays, which could significantly reduce the time and cost of new drug development .[8]

In Chapter 3, HeLa cells were cultured on a gold chip, and then drug-cell interaction was monitored in real-time using the SPR technique. Our results indicate that different concentrations of the drug propranolol (POA) have a different mode of interaction with HeLa cells, which is reflected by both the main SPR peak angular position (PAP) and main SPR peak minimum intensity (PMI). At high concentrations in the mM range, POA results in fast cell shrinkage and detachment, which dominates the optical signal obtained (decrease in both PAP and PMI). However, at low concentrations in the μM range, the

doses were insufficient to cause cell detachment. Instead, this β-blocker drug induces HeLa cell apoptosis via a G-protein coupled receptor (G-PCR) signaling pathway, as the SPR optical signature is in alignment with that produced when G-PCRs are stimulated.[10] In addition, to predict the behavior of SPR spectra to the % of cell coverage on the sensor slide, theoretical curves from averaging models were compared to the experimental data. At a high concentration (2 mM) of POA, the experimental SPR response agreed with results extracted from microscopic image based on confluency. In contrast, at lower concentrations (500 μM), the SPR responses show an increase in the signal; however, the signal was observed to decrease based on cell confluency. SPR is a label-free technique that can simultaneously detect a large range of apoptotic events in the same cell population. The change in the cell adhesion area to a sensor chip is insufficient to explain the entire SPR response to the activation of a living cell.

The biosensor-based cell assays have lagged behind the affinity-based application. More studies and investigations are needed to see more growth in this type of application. Therefore, future work should study different drug-cell interaction systems taking the advantage of SPR optical signature and the integrated responses such as PAP and PMI, which can help gain more information on the signal pathway and simultaneous interaction at the cell system targeting.

Lack of sufficient sensitivity and a proper sensing interface could be an issue for SPR sensors while detecting protein biomarkers. Chapter 4 focuses on investigating two types of interfaces: a) an affinity interface based on developing chemically modified antibody self-assembly and b) a covalent interface based on thiolated self-assembly

monolayer. IgE was chosen as a target protein biomarker molecule. Our results indicate that IgE immobilized by an affinity interface shows a higher binding capacity level than IgE coupled through a covalent interface. This could be explained by the steric hindrance induced by the improper orientation of IgE on the monolayer surface (MUA). The binding kinetics of the SPR sensogram indicates a slow association rate of IgE/anti-IgE binding, while IgE/MUA binding represents the ideal curvature association phase. This slow kinetic could be attributed to the bivalent nature of the IgE/anti-IgE binding compared to the chemical binding of IgE to the EDC/NHS surface. In addition, SPR signal amplification using AgNP conjugate was compared on the two interfaces. The results show higher signal enhancement induced by AgNP conjugate binding to the SPR surface based on the affinity interface than that of the covalent interface. This is reasonable as there is more IgE attached to the thiolated IgE interface than the MUA interface. However, comparison of the signal enhancement with the signal before amplification shows comparable enhancements. This suggests that even there are fewer IgE coupled to the MUA surface, most of them bind to the surface in such a way that the IgE epitope is available and exposed to the solution to facilitate the binding of the aptamer conjugated to AgNP. Further experiments are needed to determine the detection range and detection limit of IgE using the affinity interface based on the developing chemically modified antibody self-assembly interface and ATRP based amplification method. This method can be applied as a general strategy to highly sensitive detection of nearly all protein biomarkers by SPR analysis.

The key concept of Alzheimer's disease is based on conformational change and aggregation of amyloid beta-protein. MD simulation studies allows analysis of

biomolecular processes in action, particularly important functional processes such as ligand-induced conformational change and protein folding, which are very difficult to monitor with any experimental technique. Therefore, we performed MD simulation to investigate conformation change of amyloid-beta fragments near the lipid bilayer. Analysis of the simulation results revealed that both Amyloid-beta fragments Aβ (15-27), Aβ (28-40), and the POPC bilayer undergo conformation change in respect to the starting structure. It is worth noticing that Aβ (15-27), which represents the N-terminus fragment, takes more time to adapt the turn structure with more fluctuation compared to the C-terminus. This could indicate a higher affinity of the C-terminus toward the POPC bilayer.

Future MD simulations may involve the use of different lipid types such as cholesterol, ganglioside, and anionic lipids. One may also investigate the main membrane component responsible for enhancing Amyloid fibril formation. The chemical nature of the bilayer components is likely to have a significant role in determining the mode and extent of the membrane binding of Amyloid-beta protein, as well as in the adaption of aggregation-prone protein conformation. Further, it would be very interesting to employ simulations of confirmations with multiple peptides on top of the bilayer, which may provide insight into the role of peptide-peptide interactions on early oligomer formation near the bilayer surface.

REFERENCES

1. DG., M., Improving biosensor analysis. *J Mol Recognit* **1999,** *12*, 279-84.

2. Baird CL, M. D., Current and emerging commercial optical biosensors. . *Journal of Molecular Recognition* **2001,** *14*, 261-268.

3. Sin, M. L.; Mach, K. E.; Wong, P. K.; Liao, J. C., Advances and challenges in biosensor-based diagnosis of infectious diseases. *Expert Rev Mol Diagn* **2014,** *14* (2), 225-44.

4. Patel, S.; Nanda, R.; Sahoo, S.; Mohapatra, E., Biosensors in Health Care: The Milestones Achieved in Their Development towards Lab-on-Chip-Analysis. *Biochem Res Int* **2016,** *2016*, 3130469.

5. Hämäläinen MD, M. P.-O., Schaal W, Karlén A, Classon B, V. L., et al.: Characterization of a set of HIV1 protease inhibitors using binding kinetics data from a biosensor-based screen. . *J Biomol Screen* **2000,** *5*, 353–359.

6. Drews, J., Strategic trends in the drug industry. *Drug Discovery Today* **2003,** *8* (9), 411-420.

7. Williams, M., Target validation. *Curr Opin Pharmacol* **2003,** *3* (5), 571-7.

8. Butcher, E., Can cell systems biology rescue drug discovery? *Nat Rev Drug Discov* **2005,** *4*, 461–467.

9. van der Greef J, M. R., Rescuing drug discovery: in vivo systems pathology and systems pharmacology. *Nat Rev Drug Discov* **2005,** *4*, 961–967.

10. Fang, Y., Label-Free Cell-Based Assays with Optical Biosensors in Drug Discovery. *ASSAY and Drug Development Technologies* **2006,** *4*, 583-95.